ENHANCING SPATIAL RESOLUTION OF REMOTELY SENSED DATA FOR MAPPING FRESHWATER ENVIRONMENTS

A thesis submitted in fulfilment
of the requirements for the degree of
Doctor of Philosophy
in
Biological Sciences
at
The University of Waikato

By
Muhammad Salman Ashraf

THE UNIVERSITY OF
WAIKATO
Te Whare Wānanga o Waikato

2011

To my parents, Tasneem & Muhammad Ashraf, to whom I owe a lot

To my sons, Shaheer & Hafi, May you live long!

To my loving wife & caring friend, Asma

who are my sources of motivation

I dedicate you this thesis,

me te aroha!

Abstract

Freshwater environments are important for ecosystem services and biodiversity. These environments are subject to many natural and anthropogenic changes, which influence their quality; therefore, regular monitoring is required for their effective management. High biotic heterogeneity, elongated land/water interaction zones, and logistic difficulties with access make field based monitoring on a large scale expensive, inconsistent and often impractical. Remote sensing (RS) is an established mapping tool that overcomes these barriers. However, complex and heterogeneous vegetation and spectral variability due to water make freshwater environments challenging to map using remote sensing technology.

Satellite images available for New Zealand were reviewed, in terms of cost, and spectral and spatial resolution. Particularly promising image data sets for freshwater mapping include the QuickBird and SPOT-5. However, for mapping freshwater environments a combination of images is required to obtain high spatial, spectral, radiometric, and temporal resolution.

Data fusion (DF) is a framework of data processing tools and algorithms that combines images to improve spectral and spatial qualities. A range of DF techniques were reviewed and tested for performance using panchromatic and multispectral QB images of a semi-aquatic environment, on the southern shores of Lake Taupo, New Zealand. In order to discuss the mechanics of different DF techniques a classification consisting of three groups was used - (i) spatially-centric (ii) spectrally-centric and (iii) hybrid.

Subtract resolution merge (SRM) is a hybrid technique and this research demonstrated that for a semi aquatic QuickBird image it out performed Brovey transformation (BT), principal component substitution (PCS), local mean and variance matching (LMVM), and optimised high pass filter addition (OHPFA). However some limitations were identified with SRM, which included the

requirement for predetermined band weights, and the over-representation of the spatial edges in the NIR bands due to their high spectral variance.

This research developed three modifications to the SRM technique that addressed these limitations. These were tested on QuickBird (QB), SPOT-5, and Vexcel aerial digital images, as well as a scanned coloured aerial photograph. A visual qualitative assessment and a range of spectral and spatial quantitative metrics were used to evaluate these modifications. These included spectral correlation and root mean squared error (RMSE), Sobel filter based spatial edges RMSE, and unsupervised classification.

The first modification addressed the issue of predetermined spectral weights and explored two alternative regression methods (Least Absolute Deviation, and Ordinary Least Squares) to derive image-specific band weights for use in SRM. Both methods were found equally effective; however, OLS was preferred as it was more efficient in processing band weights compared to LAD.

The second modification used a pixel block averaging function on high resolution panchromatic images to derive spatial edges for data fusion. This eliminated the need for spectral band weights, minimised spectral infidelity, and enabled the fusion of multi-platform data.

The third modification addressed the issue of over-represented spatial edges by introducing a sophisticated contrast and luminance index to develop a new normalising function. This improved the spatial representation of the NIR band, which is particularly important for mapping vegetation.

A combination of the second and third modification of SRM was effective in simultaneously minimising the overall spectral infidelity and undesired spatial errors for the NIR band of the fused image. This new method has been labelled Contrast and Luminance Normalised (CLN) data fusion, and has been demonstrated to make a significant contribution in fusing multi-platform, multi-sensor, multi-resolution, and multi-temporal data. This contributes to improvements in the classification and monitoring of fresh water environments using remote sensing.

Acknowledgements

There are a number of people without whom this thesis might not have been written, and to whom I am greatly indebted.

I am thankful to my Chief supervisor, Dr. Lars Brabyn whose guidance, supervision, and concern for my best interests enabled me to structure this thesis in its current form. I thank you for providing me opportunity to deliver remote sensing lectures and GIS tutoring to your graduate students. My research and work experience with you has been integral to furthering my professional career.

My special thanks to my co-supervisors, Associate Professor Brendan Hicks and Professor David Hamilton for their trust upon me, and vision in directing this research. I appreciate their generous efforts in managing funds for this research, and offering a scholarship for my doctoral studies through the Foundation for Research, Science and Technology (FRST) OBI contract UOWX0505. I am also grateful for the technical and financial support that I have received from Dr. Kevin Collier and Environment Waikato. I am also thankful to Mr. Tim Frasser, Aerial Mapping NZ for providing Vexcel aerial image for analysis.

I am also thankful to my colleagues Mathew Allan and Glen Stichbury for having healthy discussions on image processing, which gave me new ideas and thoughts to do something different, and something better.

A special thanks to Ms. Andrea Haines from the Student Learning Centre for guiding and facilitating me to improve my academic writing skills.

I offer my gratitude to my parents (who visited New Zealand to cheer me up), and my mother-in-law for their endless prayers. Big thanks to my family, and my sisters-in-law, in particular Dr. Sobia & her family who visited us twice and

with whom we share many memories of seeing the marvels of New Zealand together.

Loving thanks to my wife, Asma, for her constant support, cooperation and taking care of lovely Shaheer and Hafi, who also waited patiently during this entire period. Despite her preparations for the PhD defence, she let me finish thesis writing without any worries. Just ahead of my thesis submission, she defended her work successfully. This thesis is bestowed upon her for the triumph.

Contents

List of Figures

List of Tables

List of Acronyms & Abbreviations

ALI	Advanced Land Imager
ALOS	Advanced Land Observing Satellite
ASTER	Advanced Space-borne Thermal Emission and Reflection Radiometer
BL	Bilinear resampling
BT	Brovey Transformation
CC	Cubic Convolution
ETM+	Enhanced Thematic Mapper Plus
HPF	High Pass Filter
HRMI	High Resolution Multispectral Image
HRPI	High Resolution Panchromatic Image
IHS	Intensity Hue Saturation
ISODATA	Iterative Self-Organising Data Analysis Technique
LAD	Least sum of minimum Absolute Deviation
LMVM	Local Mean and Variance Matching
LPF	Low Pass Filter
LRMI	Low Resolution Multispectral Image
LRPI	Low Resolution Panchromatic Image
MMU	Minimum Mapping Unit
NF	Normalising Function
NIR	Near Infra-Red
NN	Nearest Neighbour resampling

OHPFA	Optimised High Pass Filter Addition
OLS	Ordinary Least Squares
PAN	Panchromatic
PCS	Principal Component Substitution
RMSE	Root Mean Squared Error
SAV	Submerged Aquatic Vegetation
SNR	Signal to Noise Ration
SPOT	Satellite Pour l'Observation de la Terre
SRM	Subtractive Resolution Merge
SRR	Spatial Resolution Ration
SVR	Synthetic Variable Ratio
SWIR	Short Wave Infra-Red
TM	Thematic Mapper
USGS	United States Geological Survey
UTM	Universal Transverse Mercator
WBS	Weighted Band Sum

Chapter 1

Introduction and the research context

1.1 Freshwater remote sensing

Freshwater margins along rivers and lakes represent highly diverse biodiversity sites that not only sustain important plant and animal life, but also possess cultural, recreational, environmental and aesthetic values for local communities (Robb and Bright 2004). The vegetation in freshwater margins has significant biophysical functions, which include sediment filtering of overland flow and reduction of its re-suspension (Coates and Folkard, 2009; James et al., 2004), de-nitrification and nutrient uptake from shallow groundwater (Chambers and Kalff, 1985), converting toxic pesticides into non-toxic forms through microbial decomposition (Narumalani et al., 1997), stream bank stability, and spawning habitats for zooplankton and fish (Collier et al., 1995; Genkai-Kato, 2007; Okun and Mehner, 2005).

For the purposes of this thesis the margin between freshwater and land and the associated emergent and sub merged vegetation is called the freshwater environment as this represents significant habitat for biota. There are considerable challenges involved with field based monitoring of freshwater margins. The length of freshwater margins is remarkably high due to the sinuous nature of water and land interaction zones. Freshwater habitats are also logistically difficult to access and traverse by boat or by road. Moreover, their approach is often limited to easy access points, which occur close to the roadside or have suitable landing to disembark from a boat. The limited access and extensive distances to travel within these habitats make field based assessments subjective, time consuming and labour intensive. Consequently, only a few

points measured along transects for each habitat unit are assessed (Gilvear et al. 2007).

The use of remote sensing (RS) for studying and mapping different vegetation habitats overcomes the challenges of difficult access and length of habitats, and is a well-established method. The use of aerial photographs has been used to record the distribution of terrestrial vegetation for the last century (Thomas, 1920). Dalke (1937) stressed the value of aerial photographs to map different freshwater zones including submersed vegetation, floating leafed species, and also rushes and cattails but his findings lacked quantitative evaluation. Successful rocket launches in the late 1940's and 50's which aloft cameras to sub-orbital heights (Holliday, 1950) as well as later developments including imaging in spectral ranges beyond the visible region (Risley, 1967) and the launch of Landsat-1 satellite in 1972, led to present-day digital remote sensing.

Raitala et al. (1985) were among the first who attempted to map aquatic vegetation using Landsat satellite images. Mapping the freshwater and marine aquatic environments is considered more challenging than its terrestrial counterpart due to the varying quantity and quality of the surrounding water. Therefore, past achievements using moderate-resolution SPOT and Landsat data were limited to coarse descriptive level mapping (Jensen et al., 1986; Malthus and Karpouzli, 2003). Substantial progress has been made in marine environments for mapping coral reefs and sea-grass ecosystems (Joyce, 2004; Mount, 2006; Sotheran et al., 1997). When mapping large scale freshwater environments, it is desirable to use images with a combination of high spatial, spectral, radiometric and temporal resolutions with large spatial extents (Ashraf et al., 2010).

Many satellites with sub-metre spatial resolution have emerged since the beginning of this century. In the past 2-3 years, new satellites with higher spectral resolution have been launched. The current-era satellites have improved temporal resolution due to their sensors' high-agility to manoeuvre for side-scan

or to place a constellation of identical sensors in the same orbit. Furthermore, airborne digital imaging sensors have replaced the conventional aerial photography (Cramer, 2005). Advancements in the field of electronics have enabled both types of sensors to capture data with higher radiometric resolution that detects subtle changes in the reflected energy. In short, technological advancements have made both air and space-borne sensors, not only compatible with each other but capable of acquiring equally versatile data (multispectral, hyper-spectral, thermal, microwave and LIDAR) for all-weather, day-or-night imaging, and for 3D mapping. As a result, many recent studies have shown success in mapping different aquatic cover types (Everitt et al., 2004; Nagler et al., 2005; Valta-Hulkkonen et al., 2003; Wolter et al., 2005) as well as identification of different aquatic vegetation species (Everitt et al., 2008; Everitt et al., 2005; Hunter et al., 2010; Maheu-Giroux and de Blois, 2005).

With image capture, there is always a trade-off between spatial and spectral resolutions. Many dual-resolution optical sensors acquire a combination of a high spatial panchromatic image and low spatial multispectral images. However, the narrower spectral coverage (bandwidth) of a multispectral sensor presents a technical limitation. Multispectral sensors gather less reflected energy that adds more noise to the received signals, causing a lower level of signal to noise ratio (SNR). This shortage of energy is compensated for by the wider instantaneous field of view (IFOV). This maintains the level of SNR of the multispectral sensor compatible with its panchromatic sensor but does compromise the spatial resolution of the multispectral image. Other manufacturing constraints relating to the RS satellite system design include restriction of on-board data storage, the data-downlink transmission rate of satellites, and image processing capabilities of the ground-stations.

In general, the resolutions of RS data have been improved in all aspects: spatial, spectral, radiometric and temporal resolution. However, individually every RS sensor is unique due to the specific characteristics of its resolutions. There is no “super-resolution” sensor, which captures perfect data for mapping freshwater environments. A rise in the number of available data sensors with

distinct resolution characteristics offers opportunities to develop new processing techniques to overcome the limited data collection abilities of sensors. Data fusion (DF) is one of the most fruitful techniques to overcome the poor spatial resolutions of multi- and hyper-spectral data. A following brief account on DF not only provides the context and perspective on how DF works but highlights certain limitations associated with different DF methods. These limitations are addressed through this research (see Chapters 4 and 5).

1.2 Data fusion – a concise preview

Data fusion is an attractive and effective field of research in many domains of applications like remote sensing, computer vision, military applications and medical imaging (Boloorani, 2008). Data fusion occurs at three different levels of processing, depending upon the intended applications and according to the stage at which data fusion takes place. These levels are: pixel (or measurement) level, feature level and decision (or information) level (Pohl and Van Genderen, 1998). This thesis focuses on pixel-level data (or image) fusion, which is also known as resolution merging and pan-sharpening (de Béthune et al., 1998a; Wang et al., 2005).

In the domain of RS, data fusion at a pixel level produces a high resolution multispectral image (HRMI) from merging a high resolution panchromatic image (HRPI) with a low resolution multispectral image (LRMI). An early DF method was the high-pass filter addition (HPFA) (Schowengerdt, 1980). This method was proposed as a way to improve the spatial resolution of the then future Landsat-4 and SPOT-1 satellites' multi-spatial multispectral data using computer based processing. Schowengerdt simulated Landsat-3's multi-spectral scanner (MSS) image by degrading three out of its four bands to a lower spatial resolution. These bands were reconstructed back to their original resolution using the fourth unaltered band using the spatial frequency (band-pass filtering) principle. Since then, many methods have been introduced for data fusion. These use different algorithms ranging from very simple arithmetic addition/multiplication to complex mathematical and statistical calculations.

Scientific literature on data fusion covers a great variety of techniques using different types of RS data for numerous applications. A comprehensive review on early data fusion methods by Pohl and Van Genderen (1998) divides different DF methods into as many as four major divisions and 15 subdivisions. More recent reviews on data fusion (Aiazzi et al., 2007a; Thomas et al., 2008; Yang et al., 2010) divide different techniques into broad but confusing divisions, because a category of one is a subcategory of another. This research adopts two logical divisions - spatially centric and spectrally centric techniques. However, there are hybrid techniques, which assimilate spatially-centric processing into their inherent spectrally-centric algorithms. Further explanation of these logical typologies is explained in Chapter 3; however, a brief account on how DF works and its limitations is explained in the following paragraphs.

A rationale of any pixel-level data fusion lies in deriving the “edges” or “boundaries”, which are either determined from the HRPI alone or through a mix of both the HRPI and LRMI. Two factors cause edges to appear in an image. The first type of edge is due to the topography and geometry of different features, e.g., ridge shadows and building or tree shades. Such edges occur in all bands of the LRMI but with varying intensities. The second type of edge is due to the varying reflectance behaviour of different adjoining features, which may emerge as different colours in a three-band formation, e.g. different colours between water and land or between two different species of vegetation. These edges may only be visible in those bands which are sensitive enough to detect subtle reflectance variations. These ‘feature edges’ and ‘colour boundaries’ occur more clearly and profoundly in the HRPI due to its better spatial resolution. This HRSE is often normalised and later added with the LRMI to derive a HRMI. Different DF methods adopt a range of algorithms to determine the high resolution spatial edges (HRSE) image and its normalisation. However, these DF techniques follow a generic framework of image fusion (Aiazzi et al., 2007a; Wang et al., 2010; Wang et al., 2005) that can be explained as:

$$\mathbf{HRMI_n} = \mathbf{LRMI'_n} + \mathbf{HRSE} \cdot \mathbf{NF_n} \quad \textbf{.....(1.1)}$$

Where:

n denotes the nth band of a multispectral image

HRMI is the high (spatial) resolution multispectral image;

$\mathrm{LRMI'_n}$ is the low resolution multispectral image that is up-sampled to the same size as HRPI, consisted of n spectral bands;

HRSE is the high resolution spatial edges image which is either determined from the HRPI alone or exploited from the difference between HRPI and LRMI; and

NF_n is a set of scalar weights, convolve a single band HRSE into n bands, before injecting into each band of the $\mathrm{LRMI'}$

Preservation of both spatial and spectral characteristics of RS data is an issue in data fusion research because the relationship between these two properties functions conversely. Consequently, most DF methods, while improving the spatial context of the LRMI, either distort its spectral fidelity or over represent certain spectral bands. In a reverse scenario, the under or over-representation of spatial details causes either an effect of overall smoothness or pseudo edges around high contrast colour boundaries such as between water and vegetation. Aiazzi et al. (2007b) and Dou et al. (2007) demonstrate through their research that HRSE and NF are the main reasons for colour infidelity and spatial distortions during image fusion process. Therefore, it is important to optimise HRSE and NF, so that the combined effect of the HRSE and NF not only limits spectral difference between the HRMI and LRMI, but maintains the right proportion of edges in the HRMI. Many existing methods, including subtractive resolution merge (SRM), have given little attention to finding a functional NF value; rather the focus has shifted towards finding ways to calculate HRSE.

Many studies have showed the importance of data fusion and its influence on improved classification accuracy for different habitat types (Amarsaikhan et al., 2010; Amarsaikhan and Douglas, 2004; Li and Li, 2010; Meenakshisundaram, 2005). It is known that a fusion process incorporates spatial details of the HRPI into the fused image which results in an increase of texture that often leads to undesired speckled classification. Colditz et al. (2006)

suggest that an image fusion technique is considered good for spectral based classification purposes if it generates less speckled classes. Fox III et al. (2002) suggest that with spectral-based classification, data fusion does not increase the ability to discern finer thematic classes of vegetation. However, DF allows mapping smaller and heterogeneous landscape features thereby avoiding the mixed pixel problem experienced with the use of LRMI. As a result, feature-based classification techniques have been greatly benefitted by employing different fusion methods (Frohn et al., 2011; Midwood and Chow-Fraser, 2010).

In New Zealand, the distinct advantage of data fusion was demonstrated in a national-scale Land Cover Database 2 (LCDB2) mapping initiative. Landsat ETM+ was pan-sharpened from 30 m to 15 m, and this enabled a minimum mapping unit of 1 ha. The spectral resolution of the ETM+ sensor enabled additional land cover classes to be mapped compared to previous land cover mapping (Thompson et al., 2004). In New Zealand, DF has also been used to accurately map snow on mountain slopes using multi-sensor MODIS data (Sirguey et al., 2008). This improved the spatial resolution from 500 m to 250 m and enhanced environmental and hydrological applications.

1.3 Motivation for this research

Environment Waikato (EW) wished to explore the feasibility of mapping the ecological conditions along the margins of large water bodies (lakes and large rivers) using remote sensing. EW's interest coalesced with the objectives of the Foundation for Research Science and Technology (FRST) funded "Restoring Freshwater Ecosystems and Resurrecting Indigenous Lake Biodiversity" project awarded to the University of Waikato's Centre for Biodiversity and Ecology Research (CBER). One of the objectives of this FRST research is to build new knowledge around controlling pest fish, which degrade aquatic ecosystems by consuming and uprooting aquatic plants, stirring up bottom sediments and preying upon the eggs of other fish species. Mapping freshwater habitats and monitoring contributes to this objective and has far-reaching implications for the conservation and restoration of New Zealand's freshwater ecosystems.

A preliminary investigation of the literature regarding freshwater habitat mapping was conducted (Ashraf et al., 2007), which summarised in Chapter 2 of this thesis. Some initial investigations on methodologies related to classifying different freshwater habitats using per-pixel and sub-pixel classification approaches and experimentation to conduct in-situ vegetation spectral reflectance data collection to aid classification process (Ashraf et al., 2008, 2009) were also performed.

Freshwater environment mapping requires high-resolution images that have appropriate spectral characteristics. These characteristics, such as the number of spectral bands and the spectral ranges of a multispectral image, cannot be modified for a particular sensor. However, DF offers opportunities to enhance the spatial context by injecting HRSE image. This partially resolves the mixed pixel problem experienced with the use of LRMI, and delimits the boundaries between small and heterogeneous vegetation features and narrow margins along large freshwater bodies. This research is, therefore, motivated by the need to enhance the spatial resolution with minimal spectral and spatial distortions of commonly used multispectral sensors for effective freshwater mapping.

1.4 Scope of this research

The scope of this thesis is to test and improve different DF methods using RS data captured from a range of aerial and space-borne sensors for different freshwater environments in the Waikato region. Commonly used and computationally swift DF techniques include Brovey transform (BT), principal component and substitution (PCS), local mean and variance matching (LMVM), optimised high-pass filter addition (OHPFA), and a contemporary subtractive resolution merge (SRM) method. These were performed to compare the accuracy and performance. It was found that SRM performed better than the other methods using QuickBird satellite data. However, three modifications were applied to SRM to further improve its performance.

Remotely sensed data sources used for evaluating different DF methods included dual-resolution (i.e., a combination of the LRMI and HRPI) images from QuickBird (QB) satellite (2.4 m and 0.6 m) and Vexcel aerial sensor (28.5 cm and 9 cm), multispectral image form SPOT-5 satellite (10 m), and scanned coloured aerial photographs (0.625 m). To speed up the process, DF techniques were performed on sub-scenes of different dimensions covering areas that ranged from 0.07 km^2 to 2.16 km^2. These sub-scenes represented different freshwater habitats as their dominating feature.

Visual qualitative assessments and a range of spectral and spatial quantitative metrics were applied. These included spectral correlation and root mean squared error (RMSE), Sobel filter based spatial edges RMSE, and unsupervised classification. ERDAS Imagine software and ERDAS Spatial Modeller were used to perform different DF techniques and to perform a range of quantitative analysis.

1.4.1 Aim of this research

The main aim of this research was to enhance the spatial resolution of multispectral images representing different freshwater habitats with minimal spectral and spatial distortions to enable improved precision in classification.

1.4.2 Specific research questions

To achieve the aim of this research, the following research questions were examined, which includes an explanation of the context.

Question 1 What are the best DF techniques for aquatic environment data and what are their limitations?

Pixel-level data fusion is a common practice for fusing multi-resolution (spatial and spectral) data to achieve the synergic effectiveness of both images. In the field of aquatic vegetation mapping, many studies show the comparative advantage of the fused data over their LRMI (Frohn et al., 2009; Midwood and Chow-Fraser, 2010). High resolution multispectral data has helped in classifying

smaller features; however, the DF techniques applied were determined arbitrarily. Fox III et al. (2002) and Riyahi et al. (2009) have suggested that the PCS technique is more effective than BT, multiplicative and Ehler's Intensity-Hue-Saturation (IHS) methods in classifying different wildlife habitats and in identifying individual tree crowns respectively. However, no studies have compared different DF techniques for mapping freshwater vegetation environments. Answering this question in the context of freshwater habitats mapping will be an important contribution to knowledge in this field.

Question 2 What is the contribution of the spectral bands for different spectrally centric DF techniques?

Spectrally centric DF techniques use different proportions of their contributing spectral bands to determine a synthetic panchromatic image, which is used in conjunction with the HRPI to determine the HRSE. Some methods apply predefined weights for their spectral bands, e.g. BT, but others determine spectral weights that are either scene-specific (e.g. PCS) or sensor-specific (e.g. SRM). Depending upon the method, the spectral band contributions may cause certain bands to be over-represented at the cost of others. Reviewing different spectrally centric DF approaches will provide valuable insights not only to answer this question, but ultimately to help in modifying the SRM technique to enable fusing beyond sensor-specific RS images using different statistical regression models.

Question 3 How to normalise the spatial edges image for freshwater environments?

Many DF methods, which determine a single-layer HRSE image, require a normalisation process to decompose the HRSE image into an equal number of bands as the LRMI before injecting the HRSE into LRMI. A normalising function (NF, as referred in Eq. 1.1) is a set of scalar values that helps to adjust the contrast of the HRSE in accordance with the contrast of a particular LRMI band into which the adjusted HRSE is injected. For a low-contrast band, the NF is smaller than any high-contrast band. Existing NF algorithms are found to be non-

effective for high variant RS images, which is a particular scenario of images showing freshwater environments. As a result, spatial edges are either over or under represented in some HRMI bands. This can therefore cause undesired spatial distortions. In particular, the near infrared (NIR) band is found to be over represented for RS images showing dominant aquatic habitats. This problem is not limited to a particular DF technique but applies to most data fusion techniques that use a normalisation function. A modified NF algorithm will help in minimising the spatial distortion in RS data displaying freshwater habitats.

1.5 Thesis structure and chapter outlines

This thesis comprises six chapters – a general introductory chapter (Chapter 1), four chapters written as manuscripts or s for publication (Chapters 2, 3, 4, and 5), and concluding chapter (Chapter 6) that synthesises the foregoing chapters. Two appendices (Appendix A and Appendix B) provide additional detail on the analysis.

The research chapters 2, 3, 4 and 5 are written in a format for journal publications. Since these papers have been submitted to different journals, they follow particular formatting and referencing styles appropriate to each journal. However, changes have been made in the formats of the individual chapters to maintain the consistency of the overall thesis.

Chapter 2 provides a literature review on the mapping needs for different freshwater environments. A detailed description of optical RS satellites and their associated data characteristics explore issues related to mapping freshwater resources for the New Zealand context. One of the conclusive statements of this discourse suggests “the need for high resolution images that have appropriate spectral characteristics”. This review concludes that the spatial resolution of multispectral images needs improvement for freshwater mapping to be effective.

Chapter 3 compares different commonly used DF techniques (as explained in the previous section) for a QB image containing different freshwater

habitats. The results are compared both qualitatively and quantitatively using spectral and spatial error metrics. SRM showed the best overall performance.

Chapter 4 explores ways to extend the SRM data fusion technique beyond its existing capability, i.e. to fuse data using fixed spectral band weights predetermined for particular sensors. This modification is performed with an aim of fusing data from any combination of RS sensors. More specifically, it explains two multivariate statistical methods, the least sum of minimum absolute deviation (LAD) and the ordinary least squares (OLS) regressions to determine spectral band weights.

Chapter 5 explores the issue of higher spatial error, in the NIR band, due to the use of a non-functional NF, which is common to many DF techniques. A new DF method, called contrast and luminance normalised (CLN) fusion, helps in limiting this error for RS data of freshwater environments.

Chapter 6 synthesises results given in previous chapters, and summarises the answers to the research questions. This chapter outlines the contribution of this research in establishing new knowledge towards pixel-level data fusion for freshwater remote sensing, and concludes that many DF fusion methods can benefit from this new knowledge and improve their performances.

Appendix A shows different spatial and spectral quantitative analyses equations and their corresponding ERDAS spatial modeller programming routines.

Appendix B shows algebraic calculations to determine multivariate regression coefficients using ERDAS spatial modeller between the degraded HRPI as an independent variable and four channels of the LRMI as dependent variables using ordinary least squares (OLS) regression technique.

Chapter 2

Remote sensing of New Zealand freshwater environments[1]

2.1 Abstract

Freshwater environments in New Zealand provide a range of ecosystem services and contain important biodiversity. Managing these environments effectively requires a comprehensive inventory of the resource and cost-effective tools for regular monitoring. The complex and extensive margins of natural water bodies make them difficult to sample comprehensively. Problems thus occur with extrapolating point-specific sampling to accurately represent the diversity of vegetation in large freshwater bodies. Mapping freshwater vegetation using satellite remote sensing can overcome problems associated with access, scale and distribution, but it requires high-resolution images that have appropriate spectral characteristics. This chapter provides an overview of the optical satellite data characteristics required for mapping riparian, submerged and emergent vegetation associated with freshwater environments in New Zealand.

2.2 Introduction

New Zealand has 425 000 km of rivers and streams, and almost 4 000 lakes that are larger than 1 ha (MfE, 2007). Inland freshwaters sustain important plant and animal life, as well as having cultural, recreational, environmental and aesthetic values to local communities (Robb and Bright, 2004). These highly

[1] **Published as "Ashraf, S., Brabyn, L., Hicks, B. J., Collier, K., 2010. Satellite remote sensing for mapping vegetation in New Zealand freshwater environments: A review. New Zealand Geographer 66(1):33-43"**

valued environments require careful and sustainable management supported by knowledge of the state and trends in ecological condition. However, their quality is threatened by a range of anthropogenic factors including drainage inputs, loss of riparian cover and also invasive weeds and pests (see Harding et al., 2004). Freshwater vegetation can respond to environmental changes in lakes and rivers, and its composition and extent are commonly used as a monitoring indicator of ecological health (Clayton and Edwards, 2006; Collier et al., 2007). Regular monitoring of the extent and composition of freshwater plant communities (riparian, emergent and submerged), at appropriate scales, is difficult because of the large number of isolated pockets distributed along riverbanks and lake margins. Furthermore, access to freshwater environments often requires the use of boats or overland visits to remote areas. On-site assessments are usually subjective and labour intensive, and are based on a discrete number of points along transects for each habitat unit that does not capture the variability present at the scales required for management (Gilvear et al., 2007).

Alternatively, remotely sensed information acquired from sensors on airborne or space-based platforms can be very time and cost-effective for water-related habitat assessment at a regional scale (Ausseil et al., 2007; Johansen et al., 2007). Recent technological advances in satellite remote sensing (SRS) have resulted in a variety of new sensors being available that capture images of different environmental phenomena and features with improved data quality. SRS is a rapidly changing discipline as new satellites are being launched every year. There have been many reviews that demonstrate its effectiveness for mapping different aquatic environments (Goetz, 2006; Muller, 1997; Ozesmi and Bauer, 2002; Silva et al., 2008). The focus of this chapter is to assess the current developments in the optical satellite data quality in relation to the specific requirements for mapping freshwater vegetation in New Zealand.

2.3 Freshwater environments

The margins of freshwater habitats are a continuum of variable-size zones, extending from terrestrial regions to deep water. They are narrow and

highly diverse in terms of physical characteristics. Moving from land towards water, these zones are called riparian (riverbank), littoral (near shore) and limnetic (open water).The riparian zone of streams and rivers is often defined by hydrological interactions such as the extent of the flood plain, but it can also encompass influences from vegetation providing shade and inputs of large wood. It may be narrow in numerous incised headwater streams that flow through constrained valleys, whereas in mid-size streams, the riparian zone is typically larger, being represented by a distinct band of vegetation whose width is determined by long-term (> 50 years) channel dynamics and the annual discharge regime. Riparian zones of large lowland rivers are characterized by well-developed, but physically complex flood plains with long periods of seasonal flooding, lateral channel migration, oxbow lakes in old river channels, a diverse vegetative community and moist soils (Naiman and Décamps, 1997).

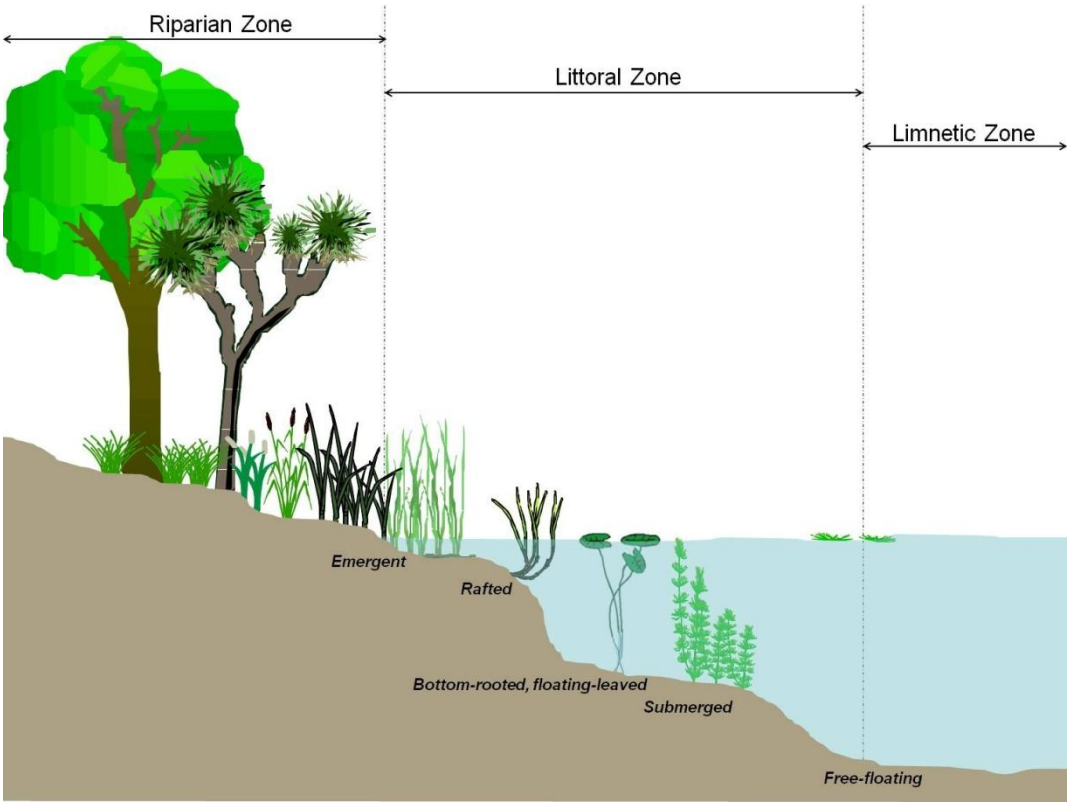

Figure 2.1: Sketch representation of freshwater environments

Most large, vascular aquatic plants (macrophytes) occur in the littoral zone, where shallow water allows light to penetrate to the bed of the water body. Macrophytes constitute a diverse assemblage of taxonomic groups and are

often separated into five categories (emergent, free floating, bottom rooted but with floating leaves, submerged and rafted or sprawling) based on their habit of growth (Coffey and Clayton, 1988). Free-floating macrophytes can occur anywhere on the system's surface where water currents allow (Fig. 2.1). In the context of this research, 'freshwater vegetation' refers to vegetation growing in the riparian zone or within the littoral zone of lakes and rivers.

2.4 Significance of image characteristics for freshwater remote sensing

Silva et al. (2008) suggest that freshwater vegetation types are more difficult to detect from RS when compared to terrestrial vegetation, and thus require thorough understanding of the physical interaction between electromagnetic energy, the vegetation and its environment. Previous studies (Malthus and George 1997; Peñuelas et al. 1993; Valta-Hulkkonen et al. 2003) have identified the following parameters that influence the ability to accurately map any freshwater vegetation, in particular submerged aquatic vegetation:

- Biophysical characteristics of the target habitat, which include biomass, canopy density and its physical form.

- Physical, chemical and environmental conditions of the surrounding matter (i.e. water and atmosphere) such as water clarity (which depends on the concentration of chlorophyll *a* and suspended sediments), height of the water column above vegetation and atmospheric condition (e.g. high concentration of the suspended aerosols such as water or dust due to humidity or other factors).

- Meteorological conditions at the time of image capture such as cloud, haze and solar azimuth.

- Sensor characteristics (e.g. spatial, spectral and radiometric resolutions, on-board data storage abilities and agility to manoeuvre for side-scan) and overpass schedules.

It is important to understand how the fundamental image parameters impact on the feasibility of freshwater vegetation mapping. There are numerous sensors currently on-board Earth Observation (EO) satellites and they vary in terms of spatial, spectral, radiometric and temporal resolutions. These parameters are explained in the following sections and are used to discuss the feasibility of using the different satellite images available. Table 2.1 summarises the optical sensors suitable for mapping freshwater environments.

2.4.1 Spatial resolution

Spatial resolution is often discussed and commonly refers to the Ground Sample Distance (GSD) of an image (i.e. how much of the earth's surface a single pixel covers). The larger the pixel, the poorer is its spatial resolution. Technological advances have enabled aerial based images to acquire up to 2 cm GSD (Booth et al., 2007); however, the highest spatial resolution of any commercially available orbital sensor is 41 cm from the GeoEye-1 satellite. Remotely sensed data with varied spatial resolutions are often referred to as low, moderate, high or very high depending upon the nature of the study. The following divisions of spatial resolutions in this chapter: (i) Very high spatial resolution (VHSR) data: below 1 m; (ii) High spatial resolution (HSR) data: 1 m to 10 m; and (iii) Moderate spatial resolution (MSR) data: 10 m to 100 m.

Spatial resolution is the most significant factor that influences the accuracy of freshwater vegetation classifications due to their limited width and their heterogeneous nature (Booth et al., 2007; Goetz, 2006; Ozesmi and Bauer, 2002). Traditionally, mapping vegetation over large areas was performed using either aerial photography or MSR satellite data. MSR satellite data (such as the early SPOT and Landsat images) have yielded degraded classifications compared to the HSR data (Congalton et al., 2002; Johansen and Phinn, 2006). Many studies have demonstrated the need for HSR to VHSR data for mapping different freshwater vegetation types (Becker et al., 2007; Lonard et al., 2000; Nagler et al., 2005; Weber and Dunno, 2001; Yang, 2007).

Table 2.1: Summary of significant medium- to high-resolution multispectral optical sensors suitable for mapping freshwater environments

Satellite(s) (Operator)	Launched on (dd-mm-yyyy)	Sensor(s)	Spectral Resolution		Spatial Resolution		Radiometric Resolution (bits)	Temporal Resolution[1] (days)	Data Supplier Data Cost[2] ($NZ/100 km^2)
			No. of bands & spectral distribution		Pixel size (m)	Swathe (km)			
Landsat-5[3]	01-03-1984	TM	1Blue, 1Green, 1Red,	7	30	185	8	16	USGS (Free)
Landsat-7 (USGS, USA)	15-04-1999	ETM+[4]	1NIR, 2SWIR	8	120/60				
			1TIR		15				
			1Panchromatic						
SPOT-2	22-01-1990	HRV	1P	4	10/10/2.5-5	60-117	8	3-26	Landcare Research, NZ ($SPOT2: 140) ($SPOT4: 245) ($SPOT5: 325)
SPOT-4	24-03-1998	HRVIR	1G, 1R, 1NIR	5	20/20/10				
SPOT-5 (SPOT Image, France)	04-05-2002	HRG	1SWIR[5]	5	20				
			1Panchromatic		5.8	70	6	5-24	
IRS-1D[6]	29-09-1997	PAN	1P	1	23.5/5.8	141/140		24/5-24	Geoscience Australia Antrix Co., India (LISS-III: 3.2) (AWiFS: 0.12)
IRS-P6 (ResourceSat-1)[7] (ISRO, India)	17-10-2003	LISS-III	1SWIR	4	70.5/23.5	148	7		
		LISS-IV	1G, 1R, 1NIR	3	23.5	24-70		5-24	
		AWiFS	1G, 1R, 1NIR, 1SWIR	4	56	370-740	10	2	
IKONOS-2	24-09-1999	Panchromatic	1P	1	1/0.41	11.3	11	5	Terralink Intl., NZ (IKONOS: ~1500) (GeoEye: ~2000)
GeoEye-1 (GeoEye, USA)	06-09-2008	Multispectral	1B, 1G, 1R, 1NIR	4	4/1.65	15.2		3	
Terra (EOS-AM) (NASA, USA)	15-12-1999	ASTER	1G, 1R, 1NIR	14	15	60	8	16	WIST, NASA Geoscience Australia (~5)
			6SWIR[8]		30		12		
			5TIR		90				
EO-1 (NASA, USA)	21-11-2000	ALI	1P	10	10	37	12	16	USGS (Free)
			2B, 1G, 1R, 3NIR, 2SWIR		30				
		Hyperion	220Hyperspectral	220	30	7.7			
QuickBird-2 (Digital Globe, USA)	18-10-2001	Panchromatic	1P	1	0.6/0.5	16.5	11	5	SKM Ltd., Australia GeoImage, Australia (~2000)
WorldView-2	08-10-2009	Multispectral	1B, 1G, 1R, 1NIR	4	2.4			1.1	
			2B, 1G, 1Y, 1R, 1RE, 2NIR	8	1.84	16.4			
PROBA-1 (ESA, EU)	22-10-2001	HRC	1Monochromatic	1	5	5	10	7	ESA, EU
		CHRIS[9]	19-62H	19-62	25-50	14	12		
AlSat-1 (Algeria) NigeriaSat-1/UK-DMC-1 Beijing-1 UK-DMC-2/Deimos-1 (DMCii, UK)	28-11-2002	CMT[10]	1P	1	4	24	8	5	Apogee, Australia DMCii, UK For 32m resolution data (>1 year old: 2.75 (<1 year old: 9.75)
	27-09-2003								
	27-10-2005								
	29-07-2009	SLIM6	1G, 1R, 1NIR	3	32/22[11]	660		1	
Formosat-2 or RoCSat-2 (NSPO, Taiwan)	20-04-2004	RSI	1P	5	2	24	8	1	Landcare Research, NZ (~1050)
			1B, 1G, 1R, 1NIR		8				
TopSat (QinetiQ, UK)	27-10-2005	RALCam	1P	4	2.9	17	10	6	Infoterra Ltd. (MS or PAN: ~1300)
			1B, 1G, 1R		5.7	12			
ALOS or Daichi (JAXA, Japan)	24-01-2006	AVNIR-2	1B, 1G, 1R, 1NIR	4	10	70	8	2-45	Geoscience Australia[12] (AVNIR: 12) (PRISM: 45)
		PRISM	1P	1	2.5	35-70	8		
Resurs-DK1 (Roscosmos, Russia)	15-06-2006	CCD	1P	4	1	28.3	10	6	Sovzond JSC, Russia (PAN: 1250) & (MS: 1550)
			1G, 1R, 1NIR		3				
KompSAT-2 or Arirang-2 (KARI, South Korea)	28-07-2006	MSC	1P	5	1	15	10	3	SPOT Image, France (~2100)
			1B, 1G, 1R, 1NIR		4				
RapidEye 1-5 (RapidEye AG, Germany)	29-08-2008	JSS-56	1B, 1G, 1R, 1RE, 1NIR	5	6.5	77	12	1	AAMHatch, Australia (~300)
THEOS (GISTDA, Thailand)	01-10-2008	PAN	1P	5	2	22	8	3-26	GISTDA, Thailand (PAN: 680;MS: 28)
		MS	1B, 1G, 1R, 1NIR		15	90			

[1] The temporal resolution is a theoretical representation of a sensor; it does not imply that sensors capture data in every single overpass

[2] Data cost is calculated for 100 km2 data from the full scene; it is mostly for radiometric corrected, archived, multispectral & panchromatic bundled, and single-user licensed data

[3] Landsat-5 is expected to continue until 2010

[4] The Scan Line Corrector (SLC) malfunctioned on 31 May 2003 that resulted in the onward acquisition of downgraded data

[5] SPOT-2 does not capture data in SWIR spectral range

[6] IRS-1D carries PAN and LISS-III sensors only

[7] IRS-P6 carries improved LISS-III, LISS-IV and AWiFS sensors; LISS-IV sensor captures data with 24 km swathe in multispectral mode or 70 km swathe for any single band (i.e. monochromatic mode)

[8] A malfunction in the SWIR detector cooler system has resulted in progressive deterioration and ultimately degraded data quality since May 2008

[9] CHRIS sensor captures data in 19 spectral bands at 25 m spatial resolution up to 62 bands at 50 m resolution

[10] Beijing-1 satellite carries an additional high resolution panchromatic sensor

[11] Recently launched UK-DMC-2 and Spain-Deimos-1 capture data at 22 m resolution

[12] Data cost is shown for the non-commercial use through Geoscience Australia; Landcare Research NZ also provides data for the commercial use

2.4.2 Spatial extent

Spatial extent is the area covered by an image. Often the spatial extent increases with decreasing spatial resolution. Aerial imaging with VHSR has restricted geographical coverage while most environmental monitoring satellites are designed to scan the earth with swathe generally ranging above 50 km. At the MSR, Landsat satellites are considered the widest swathe (185 km) for the last 35 years for vegetation mapping but a careful design has enabled Disaster Monitoring Constellation (DMC) satellites to capture data with much wider swathe (600 km) at similar or better spatial resolution than the Landsat TM sensor. Recently launched HSR to MSR sensors, such as HRG on SPOT-5 and LISS-III on ResourceSat-1, have considerably improved their spatial resolution as compared to their earlier sensor models without compromising their spatial extent. The latest MSR satellites have also focused on larger spatial extent such ALOS (70 km), Terra (60 km) and RapidEye (77 km) to ensure that the coverage of large regions remains cost effective. In contrast, high to very high spatial resolution satellites usually scan the Earth with swathe ranging between 10 to 15 km. Their limited spatial extent requires many images for mapping a large region, which adds to acquisition costs, seasonal inconsistency, and processing complexity.

2.4.3 Spectral resolution

Spectral resolution is a measure of the sensitivity of a sensor to record information across the electromagnetic spectrum. It is often defined as the number of spectral bands per image and their band widths. Remote sensors have three main types of spectral resolution: i) very broad spectral bands (i.e. panchromatic), ii) multiple discrete and broad spectral bands (i.e. multispectral) or iii) contiguous and very narrow spectral bands (i.e. hyperspectral). More bands mean that more data are collected, requiring more resources and time to process them. The spectral characteristics of freshwater vegetation resemble those of terrestrial vegetation; however, the interaction of light with water and the requirement to distinguish between submerged, emergent or floating plants

adds complexity. The spectral resolution thus critically influences what can be extracted from satellite images. The lower spectral resolution of SPOT HRV data as compared to Landsat TM has shown restricted accuracy for different aquatic habitats and vegetation types (Arbuckle et al., 1998; Gao, 1999; Harvey and Hill, 2001).

For sensing freshwater macrophytes, the green region of the spectrum is the most suitable followed by red and red-edge regions within the visible spectrum in tandem with near infrared (NIR) (Silva et al., 2008). The red-edge band lies in the region of an abrupt change (between 680-750 nm) of the reflectance spectra of vegetation that is caused by the combined effects of strong chlorophyll absorption and leaf internal scattering in healthy vegetation. Information recorded in this region provides the basis for vegetation identification procedures and is valuable for the assessment of vegetative chlorophyll status, leaf area index, early stress detection and detection of different submerged aquatic species (Artigas and Yang, 2006; Horler et al., 1983). Almost all multispectral EO satellites lack a band in the red-edge region with the exception of a recently launched constellation of five identical satellites (RapidEye 1-5) that carry red-edge enabled sensors to acquire 6.5 m HSR data. A successful launch of WorldView-2 satellite on 8 Oct 2009 now provides 1.84 m spatial resolution data in eight multispectral bands including a red-edge band.

In traditional multispectral data, differences among different floral species are not significantly recognisable due to relatively broad spectral band widths. Becker et al. (2007) suggest that band centres of commonly available high-resolution satellite systems are not optimal for differentiating wetland vegetation. Alternatively, narrow and contiguous hyper-spectral data provide information about the composition and physical properties of different materials observed in the freshwater system. Available hyper-spectral satellite sensors (e.g. Hyperion and CHRIS) are heavily compromised on either spatial resolution or spatial extent, and are therefore inappropriate for detailed large scale mapping.

Aerial spectrometry is not only costly but requires more resources and time to store and analyse collected data if captured over a large region at maximum spatial and spectral resolution. Becker et al. (2005) used two combinations of spectral and spatial settings; i.e. 1 m resolution imagery with 18 non-contiguous bands and 4 m resolution imagery with 46 contiguous bands. Their research verified that a minimum of seven, strategically located band centres (425.4 nm, 514.9 nm, 560.1 nm, 685.5 nm, 731.5 nm, 812.3 nm, and 916.7 nm) in the visible to NIR wavelength region is necessary to maintain classification accuracy above the 85% threshold. These seven bands generated a mildly degraded classification result compared to that obtained from full-spectral-resolution hyper-spectral imagery.

2.4.4 Radiometric resolution

Radiometric resolution refers to how precisely a sensor can measure intensity within a particular wavelength band. The radiometric resolution of an imaging system describes its ability to discriminate slight differences in electromagnetic radiation. The finer the radiometric resolution of a sensor, the more sensitive it is to detecting small differences in reflected or emitted energy. Traditionally, RS data are captured in 256 intensity levels (i.e. 8-bit), but new satellites offer greater resolution, usually up to 12-bit or 4096 intensity levels per band. These data cannot be completely visualised on computer screens; however, their higher radiometric resolution contributes mathematically to identifying subtle variations in the reflectance of different features and thus improves classification results.

Small rivers provide difficult conditions for mapping underwater vegetation, because of trees on the riverbanks overhanging and overshadowing the water surface to a large extent (Schulz et al., 2003), and low radiometric resolution data make it difficult to differentiate between SAV and shaded water surface due to bank vegetation. Large rivers like the Waikato River provide sufficient habitats for SAV that are un-obscured by bank vegetation or shadow. High radiometric resolution data provide a means to differentiate between SAV

and shaded water surfaces; alternatively, data should be acquired at dates close to summer solstice to minimize shadows (Sawaya et al., 2003).

2.4.5 Temporal resolution

Temporal resolution refers to the frequency of image acquisition for a given area, or the revisit period of a satellite to pass over the same area. EO sensors use circular, near-polar, sun-synchronous orbits where each orbit is phased out with the preceding one due to the Earth's rotation on its axis. Over a period of several days, these sensors perform a cycle of orbits of the Earth that returns them to their initial position and enable each area of the globe to be viewed. High temporal resolution becomes critical when an area is often cloudy, as several passes may be required before a cloud-free image is obtained.

The revisit period of an orbital sensor depends upon a variety of factors such as spatial extent (or swathe) of the sensor, its ability to capture off-nadir data, on-board data storage capability and the latitude of the target area. As most Earth observation satellites operate in near-polar sun-synchronous orbits, there is higher revisit frequency for the regions at higher latitudes. Satellite sensors with larger spatial extent also have higher temporal resolution. Broad swathe sensors such as MODIS and AVHRR have 1-3 days global repeat cycles. Medium swathe satellites like Landsat and SPOT revisit areas every 2-4 weeks and narrow swathe satellites of 10-20 km revisit every 3-6 months. To overcome their poor revisit capability, medium and narrow swathe satellites can swivel their sensors to capture off-nadir (side viewing) images. High-agility swivels enable the IKONOS-2 satellite to scan 4,700 km^2 of contiguous areas. The high agility coupled with large on-board data storage capacity on newly launched and future satellites i.e. 1 Terabyte for GeoEye-1 and 2199 Gigabyte for WorldView-2, enable them to scan 15,000 km^2 (i.e. 300 x 50 km) and 7,200 km^2 (i.e. 110 x 65.6 km) contiguous area (about the sizes of Hawke's Bay and Auckland regions), respectively, in a single pass.

The use of relatively inexpensive micro-satellites, weighing less than 100 kg, has provided an alternative to meet the needs for higher temporal resolution by means of launching an affordable constellation of EO satellites. A constellation of six DMC satellites launched over a time frame of seven years has a combined ability to capture the entire globe on a daily basis. The launch of five equally spaced RapidEye satellites over a single sun-synchronous orbit on 29 Aug 2008 has ensured a global daily revisit to acquire HSR (6.5 m) data. The launches of WorldView-2 and GeoEye-2 now supplement their existing networks and have substantially improved the rapid imaging capability for VHSR data.

Acquired digital SRS data requires further processing using specialised software to convert it into a thematic map. There are numerous computerised classification algorithms that have been used to map different aquatic habitats (Ozesmi and Bauer, 2002). However, it is generally difficult to say that one classification technique is always better than another since performance also depends on the SRS data (Schowengerdt, 2007).

2.5 Freshwater remote sensing of New Zealand

Remote sensing is not new to New Zealand; the first aerial surveys were flown over Christchurch in 1926, and the first SRS data for New Zealand became available in 1973 from Landsat-1 (Belliss, 1984; Stephens, 1991). The soil maps by the NZ Soil Bureau (1954, 1968) and Water and Soil Division (1979) were the earliest sources of information which identified the extent of wetland soils and modified and improved the mapped boundaries at scales 1:50,000 or smaller by using manual interpretation of remotely sensed imagery (Ward and Lambie, 1999). Other studies that show the effectiveness of SRS data for vegetation mapping at a local level in marine environments include Gao (1999), Gao et al. (2004) and Israel & Fyfe (1996). A low-cost aerial RS technique to map macro-algae in estuarine environments by Alexander (2008) has shown the utility of this approach for the study of freshwater systems. Within the riparian zone Arbuckle et al. (1999) used SPOT XS data to map riparian zone of the Taieri River. They reported a partial success due to the moderate spatial and low spectral nature of

data. There is no reporting of any remote sensing studies that have addressed emergent or submerged freshwater environments in New Zealand, the techniques used to process data have been established in other aqueous environments (Everitt et al., 2008; Wolter et al., 2005; Yuan and Zhang, 2008).

The Land Cover Database (LCDB) represents the first nationally comprehensive vegetation monitoring undertaken in New Zealand (Walker et al., 2006). The LCDB1 used 1996/97 SPOT-2 XS images, while the LCDB2 used 2001/02 Landsat-7 ETM+ images. However, they provide only a coarse assessment of indigenous habitats and ecosystems, due to the broad, qualitative nature of LCDB cover classes, the reliance on subjective manual distinction of spectral signatures, and resolution issues associated with the 1 ha minimum mapping unit (MMU) used (Thompson et al., 2003). Jensen et al. (1986) have reported a MMU of less than 0.5 ha for the classification and mapping of freshwater habitats which means that small freshwater environments have not been accurately mapped in case of LCDB.

While SRS offers certain advantages over conventional aerial photography (such as wider area coverage and increased spectral resolution), cloud cover has been a significant problem in New Zealand (Belliss, 1984). To capture cloud-free optical satellite images requires high temporal resolution, but such satellites are often associated with low spatial and limited spectral resolutions, e.g. geostationary, weather observation satellite sensors. Aerial photography is often seen as a good alternative in New Zealand because of the greater flexibility and availability to utilise the sensor when the sky is cloud free. However, aerial photography also has problems with weather, which has delayed the complete capture of aerial photography of the Waikato Region for three years under Waikato Region Aerial Photography Syndicate (WRAPS) initiative. SRS thus possesses certain advantages over aerial imaging for mapping freshwater environments over a large region.

Two national-level mapping initiatives are envisaged to ensure cloud-free data acquisition from moderate to high resolution satellites. These are the Land

Use and Carbon Analysis System (LUCAS) project and the 'All of Government' KiwImage initiative. The Ministry for the Environment (MfE) acquired 10 m resolution images of SPOT-5 satellite to analyse the carbon stocks of New Zealand's forest and soils, which is required for the country's reporting requirements under the Kyoto Protocol to the United Nations Framework Convention on Climate Change. Under the title of KiwImage, the New Zealand Defence Force (NZDF) is purchasing QuickBird-2 satellite data for the whole of New Zealand and its offshore islands. These images will be available to the participating central or local government agencies. Although per-scene area coverage of QuickBird-2 is far less than SPOT-5, its availability to regional councils and crown research institutes at a national scale provides a better prospect for detailed mapping of aquatic habitat due to its improved spatial resolution.

The KiwImage project may take 5 years or more to capture the whole of New Zealand, necessitating a mosaic to cover a region. Seasonal variability may compromise monitoring of macrophytes, which requires consistent reflectance for given vegetation classes. However, LUCAS SPOT-5 imagery acquired over two summers (2006/07 and 2007/08) can provide a baseline for freshwater environments.

2.6 Conclusions

The frequent launches of many experimental and low-cost microsatellites have made it difficult to determine exactly the number of satellites in orbit at any time. In 2008 alone, 11 new satellites carrying optical sensors were successfully added to an already long list of EO satellites. SRS has become viable as its spatial resolution and cost are competitive with aerial images. Table 2.1 attempts to provide a summary of significant medium- to high-resolution multispectral optical sensors suitable for the regional/national level mapping of freshwater vegetation. While there are many other EO satellites, many of these cannot be accessed easily as their operating agencies are either only interested in providing data for their own country or region, or they lack a user-friendly data search/retrieval mechanism for international clients. Most commercially

orientated satellite operators either offer online mechanisms of archived data search and its acquisition, or facilitate launching of new data acquisition requests directly into their systems.

The cost of SRS data is an important consideration for any large regional mapping project. In New Zealand, Landsat, SPOT-5 and QuickBird-2 are cost-effective for mapping large areas. Landsat data have been effectively provided free of charge by the U.S. government, while SPOT-5 and QuickBird-2 are being purchased effectively by New Zealand government organisations, and will be available free in the case of SPOT-5, or at a bulk purchase cost for QuickBird-2.

A combination of high spatial, spectral, radiometric and temporal resolution is required, as well as large spatial extents. With image capture, there is a trade-off between these parameters, and therefore no available image is ideal. QuickBird-2 multispectral data have advantages because of their HSR compared to Landsat TM/ETM+ and SPOT XS. The small spatial extent of QuickBird-2, and the fact that collecting regional coverage takes time, means that QuickBird-2 imagery under the KiwImage project will not be seasonally consistent. The recent additions of RapidEye1-5 and WorldView-2 satellites have widened options to choose suitable data to map freshwater habitats at a regional/national scale in New Zealand. They have higher spatial, and better spectral and radiometric data with more frequent revisit capabilities compared to SPOT-5, ALOS and TERRA, and IKONOS-2, QuickBird-2 and GeoEye-1, respectively. Considering the current availability of archived images and data characteristics, a good choice of sensor for mapping vegetation in New Zealand freshwater environments is QuickBird-2. This does not mean that other sensors will not provide better information in the future, but additional negotiations are required to ensure data capture.

This is a fruitful time for research in remote sensing and the development of applications such as freshwater vegetation mapping. The availability of satellite images has been improved dramatically not only because of advances in technology and the number of satellites that have been launched, but also

because New Zealand government organisations have invested millions of dollars in purchasing images of the country. It is imperative for geographers and natural resource managers to be aware of these developments, and also to understand the basic limitations and advantages of different satellite images.

Chapter 3

Image data fusion for the remote sensing of freshwater environments[2]

3.1 Abstract

Remote sensing based mapping of diverse and heterogeneous freshwater environments requires high resolution images. Data fusion is a useful technique for producing a high-resolution multispectral image from the merging of a high-resolution panchromatic image with a low-resolution multispectral image. Given the increasing availability of images from different satellite sensors that have different spectral and spatial resolutions, data fusion techniques that combine the strengths of different images will be increasingly important to Geography for land-cover mapping. Different data fusion methods however, add spectral and spatial distortions to the resultant data depending on the geographical context; therefore a careful selection of the fusion method is required. This chapter compares a technique called subtractive resolution merge, which has not previously been formally tested, with conventional techniques such as Brovey transformation, principal component substitution, local mean and variance matching, and optimised high pass filter addition. Data fusion techniques are grouped into spectral and spatial centric methods. Subtractive resolution merge belongs to a new class of data fusion techniques that uses a mix of both spatial and spectral centric approaches. The different data fusion techniques were applied to a QuickBird image of a semi-aquatic freshwater environment in New

[2] **Major contents of this chapter have been published as "Ashraf, S., Brabyn, L., Hicks, B. J., 2012. Image data fusion for the remote sensing of freshwater environments. Applied Geography 32(2): 619-628, DOI: 10.1016/j.apgeog.2011.07.010"**

Zealand. The results were compared both qualitatively and quantitatively using spectral and spatial error metrics. This research concludes that subtractive resolution merge performed better than all the other techniques and will be a valuable technique for enhancing images for freshwater land-cover mapping.

3.2 Introduction

The role of remote sensing has been pivotal for accurately mapping land cover and monitoring environmental changes in different habitats. This has been demonstrated by Melendez-Pastor et al. (2010) who used remote sensing to compare wetlands inside and outside a protected park using Landsat-5 TM and Landsat-7 ETM+. Remote sensing is often combined with standard Geographical data such as elevation to extract detailed features such as hedgerows (Tansey et al., 2009) and other agricultural features that are an important part of landscape character. In developing countries, remote sensing is particularly valuable because it is a cost effective mapping tool and these countries often have very few base maps (Shalaby and Tateishi, 2007). A common technique used in enhancing images for land cover mapping is to sharpen multispectral bands with panchromatic images. Mallinis et al. (2011) used such a technique prior to classifying land-cover/land-use changes in the Nestos Delta, Greece.

Remote sensing is rapidly advancing with the increasing availability of satellite images, and improved image enhancement and analysis techniques. Many remote sensors do not capture both high spatial and spectral images at the same time due to their technical limitations. Instead, dual images are often captured; one is a high (spatial) resolution panchromatic image (HRPI), which is good for identifying spatial details, and the other is a low (spatial) resolution multispectral image (LRMI), which is suitable for detecting features based on their spectral properties. Examples of these dual resolution satellites are; Landsat-7, SPOT 1-5, EO-1, IKONOS, QuickBird-2, WorldView-2, GeoEye-1 and FormoSat. There is considerable benefit from integrating HRPI and LRMI to produce a high-resolution multispectral image (HRMI) for further image analysis. This process is commonly labelled data fusion, pan sharpening, or resolution

merging (de Béthune et al., 1998a; Wang et al., 2005), and is a common image enhancement process used in many land-cover mapping applications (Fox III et al., 2002; Mallinis et al., 2011; Midwood and Chow-Fraser, 2010; Munechika et al., 1993).

The choice of data fusion technique is dependent on the application of the image analysis because the reflectance varies with different environmental features. In a freshwater environment there is a high reflectance of blue light compared to the infra-red. When there is a high amount of vegetation, the infra-red intensity is high compared to the blue light. These variabilities make it difficult to use data fusion techniques. In freshwater environments that have submerged and emergent vegetation, the choice of data fusion method becomes critical. This chapter therefore focuses on a freshwater environment to compare data fusion techniques. Freshwater environments are highly diverse, heterogeneous, and widely distributed due to the elongated and sinuous nature of water and land interaction zones. Access for ground surveys of freshwater environments are logistically difficult making remote sensing a preferred option. To map large scale freshwater environments, it is desirable to use images with a combination of high spatial, spectral, radiometric and temporal resolutions with large spatial extents (Ashraf et al., 2010).

A technique known as subtractive resolution merge (SRM) is a recent addition to existing data fusion algorithms that is in use by image processing software (ERDAS Imagine ver. 9.2). This chapter reviews this technique and quantifiably compares its performance with standard techniques, such as Brovey transformation (BT), principal component substitution (PCS), local mean and variance matching (LMVM), and optimised high pass filter addition (OHPFA). A QuickBird image representing a lacustrine habitat is used for this comparison.

Ideally, data fusion techniques add the spatial and spectral contents of both the HRPI and LRMI respectively to produce an enhanced HRMI; however, these techniques often focus on either one of these qualities and offer only one result (Chen et al., 2006). Different applications may require different balances

between spectral characteristic preservation and high spatial detail retention. For classification purposes it is important to preserve the spectral information whereas other applications (e.g., feature extraction and cartography) may only require a sharp and detailed display of the scene (Cetin and Musaoglu, 2009; Chen et al., 2006). SRM offers the user the control to adjust spectral and spatial retention to suit the purpose of the data fusion.

This chapter reviews the different data fusion techniques available, including a description of the SRM algorithm, which uses a technique to produce a synthetic panchromatic image from the LRMI. The different data fusion techniques are applied to a QuickBird image and the results are then downgraded to the original resolution and compared with the original LRMI using Pearson's correlation coefficient and Root Mean Squared Error (RMSE). A Sobel filter based RMSE is also used to compare the magnitudes of edges between the HRPI and the HRMI.

3.3 Overview of data fusion techniques

A comprehensive review of early data fusion methods can be found in (Pohl and Van Genderen, 1998; Yang et al., 2010). These methods can be divided into spatially-centric and spectrally-centric techniques. The spatially-centric techniques have more focus on the retention of the spatial content of an HRPI. Spectrally-centric techniques provide better spectral details for when distinction between classes is required.

Spatially-centric techniques use two different approaches: a simple intensity modulation (Liu, 2000; Schowengerdt, 1980) or a complex wavelet transformation based on multi-resolution decomposition (Garguet-Duport et al., 1996; Ranchin and Wald, 2000; Teggi et al., 2003; Yocky, 1996). An intensity modulation uses high-pass or low-pass kernels applied to the HRPI that help detect edge features. Common techniques within this category include the High Pass Filter Addition (HPFA) (Gangkofner et al., 2008), Smoothing Filter-based

Intensity Modulation (SFIM) (Liu, 2000), and Local Mean and Variance Matching (LMVM) (de Béthune et al., 1998a; de Béthune et al., 1998b).

Spectrally-centric techniques can be divided into three groups: (i) Projection and substitution models, (ii) Arithmetic models, and (iii) Synthetic variable ratio based models.

Projection and substitution models use statistical techniques and a range of transformations such as Intensity, Hue, Saturation (IHS) (Gillespie et al., 1986), Principal Component (PC) (Chavez Jr. et al., 1991), and Gram-Schmidt (GS) (Laben and Brower, 2000).

Arithmetic models operate at the individual pixel level to proportion spectral information to the resulting HRMI so that the bands can be assigned spectral brightness near to the HRPI. Such models include the Brovey Transformation (BT), Multiplicative Model, and Pixel Block Intensity Modulation (PBIM) (Cliche et al., 1985; Crippen, 1989; Gillespie et al., 1987; Liu and Moore, 1998).

Synthetic variable ratio (SVR) based procedures produce low resolution synthetic panchromatic images ($LRPI_{SYN}$) from LRMI by assigning different weights to the bands (Rahman and Csaplovics, 2007). A common practice for deriving such weights is through multivariate regression analysis as initially proposed by Munechika et al. (1993) and later modified by Zhang (1999). An HRMI is then produced from the $LRPI_{SYN}$ using arithmetic models.

There is now a new class of data fusion techniques that use a mix of both spatial and spectral centric approaches. These techniques include SRM (ERDAS, 2009), fast Fourier transformation (FFT)-enhanced Intensity Hue Saturation method (Ling et al., 2007), and wavelet integrated HIS method (Zhang and Hong, 2005). SRM is described in detail in a later section.

As this compares SRM with Brovey transformation (BT), principal component substitution (PCS), optimised high pass filter addition (OHPFA), and

local mean and variance matching (LMVM), each of these techniques are summarised below.

3.3.1 Brovey transformation (BT)

BT, as popularised by R. L. Brovey, is one of the most widely used methods and is relatively simple and efficient (Li et al., 2007). It has limitations because it uses only three bands, and also results in colour distortion (Dong et al., 2009). The BT was developed to visually increase contrast in the low and high ends of the image histogram and for producing visually appealing images (ERDAS, 2009). The formula for the BT is:

$$\mathbf{HRMI_n} = \frac{\mathbf{LRMI_n} \times \mathbf{HRPI}}{\mathbf{LRPI}} \quad \textbf{.....(3.1)}$$

where:

HRMI is a high resolution multispectral image – subscript n represents one of the three bands

LRMI is a low resolution multispectral image

HRPI is a high resolution panchromatic image

LRPI is a low resolution panchromatic image derived from the sum of any three LRMI bands.

3.3.2 Principal component substitution (PCS)

With principal component substitution (PCS), the LRMIs are transformed to the principal component (PC) images according to the eigenvectors of their corresponding covariance matrices. The first PC (PC1) image is replaced by the HRPI. Prior to its replacement, the HRPI is statistically adjusted to match with the PC1 through two commonly used methods – the min-max stretch method, and the mean and variance stretch method. The fused images are obtained by applying an inverse transformation on the new set of components (Cetin and Musaoglu, 2009; Chavez Jr. et al., 1991; Shettigara, 1992; Wang et al., 2005).

3.3.3 Optimised high pass filter addition (OHPFA)

Within the spatial centric method of data fusion, there are many variants that use filters to calculate edge features directly from an HRPI. Edges can be detected by convolving low pass filters (LPF) and high pass filters (HPF). An LPF is a focal mean, while an HPF is a weighted focal mean. Schowengerdt (1980) introduced a simple high pass filter addition (HPFA) method where edge features were obtained by applying an LPF to an HRPI, which is then subtracted from the HRPI and added to an LRMI on a pixel-by-pixel basis. An algorithm for the Schowengerdt's HPFA is:

$$\mathbf{HRMI_n} = \mathbf{LRMI_n} + (\mathbf{HRPI} - \mathbf{LPF} * \mathbf{HRPI}) \quad \textbf{.....(3.2)}$$

where:

n represents one of the n bands

LPF represents low-pass filter and

* represents convolution process

In a comparison with the PCS and IHS techniques, Chavez Jr. *et al*. (1991) have found that the HPFA technique improves the preservation of the spectral content of the original LRMI.

Gangkofner et al. (2008) have introduced and evaluated an optimised HPFA (OHPFA) algorithm that uses varying kernel sizes, central kernel mean weights, and a panchromatic contribution weight (also referred to as an injection weight), which allows the user to control the contribution of edges. The OHPFA is further optimised using a normalisation function (NF) which was first suggested by de Béthune et al. (1998a). The NF is required because panchromatic images do not usually break down to equal contributions from each multispectral band, therefore the edge values from the HRPI need to be normalised to the varying band intensities of the LRMI. The equation for the normalisation function is calculated from the whole image and is the standard deviation of the $LRMI_n$ divided by the standard deviation of the HRPI. The basic algorithm for the OHPFA is:

$$\mathbf{HRMI''_n = HRMI'_n + (HPF * HRPI) \times PCW \times NF_n} \quad \textbf{(3.3)}$$

where:

HRMI" is an intermediate HRMI through the fusion process

HRMI' is an up sampled LRMI using bilinear interpolation

HPF is a weighted focal mean convolution filter

PCW is a panchromatic contribution weight

NF is a normalising function

n represents one of the n bands

The HRMI" is stretched to match the mean and the variance of the LRMI by using the following formula:

$$\mathbf{HRMI_n = \frac{HRMI''_n - \mu HRMI''_n}{\sigma HRMI''_n} \times \sigma LRMI_n + \mu LRMI_n} \quad \textbf{(3.4)}$$

where:

n represents one of the n bands

μ is mean and σ is standard deviation of the corresponding LRMI and HRMI bands

Gangkofner et al. (2008) experimented with kernel size and found that when there is a larger spatial resolution ratio between the LRMI and HRPI, a larger HPF kernel size is required to capture the edge features. With a different kernel size, a different central kernel mean weight is required because the kernel sum varies with kernel sizes. A panchromatic contribution weight controls the intensity of these edges relative to the rest of the image.

As a general rule, the best kernel size is approximately twice the size of the LRMI and HRPI spatial resolution ratio (Chavez Jr. et al., 1991). Wang *et al*. (2005) have suggested a 3x3-kernel size when this ratio is 1:2 and 5 x 5-kernel size when the ratio is 1:4. Gangkofner et al. (2008) has suggested that the kernel size be twice the ratio plus one (to ensure it is an odd number). For QuickBird the ratio is 1:4; therefore a kernel size of 9 x 9 and a central weight of 80 is optimal. For this kernel size, a panchromatic contribution weight of 0.5 is optimal.

3.3.4 Local mean and variance matching (LMVM)

The LMVM was introduced by de Béthune et al. (1998a; 1998b) and is similar to the Schowengerdt's HPFA but the spectral distortions of the edges are reduced by applying a focal mean (LPF) to the LRMI and also including the normalisation function previously mentioned. The LMVM equation is:

$$\mathbf{HRMI_n} = (\mathbf{LPF} * \mathbf{LRMI_n}) + (\mathbf{HRPI} - \mathbf{LPF} * \mathbf{HRPI}) \times \mathbf{NF_n} \quad \textbf{.....(3.5)}$$

where:

NF is determined for pixels within the low-pass convolution window instead of using global statistics.

3.3.5 Subtractive resolution merge (SRM)

SRM is used by ERDAS Imagine software ver. 9.2 (ERDAS, 2009) but has not yet been reviewed and fully explained in the literature. SRM produces a low-resolution panchromatic synthetic image ($LRPI_{SYN}$) from the weighted sum of the LRMI bands. This $LRPI_{SYN}$ is then up-sampled to a high-resolution panchromatic synthetic image ($HRPI_{SYN}$) and then subtracted from HRPI (which is not synthetic) and this provides the edge details. The SRM also uses a mix of HPF and LPF to control spatial details. Spectral detail is maintained through the use of a normalisation function, and panchromatic contribution weights. ERDAS Imagine software offers panchromatic contribution weights ranging from 0.7 to 1.3 so that the user can choose a balance between spectral fidelity and spatial contrast.

The SRM data fusion method is summarised as a flow diagram in Figure 3.1 and the calculations are presented in the following equation as:

$$\mathbf{HRMI_n} = (\mathbf{LPF} * \mathbf{LRMI'_n}) + (\mathbf{HPF} * \mathbf{HRPI} - \mathbf{LPF} * \mathbf{HRPI_{SYN}}) \times \mathbf{PCW} \times \mathbf{NF_n} \quad \textbf{.....(3.6)}$$

Where:

LRMI'_n is a bilinear convolution up-sampled LRMI;

n represents one of the n bands;

LPF is a 5x5 kernel low-pass filter;

HPF is a 3x3 kernel high-pass filter using central weights of 11, 14, 17, 20 and 23 or 1000 if no high-pass filtering effect is required;

$HRPI_{SYN}$ is a bilinear convolution up-sampled $LRPI_{SYN}$;

PCW is a panchromatic contribution weight ranging from 0.7 to 1.3 with 0.1 increments. Its default value is 1.0;

NF is a normalising function $\left(\frac{\sigma \mathrm{LRMI}_n}{\sigma \mathrm{HRPI}}\right)$; and

σ represents standard deviation of the corresponding band of the LRMI

The essence of SRM is to calculate $HRPI_{SYN}$ as close as possible to HRPI to determine spatial edges. A fundamental assumption in the SRM algorithm is that the spectral radiance response of the HRPI overlaps with the LRMI (explained in section 4.3). The $LRPI_{SYN}$ is calculated from the weighted band sums (WBS) of the LRMI bands. The WBS is stretched to the same mean and variance of the HRPI to generate the $LRPI_{SYN}$ using the following equation.

$$\mathbf{LRPI_{SYN}} = \frac{\mathbf{WBS} - \boldsymbol{\mu}\mathbf{WBS}}{\boldsymbol{\sigma}\mathbf{WBS}} \times \boldsymbol{\sigma}\mathbf{HRPI} + \boldsymbol{\mu}\mathbf{HRPI} \quad \textbf{(3.7)}$$

where:

WBS is a weighted band sum of LRMI

μ is mean and σ is standard deviation

The band weights developed by ERDAS for the QuickBird sensor are 0.2, 0.7, 1.2, and 1.4 for blue, green, red, and near infra-red (NIR), respectively. These weights are calculated using a least absolute deviations (LAD) multiple linear regression and are sensor specific.

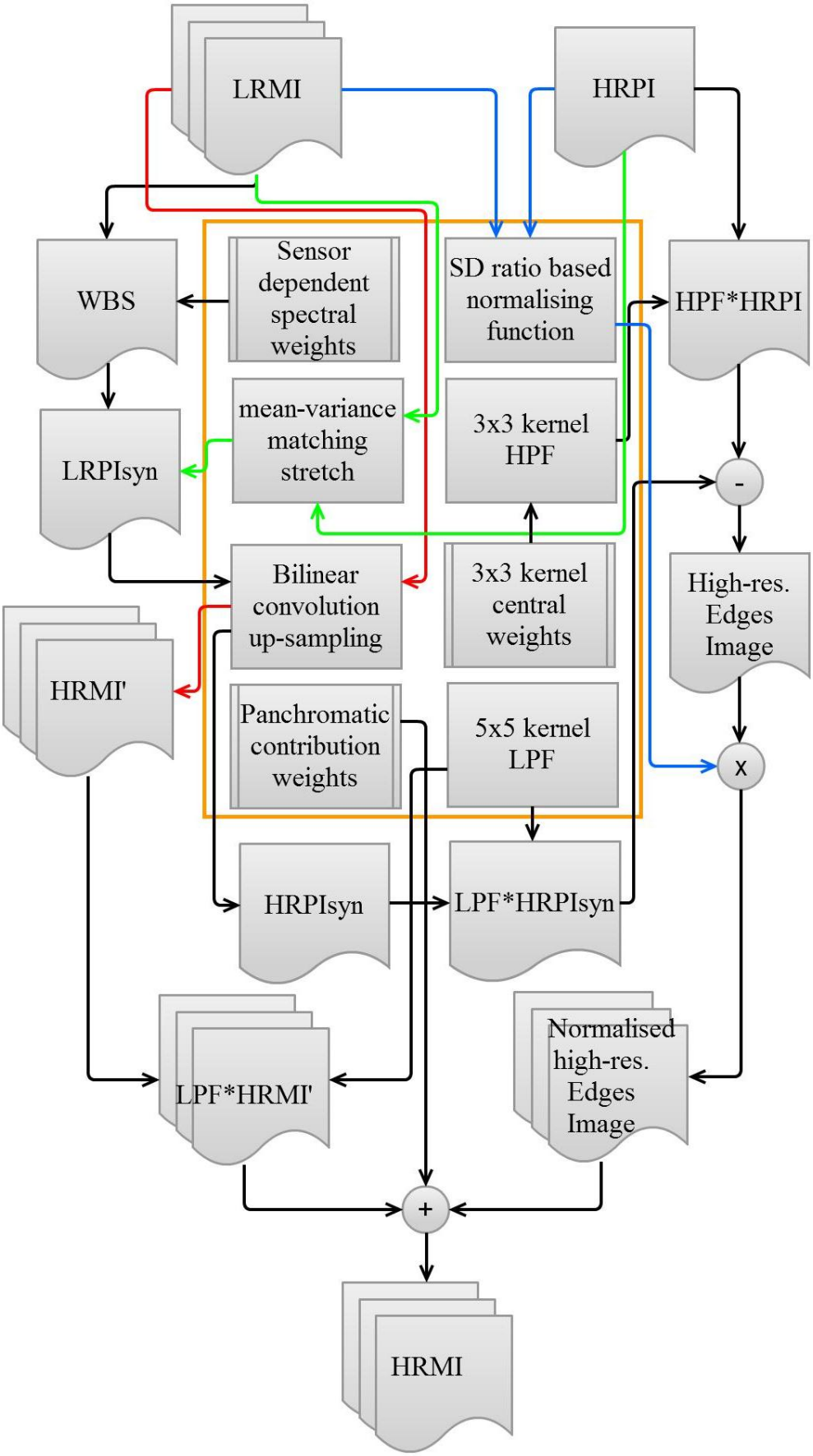

Figure 3.1: Flow diagram of SRM DF method

3.3.6 Refinement of parameters for data fusion techniques

For each data fusion technique, there are certain parameters that need to be defined. These parameter settings were each tested to determine the optimal settings. The BT resolution merge uses only three bands for data fusion thus provide inconsistency in the outcome depending upon the bands used for the process. We determined all four possible outcomes (i.e. bands 1, 2, 3; bands 1, 2, 4; bands 1, 3, 4; and bands 2, 3, 4) for the QB LRMI, which resulted in three possible images for each band. The results used the average of these three images. ERDAS Imagine software offers three re-sampling choices for BT and PCS; nearest neighbour (NN), bilinear (BL), and cubic convolution (CC). All three were experimented with and there was found to be very little variation. For BT and PCS, all calculations used NN re-sampling, as this is the simplest method. The other data fusion techniques have predefined re-sampling techniques.

For the PCS technique, two methods were experimented with to statistically adjust the HRPI with the PC1; the minimum-maximum stretch method, and the mean and variance method. The mean and variance method produced better quantitative results and these are presented in the final metrics. It should be noted that the OHPFA and SRM techniques also use the mean and variance stretch.

For the OHPFA, the default values were used, i.e. HPF kernel of 9 x 9 with central weight of 80 and injection weight of 0.5 to compare its performance with SRM and LMVM. For the LMVM method, different kernel sizes of LPF were used ranging from 5 x 5 to 13 x 13. The results showed that 5 x 5-kernel achieved lower spectral distortion and better correlation among MS bands but at the cost of high Sobel filter based edge RMSE between HRPI and HRMI. An increase in the kernel size reverses these results, thus fusion results for LMVM are shown for the mean kernel size, i.e. 9 x 9, which is the same used for the OHPFA method. For the SRM, all possible options of different centre values of the high-pass filter kernel were tested, however, the PCW was controlled (set to default 1.0) to avoid any spatial or spectral bias. The variation in the central value of the high-

pass filter kernel behaved as theoretically expected, i.e. lower values generate better contrast but at the expense of higher spectral distortion in the HRMI. For convenience, the SRM results are based on the default central HPF kernel weight, i.e. 17.

3.4 Data

The images used for comparing the data fusion techniques were a sub-scene consisting of 500 x 500 pixels of LRMI (figure 3.2*c*) and 2000 x 2000 pixels of HRPI (figure 3.2*d*) from the QuickBird satellite; captured on 22 March 2007. These images were geometrically projected to UTM zone 60S and have 2.4 m and 0.6 m resolution for the LRMI and HRPI, respectively. They are stored in 16-bit integer format. To appraise the performance of different fusion methods using pre-fusion degradation the LRMI and HRPI were degraded to 9.6 m and 2.4 m resolution using the pixel-block average (PBA) method. The $LRMI_{PBA}$ and $HRPI_{PBA}$ consist of 125 x 125 pixels (figure 3.2*e*) and 500 x 500 pixels (figure 3.2*f*) respectively. During analysis, all derived or degraded images were stored as 16-bit floating point.

These images display a typical habitat of emergent and submerged vegetation, which is located at the southern edge of the Lake Taupo and is part of the Tongariro River delta. The image contains approximately 50% water, which is located in the upper half of the image. The rest of the image is composed of herbaceous wetland vegetation dominated by raupo (*Typha orientalis*), rush (*Baumea rubiginosa*), and flax (*Phormium tenax*); scrub such as kanuka (*Kunzea ericoides*), manuka (*Leptospermum scoparium*), and grey willow (*Salix cinerea*); and emergent and submerged freshwater vegetation such as hornwort (*Ceratophyllum demersum*) and oxygen weed (*Lagrosiphon major*) (Cromarty and Scott, 1995; Eser, 1998). Structures such as roads, buildings and a boat marina are also visible.

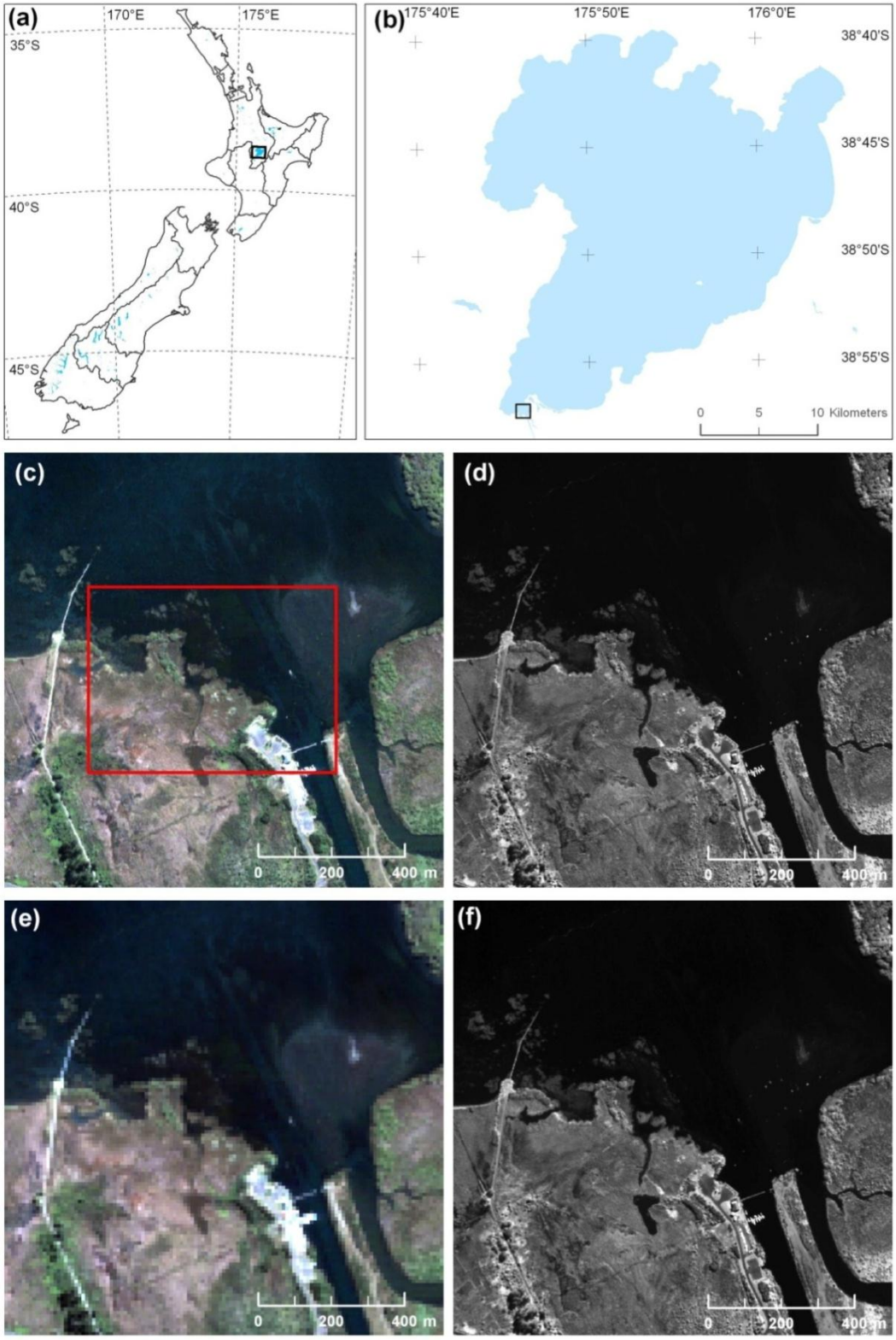

Figure 3.2: QuickBird images used for the evaluation of data fusion techniques; (a) Index map; (b) Location map of study area - Southern edge of the Lake Taupo, New Zealand; (c) Sub-scene of the true colour composite LRMI; (d) HRPI; (e) Degraded LRMI at 9.6 m resolution; and (f) Degraded HRPI at 2.4 m resolution. The square box in (c) is the extent of the zoomed in area shown in figures 3.3 & 3.5.

3.5 Method for evaluating data fusion techniques

The most common approach to compare data fused techniques is qualitative assessment by visual inspection; however, it is subjective and depends upon many factors including (i) displaying images at consistent scale, (ii) consistent data stretching, (iii) using same band combinations, and (iv) quality of graphic display. Quantitative comparisons provide a more objective assessment of both the spatial sharpening and retention of spectral fidelity, however to be effective, they require a valid reference image to compare against, which as explained later is problematic.

There are two approaches to the quantitative evaluation of data fusion techniques – a post-fusion degradation and a pre-fusion degradation. The post-fusion degradation approach first fuses the LRMI and HRPI to produce an HRMI and then degrades the HRMI to the same spatial resolution as the LRMI using pixel-block averaging. The degraded results are then quantitatively compared to the original LRMI (Li et al., 2010; Wald et al., 1997). This method is problematic because the purpose of data fusion is to improve the original LRMI, and therefore the resulting HRMI should be different to the LRMI. The alternative pre-fusion approach degrades the original LRMI and HRPI to lower resolutions prior to data fusion and then fuses back to the original resolution (Li et al., 2010; Wald et al., 1997). Pre-fusion is also problematic because the SRM technique uses band weights which are determined for the resolution of the original image, not for the degraded image. For this research the primary approach used was post-fusion degradation. There were two reasons for this. First, the objective was to improve the resolution of the original LRMI. The second reason was that with pre-fusion degradation, both the HRPI and LRMI are degraded, which increases the level of generalisation, while with post-fusion degradation only one image is degraded. However, for comparison a pre-fusion degradation approach was also used. There is no ideal reference image, therefore the results need to be carefully interpreted, and a mix of qualitative and quantitative techniques is required.

When using quantitative techniques, it is necessary to use both spectral and spatial metrics (Gangkofner et al., 2008). These tend to show opposite trends and reflect the trade-off between the spatial and spectral qualities of the fusion results. To measure spectral quality, Pearson's correlation coefficient and root-mean squared error (RMSE) are used. To measure spatial quality, the RMSE of Sobel filtered images are used.

Pearson's correlation coefficient is the most popular similarity metric in image fusion (Wang et al., 2005). It measures spectral similarity by determining the degree of linear relationship between the original LRMI and the fused HRMI, which is at same resolution as the LRMI after degradation. The problem with the correlation coefficient is its insensitivity to a constant gain and bias between two images.

The Root Mean Squared Error (RMSE) measures the standard error between the LRMI and the degraded HRMI (Gangkofner et al., 2008; Li et al., 2010; Pradhan et al., 2006). It is a more sensitive criterion than Pearson's correlation. Thus, if the correlation of the two image fusion algorithms is almost identical, the RMSE can better distinguish the degree of similarity between LRMI and degraded fused HRMI than can the correlation coefficient (Gangkofner et al., 2008). It can be calculated at a global level and a pixel level. The global RMSE value indicates how close both datasets match, however it does not provide any detail about which features have changed or the magnitude of these changes. Such changes can be assessed qualitatively if mapped at the pixel level.

The Sobel filter based RMSE is a quantitative method for comparing the absolute edge magnitude difference of the HRPI and the fused HRMI. It is also used to compare the edge magnitudes of the LRMI and degraded HRMI. The Sobel filter measures the gradient of edge intensities, using two 3 x 3-kernel Sobel filters, in horizontal and vertical directions. The Euclidian distance of these two horizontal and vertical edge intensities returns an edge magnitude. The equation for the Sobel filter edge magnitude is:

$$\mathrm{M} = \sqrt{\mathbf{M_x^2} + \mathbf{M_y^2}} \quad \textbf{(3.8)}$$

where:

$$\mathrm{M_x} = \begin{bmatrix} -1 & 0 & +1 \\ -2 & 0 & +2 \\ -1 & 0 & +1 \end{bmatrix} * \text{Image and}$$

$$\mathrm{M_y} = \begin{bmatrix} -1 & -2 & -1 \\ 0 & 0 & 0 \\ +1 & +2 & +1 \end{bmatrix} * \text{Image}$$

3.6 Results and discussion

Figure 3.3 provides a qualitative assessment of the five data fusion techniques for a zoomed in area of the original LRMI. All images in figure 3.3 are displayed using the same colour lookup values and are stretched by three standard deviations. The OHPFA and SRM techniques appear similar in quality and stand out as being significantly sharper and more colour balanced than the other three techniques. The quality of the OHPFA supports similar findings by Gangkofner et al. (2008) and is expected since it is a modern and well-researched technique. The BT and PCS techniques show significant colour distortion, however the BT does have improved spatial detail. The LMVM appears very similar to the original LRMI in both spatial and spectral detail, and therefore shows insignificant improvement.

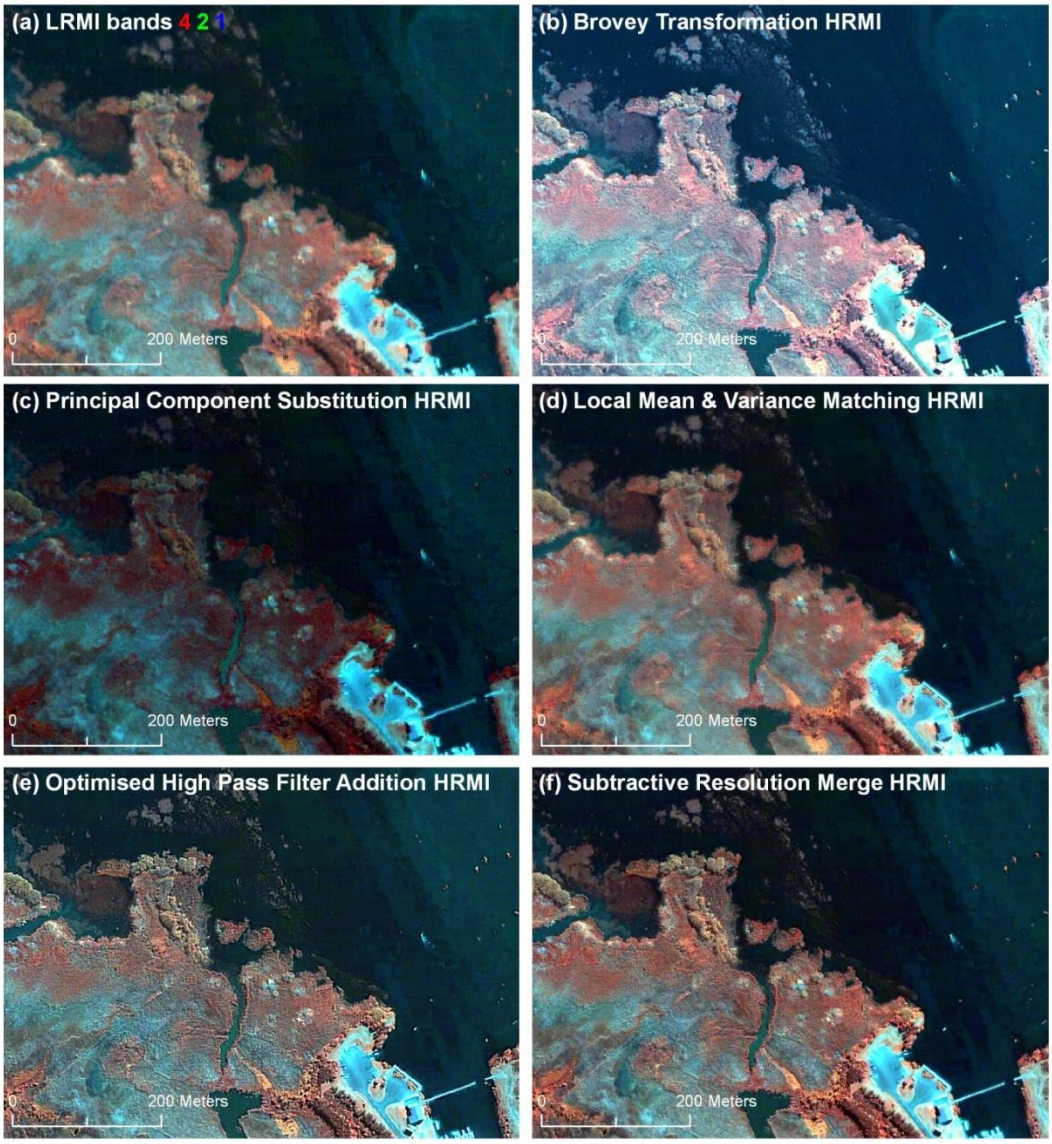

Figure 3.3: A representative portion of the original and fused QuickBird images; (a) False colour composite of LRMI bands 4, 2, 1 shown as R, G, B; (b) fused image from the Brovey transformation; (c) fused image from the principal component substitution method; (d) fused image from the local mean and variance matching method; (e) fused image from the optimised high-pass filter addition method; and (f) subtractive resolution method.

Figure 3.4 summarises the results from the quantitative evaluation metrics using the post-fusion degradation approach and shows a different result. The LMVM is the closest to the original LRMI overall. This is to be expected given that the qualitative assessment showed the two images are similar and that there were no significant improvements. The BT has the least overall spatial distortion but performs badly on the spectral preservation. The PCS performs similar to the LMVM in retaining spatial detail but has a significant visual spectral distortion as confirmed in figure 3.3*c*. The quantitative assessment is important

for comparing SRM with OHPFA, as these techniques visually enhanced the original LRMI both spectrally and spatially, as shown in figure 3.3*e* and 3.3*f*. The summary metrics show that the SRM enhancement distorts the image less than the OHPFA technique for all four metrics.

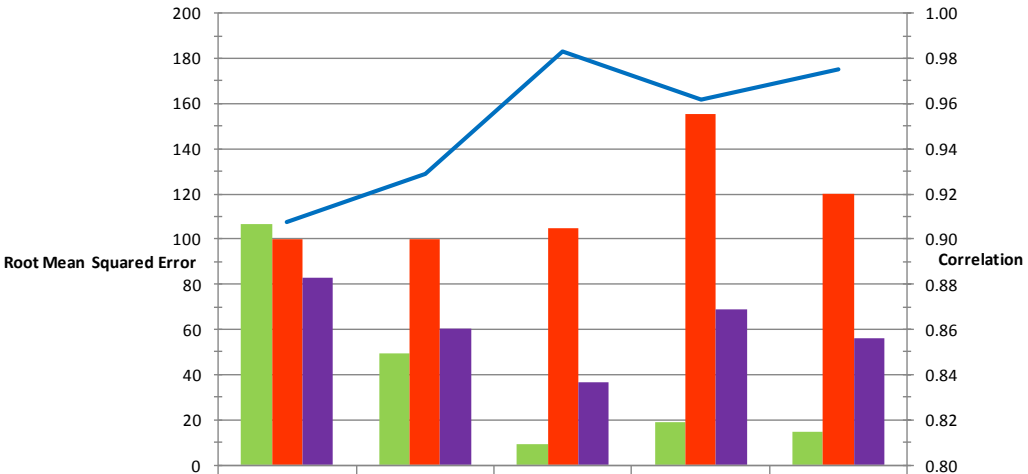

	BT	PCS	LMVM	OHPFA	SRM
Spectral RMSE	106.74	49.47	9.45	18.72	14.46
Sobel Filter RMSE-I	99.71	100.12	104.76	155.44	120.13
Sobel Filter RMSE-II	82.85	60.57	36.53	69.00	55.83
Correlation	0.907	0.929	0.983	0.962	0.975

Figure 3.4: Average correlation and RSME metrics for the different data fusion techniques using the post-fusion degradation approach.

Table 3.1 shows the quantitative assessment for each band. When SRM is compared with OHPFA at the individual band level, SRM is closest to the original LRMI for all bands, both spectrally and spatially, except the blue Sobel RMSE. There are two anomalies shown in table 3.1. Firstly the spectral correlations for all bands and techniques are 90 % or better except for the blue band of the BT technique. The second anomaly is the Sobel RMSE for the NIR band has a high range of values for the different techniques. The PCS technique is significantly low (27.21) and the OHPFA and SRM have high values (360.46 and 232.47, respectively).

Table 3.1: Evaluation of spectral and spatial metrics using post-fusion degradation for a QuickBird satellite image

Data Fusion Techniques	Spectral measure between LRMI and degraded HRMI bands								Spatial measure between HRMI & HRPI and LRMI and degraded HRMI bands							
	Correlation				Spectral RMSE				Sobel Filter RMSE-I (between HRMI & HRPI)				Sobel Filter RMSE-II (between LRMI & degraded HRMI)			
	Blue	Green	Red	NIR	Blue	Green	Red	NIR	Blue	Green	Red	NIR	Blue	Green	Red	NIR
BT	0.778	0.903	0.958	0.990	93.89	111.85	57.72	163.48	111.28	99.42	117.96	70.18	33.29	56.47	48.86	192.79
PCS	0.929	0.902	0.903	0.981	9.28	24.81	25.82	137.98	133.73	119.82	119.73	**27.21**	**9.51**	**26.86**	26.04	179.86
LMVM	0.969	**0.982**	**0.988**	**0.994**	4.23	**7.37**	**6.27**	**19.93**	127.09	106.73	112.71	72.52	16.45	29.02	**25.17**	**75.49**
OHPFA	0.962	0.962	0.961	0.962	4.73	10.52	11.25	48.38	**108.86**	76.59	75.86	360.46	16.98	37.73	41.32	179.96
SRM	**0.970**	0.975	0.976	0.979	**4.19**	8.62	8.87	36.16	112.14	**68.89**	**67.02**	232.47	15.99	32.75	34.26	140.06

N.B. Best results are shown as bold values

The low blue band correlation for the BT and the low NIR Sobel RMSE value for the PCS methods are due to the spectral centric nature of data fusion. Spectral centric fusion methods determine weighted band sum (WBS) images using band weights for the LRMI bands and their difference with the HRPI returns edge detail images. The values of their band weights and their correlation with the degraded HRPI are shown in the Table 3.2. For the PCS, 70 % of NIR band is contributing to the PC1, which is then replaced with the HRPI during the substitution process. The NIR band is over represented for the PCS method and the RMSE for the NIR band between HRMI and HRPI is therefore low. For the BT, there is always equal representation (33 %) for the participating three bands in the data fusion process. For the QuickBird image used in this research, which has a combination of vegetation and water, the average of all possible combinations of BT was 33 % for the blue band and 22 % each for the other three bands. The blue band has high reflectance for water and low reflectance for vegetation, while the other three bands behave in reverse to this trend. This reverse trend caused by the other bands generates low blue band correlation.

SRM and OHPFA have high RMSE values for the NIR band, both spectrally and spatially, compared to the other bands. The underlying cause of this problem is because, in a freshwater environment, the standard deviation of the NIR band will be higher than the HRPI's standard deviation. Under such conditions, the normalisation function that is used will always have an over representation of edge features for the NIR band, which causes undesired spectral and spatial distortion. The inclusion of Panchromatic Contribution Weight (PCW) in SRM and OHPFA techniques aims to address this issue; however, our experimentation with varying PCW values identified it as counterproductive to the visible bands. A lower PCW values resulted in higher spatial edge RMSE in the visible bands whereas RMSE for the NIR band, both spectrally and spatially, was not reduced significantly.

Table 3.2: Band weights and the correlation between the weighted band sum images and degraded HRPI for the different spectral centric techniques

Data Fusion Techniques (band weight calculation approach)	Blue	Green	Red	NIR	Correlation between WBS and the degraded HRPI
PCS (Eigen values for PC1)	0.063	0.172	0.179	0.967	**0.977**
BT (linear weights)	1.0	1.0	1.0	1.0	**0.978**
SRM (LAD regression coefficients)	0.2	0.7	1.2	1.4	**0.982**
LMVM & OHPFA (9x9 LPF)	-	-	-	-	**0.969**[1]

[1] In absence of band weights for the spatial centric LMVM and OHPFA techniques, a correlation is directly derived between the HRPI and low-pass filter applied HRPI

The NIR band is important for mapping terrestrial and freshwater vegetation; therefore the effects of data fusion on this band require careful assessment. Figure 3.5 shows the NIR RMSE map for the five different data fusion techniques. BT and PCS have higher NIR RMSE for most of the vegetation types (see figures 3.5*a* and 3.5*b*). The LMVM has the lowest overall error (figure 3.5*c*) and the major errors are located around high contrast features, such as infrastructure. However, as shown in figure 3.3*d*, the LMVM does not provide spatial enhancement unlike OHPFA and SRM. The SRM has less overall RMSE than the OHPFA (figures 3.5*d* and 3.5*e* show that this difference is explained mostly by the representation of water, where OHPFA has more RMSE). Water is often perceived as being homogenous, however in this study area, the water is shallow and freshwater vegetation is visible therefore making the water heterogeneous.

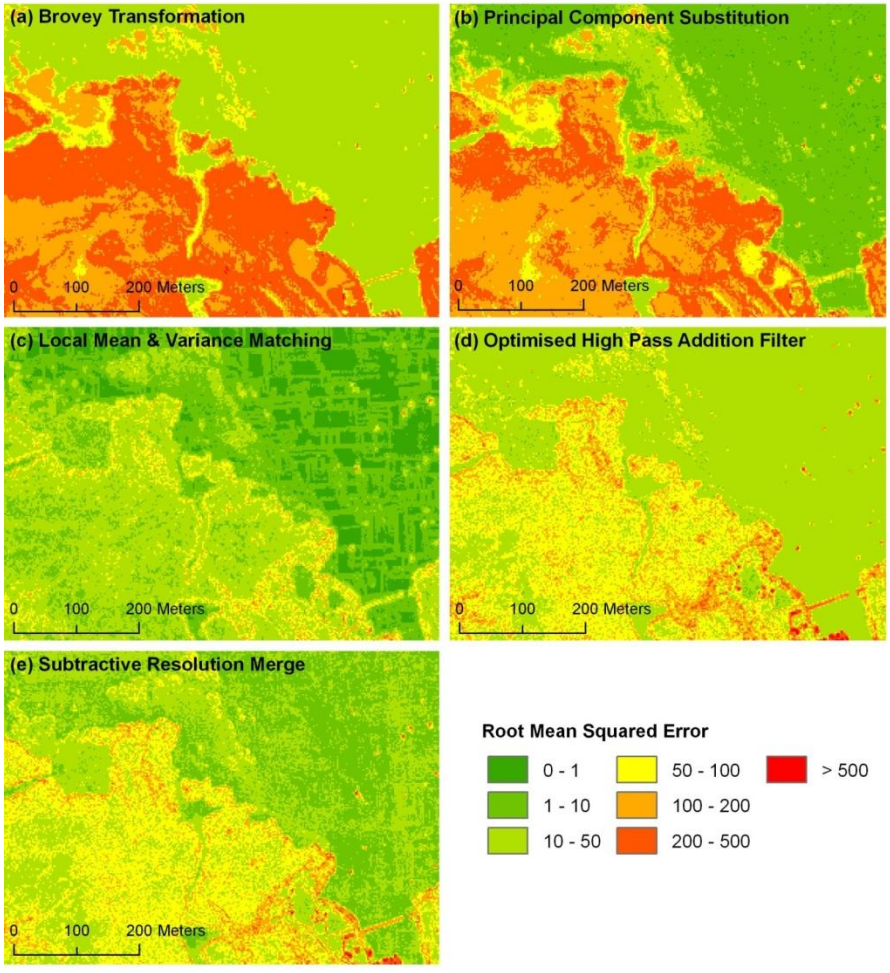

Figure 3.5: Spectral RMSE map showing the error values for each pixel of band 4 (NIR) of QB image; (a) BT; (b) PCS; (c) LMVM; (d) OHPFA; and (e) SRM.

Figure 3.6 shows the summary metrics that are obtained when the evaluation is based on the pre-fusion degradation. The results show differences in quantitative values but the evaluation of data fusion techniques does not change. SRM is still closer to the reference image than the OHPFA for all the spectral and spatial metrics. The RMSE values are higher for the pre-fusion degradation process and because there is more degradation (generalisation) of the images associated with pre-fusion degradation, i.e. both LRMI and HRPI are degraded. This additional generalisation could produce higher or lower values and it is by chance that they are higher. The performance of SRM relative to LMVM does decrease slightly for the blue spectrum for the spectral similarity and spectral difference metrics when using pre-fusion degradation because, with pre-fusion degradation, the band weights required for SRM are calibrated to the original LRMI, not for the degraded LRMI.

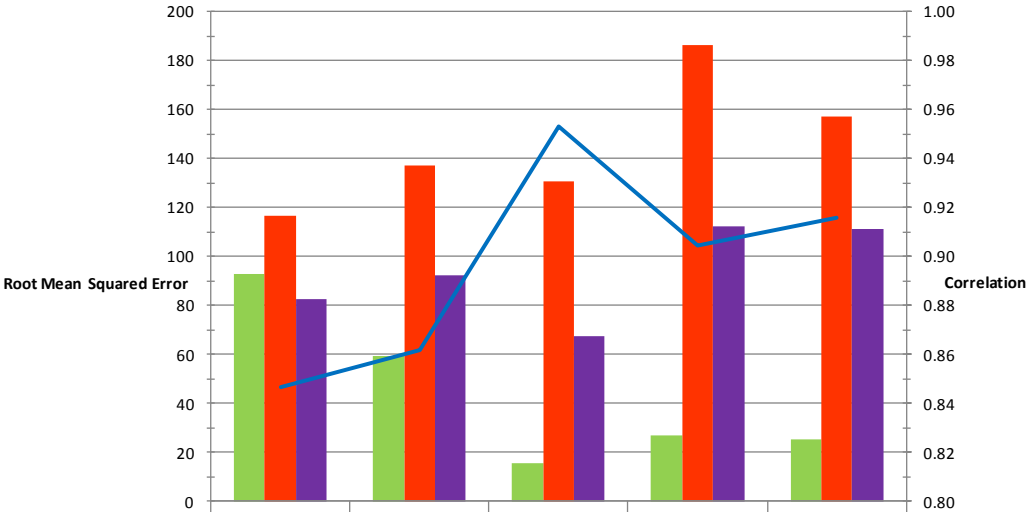

	BT	PCS	LMVM	OHPFA	SRM
Spectral RMSE	92.64	59.22	15.34	26.69	25.14
Sobel Filter RMSE-I	116.70	137.33	130.49	186.12	157.20
Sobel Filter RMSE-II	82.46	92.15	67.34	112.08	111.27
Correlation	0.847	0.862	0.953	0.905	0.916

Figure 3.6: Average correlation and RSME metrics for each data fusion techniques using the pre-fusion degradation approach.

Table 3.3 evaluates the spectral and spatial metrics for each band for pre-fusion degradation images. This underscores the good performance of SRM when compared with OHPFA at the individual band level.

Table 3.3: Evaluation of spectral and spatial metrics using pre-fusion degradation for a QuickBird satellite image

Data Fusion Techniques	Spectral measure between $HRMI_{PBA}$ and LRMI bands								Spatial measure between $HRMI_{PBA}$ & $HRPI_{PBA}$ and $HRMI_{PBA}$ & LRMI							
	Correlation				Spectral RMSE				Sobel Filter RMSE-I (between $HRMI_{PBA}$ & $HRPI_{PBA}$)				Sobel Filter RMSE-II (between $HRMI_{PBA}$ & LRMI)			
	Blue	Green	Red	NIR	Blue	Green	Red	NIR	Blue	Green	Red	NIR	Blue	Green	Red	NIR
BT	0.679	0.842	0.903	0.963	91.02	104.98	53.71	120.85	126.51	105.34	138.66	96.28	47.30	62.31	52.26	167.95
PCS	0.819	0.817	0.832	0.980	12.61	30.93	31.87	161.45	170.50	155.65	154.78	**68.39**	35.66	65.55	55.53	211.86
LMVM	**0.916**	**0.950**	**0.962**	**0.984**	**6.90**	**12.02**	**11.13**	**31.31**	161.57	134.31	137.95	88.11	**29.60**	**53.08**	**46.71**	**139.98**
OHPFA	0.872	0.905	0.911	0.931	8.47	16.45	16.85	65.01	151.09	118.93	117.43	357.05	36.46	68.51	72.28	271.05
SRM	0.884	0.918	0.917	0.946	8.18	15.63	16.79	59.96	**140.61**	**83.86**	**78.93**	325.39	35.99	67.17	73.56	268.37

N.B. Best results are shown as bold values

3.7 Conclusions and future research

This research has classified data fusion techniques into spectral centric, spatial centric, and a mix of both, depending on how edge features are calculated. SRM is a mixed technique and the results show that it is an improvement over BT, PCS, LMVM, and OHPFA, for QB data and a semi-aquatic environment.

The SRM produced a visually similar result to the OHPFA technique but the quantitative metrics suggests that the SRM is an improvement. A reason for this improvement is that the SRM uses a small kernel for both the high-pass (5 x 5) and low-pass filters (3 x 3), while the OHPFA uses a 9 x 9-kernel size for just a high-pass filter.

The more significant feature of SRM is that it combines the advantages of spectral and spatial centric fusion techniques. Its uses intensity modulation functions, which are spatial centric fusion methods, and synthetic variable ratio, which is a spectral centric technique. It also enables users to fine-tune the mix of spectral and spatial parameters to produce a result that suits the purpose of data fusion.

This research has identified Sobel filter RMS errors ranging from 30 to 360. These digital numbers cannot be compared with similar research, such as Gangkofner et al. (2008), which has a range of Sobel filter RMS errors from 2 to 18. Their research used Landsat 7 images that have a radiometric resolution of 8 bits, while the QuickBird image has a radiometric resolution of 11 bit. In theory, maximum values between Landsat-7 and QuickBird are 256 and 2,048 respectively.

A challenge for data fusion is to fuse images from different sensor platforms that do not capture dual multispectral and panchromatic images, such as RapidEye, Terra ASTER, or aerial sensors. Now that SRM has been shown to be a superior approach, the technique needs to be modified to address data fusion

across sensors. This may involve adjustments to kernel sizes and mean weights, and the up-sampling approach used for the synthetic HRPI.

Another avenue for future research is to address the issue of normalisation between the visible and NIR bands. As demonstrated in the results, the visible bands' values have a lower standard deviation in a freshwater environment compared to the NIR band values. The NIR values become over represented producing an error. Given that the NIR band is important for vegetation mapping, this issue needs to be addressed.

Quantitative techniques for comparing image enhancements need improvement, particularly with spatial details. Any improved multispectral image when compared to the original LRMI will have difference, otherwise there is no improvement. A valid HRMI reference is required for comparison, which is not possible unless there is a similar sensor with higher resolution. With this research, quantitative metrics did not agree with the visual comparison. The quantitative metrics were only useful for comparing the techniques that clearly showed visual improvement, which in this case were the OHPFA and SRM. Identifying what defines the best compromise between spectral RMSE and Sobel RMSE is an additional problem. There will always be a trade-off between these errors and the best compromise will be specific to the end use.

The use of data fusion for enhancing LRMI from HRPI is important for maximising the information that can be obtained from remote sensing. Many image processing software packages provide data fusion tools, and it is important that these techniques are well understood and their performances compared. The enhancement and robust comparison of data fusion techniques will ultimately lead to improved image analysis and land-cover mapping.

Chapter 4

Alternative solutions for determining the spectral band weights for the SRM technique[3]

4.1 Abstract

Data fusion using subtractive resolution merge (SRM) is limited because it currently requires fixed spectral band weights predetermined for particular sensors. This is problematic because there is an increasing availability of new and emerging sensors that have no predetermined band weights. There is also a need for fusion across sensors, which potentially requires a large number of sensor combinations and band weight calculations. This demonstrates how least sum of minimum absolute deviation (LAD) and ordinary least squares (OLS) regressions can calculate band weights for application in the SRM technique using QuickBird satellite and Vexcel aerial images. Both methods were effective in improving image details. The results of LAD and OLS are shown using qualitative and quantitative metrics and through unsupervised classification of freshwater habitat. OLS and LAD produce similar results; however, OLS is computationally simpler and easier to automate. The ability of the user to calculate their own scene specific band weights eliminates the dependence on predetermined sensor band weights. This research concludes that OLS band weight calculations should be integrated into the SRM technique to diversify its application.

[3] **Major contents of this chapter have been published as "Ashraf, S., Brabyn, L., Hicks, B.J., 2011. Alternative solutions for determining the spectral band weights for the subtractive resolution merge technique. International Journal of Image and Data Fusion, DOI: 10.1080/19479832.2011.607473"**

4.2 Introduction

Increasingly, new satellites with dual resolutions capabilities are available, which include Landsat 7, SPOT 1-5, EO-1, IKONOS, QuickBird, WorldView-2, GeoEye-1, FormoSat and DubaiSat. Such sensors capture simultaneously a high (spatial) resolution panchromatic image (HRPI), which is good for identifying spatial details, and a low (spatial) resolution multispectral image (LRMI), which is pertinent for the spectral classification of features. Spatial resolution is the most significant factor that influences the accuracy of freshwater vegetation classifications because of their limited width and their heterogeneous nature (Booth et al., 2007; Goetz, 2006; Ozesmi and Bauer, 2002). Data fusion (DF) techniques aim to integrate HRPI and LRMI to produce a high (spatial) resolution multispectral image (HRMI) for further analysis. Many earlier techniques produce one possible HRMI; however, different applications, according to their purpose of data fusion, require a focus either on the spectral information from the LRMI or on the spatial details from the HRPI (Chen et al., 2006). Contemporary data fusion methods use sophisticated algorithms to balance these characteristics to ensure the best integration of spectral and spatial qualities of the input data (Boloorani et al., 2005). Different applications may require different balances between spectral characteristic preservation and high spatial detail retention. For classification purposes it is important to preserve the spectral information, whereas other applications (e.g. feature extraction and cartography) may only require a sharp and detailed display of the scene (Cetin and Musaoglu, 2009; Chen et al., 2006).

Subtractive resolution merge is a contemporary DF technique, which offers users the control to adjust spectral and spatial retention to suit their purpose of the data fusion. SRM is in use by image processing software ERDAS Imagine ver. 9.2 and targets specific dual-resolution sensors using predefined spectral band weights. SRM has been demonstrated to outperform conventional fusion methods, such as Brovey transformation, principal component substitution, local mean and variance matching, and optimised high pass filter

addition (Ashraf et al., 2012). This reason for the high performance of SRM is because it uses robust statistical approach to determine band weights, while most conventional techniques use a generalised mathematical method.

This chapter explores how SRM based spectral band weights can be determined using least absolute deviations (LAD) regression. LAD regression is a robust method that uses an iterative process to optimise the least absolute deviation between LRPI and the weighted sum of the LRMI bands. The limitation is the intensive computation required for the iterations. The emergence of new dual resolution sensors stresses the need of simpler calculations to determine band weights for data fusion. An ordinary least squares (OLS) regression estimators is also demonstrated in this as a comparison with LAD.

A current limitation of SRM is the reliance on predetermined band weights provided by ERDAS Inc. which is currently limited to three sensors: QuickBird, IKONOS and FormoSat. These weights are calculated using LAD regression. The process of calculating band weights in the SRM technique is explained in the following section. The purpose of this research is to diversify the scope of the SRM technique beyond its current limitation to fuse data of dual resolution sensors with known band weights. QuickBird and Vexcel aerial sub images, representing lacustrine and riverine freshwater habitats respectively, are used to demonstrate LAD and OLS band weight calculations for use in SRM.

The results are compared using visual qualitative assessments and a range of spectral and spatial quantitative metrics, which include spectral correlation and root mean squared error (RMSE), Sobel filter based spatial edges RMSE, and unsupervised classification.

4.3 Overview of spectral band weights calculations

Spectrally centric data fusion methods derive a synthetic LRPI ($LRPI_{SYN}$) from the multispectral bands (LRMI), either indirectly or directly. With most satellite images, not every band will contribute equally to a panchromatic image. Some simple data fusion techniques, such as Brovey Transformation and its

modification (Li et al., 2007), assume each band does contribute equal weight and this causes serious over and under representation of certain bands. Figure 4.1 shows the spectral radiance response for the Quickbird and Vexcel sensors. For the Quickbird, the NIR band makes a significant contribution to the panchromatic curve, while for the Vexcel sensor the NIR is insignificant. The calculation of band weights is therefore important for deriving a $LRPI_{SYN}$ from a LRMI.

There is a range of techniques for calculating band weights. Projection and substitution models use indirect mathematical algorithms to first project the LRMI into a new colour space. One of the projected bands is then substituted with the statistically adjusted HRPI. An inverse projection returns the HRMI. Commonly used techniques under this category include Intensity, Hue, Saturation (IHS) (Gillespie et al., 1986), Principal Component Substitution (PCS) (Chavez Jr. et al., 1991), Gram-Schmidt (GS) (Laben and Brower, 2000), and a recently introduced hyper-spherical colour sharpening (HCS) (Padwick et al., 2010). Arithmetic models also indirectly calculate band weights and operate at the individual pixel level to proportion spectral information to the resulting HRMI so that the bands can be assigned spectral brightness near to the HRPI. Such models include the Brovey Transformation (BT) (Gillespie et al., 1987), Multiplicative Model (Crippen, 1989), and Intensity Modulation (IM) (Cliche et al., 1985).

Alternatively, band weights can be directly calculated, which are either sensor-specific or image-specific. Sensor-specific weights are predetermined by remote sensing software companies, while image-specific band weights are calculated by the user prior to data fusion, which requires additional computation. Some synthetic variable ratio (SVR) models calculate band weights directly while others such as SRM use predetermined sensor specific weights. These weights produce a $LRPI_{SYN}$ from the LRMI (Rahman and Csaplovics, 2007). There are two methods for calculating band weights, an a linear method that assumes spectral radiance responses such as developed by Wang et al. (2008) or

Svab and Ostir (2006) and multiple linear regression analysis as initially proposed by Munechika et al. (1993) and later modified by Zhang (1999).

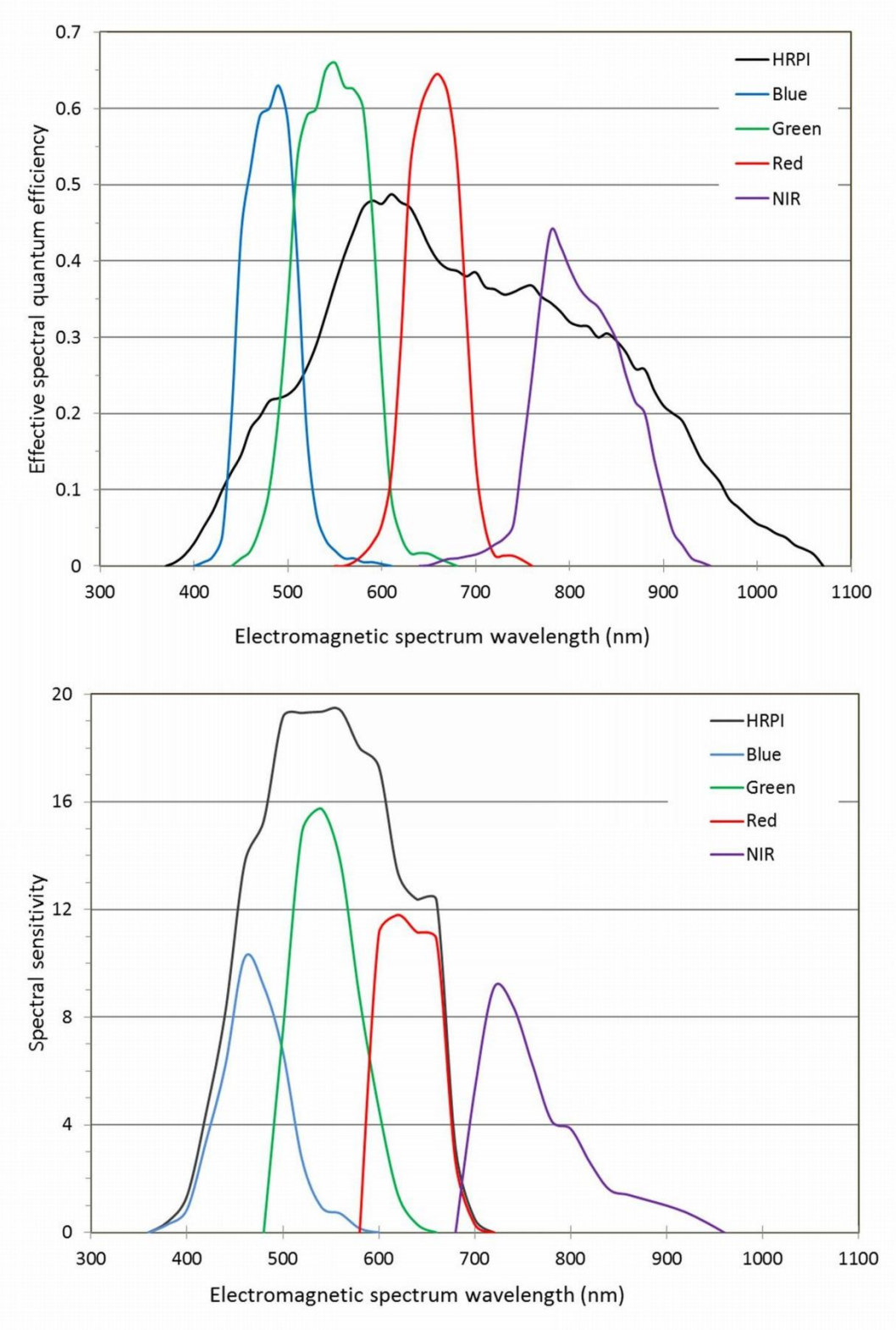

Figure 4.1: Absolute spectral radiance response of QB (above) and Vexcel (below) sensors. Source: Otazu et al. (2005) for QB and Haest et al. (2009) for Vexcel.

The linear approach, called improved synthetic variable ratio (ISVR), estimates the spectral radiance for the gaps between the LRMI bands using an average based on the surrounding bands (Wang et al., 2008). These gaps complete the spectral radiance curve for non-contiguous LRMI bands, allowing the percentage contribution of each band to be estimated. Equation 4.1 shows the formula for calculating band weights (ϕn) with this method. A limitation of this approach is that the spectral response in the gaps is assumed to be linear. Figure 4.1 shows that this is not the case for both the QuickBird and Vexcel sensors.

$$\boldsymbol{\varphi_n = 1 + t_1 + t_2} \quad \textbf{(4.1)}$$

where:

$$t_1 = \begin{cases} \frac{\lambda_{i,1} - \lambda_{(i-1),2}}{2(\lambda_{i,2} - \lambda_{i,1})} & (2 \le i < n) \\ 0 & (i = 1) \end{cases};$$

$$t_2 = \begin{cases} \frac{\lambda_{(i+1),1} - \lambda_{i,2}}{2(\lambda_{i,2} - \lambda_{i,1})} & (1 \le i < n) \\ 0 & (i = n) \end{cases};$$

$\lambda_{i,1}$ and $\lambda_{i,2}$ are the two ends' wavelengths of *i*th band of the LRMI; and

n is the total number of bands used to construct $LRPI_{SYN}$.

Svab and Ostir (2006) have determined theoretical spectral band weights by adopting the band-integrated (in-band) radiance at the sensor aperture for different satellite sensors (as shown in the equation 4.2) and comparing the responses of the panchromatic band and individual bands of the sensor (Otazu et al., 2005).

$$\boldsymbol{L_n = \int_0^\infty L(\lambda) \cdot R_n(\lambda) \cdot d\lambda} \quad \textbf{(4.2)}$$

where:

λ is the wavelength and n is the band number;

L_n is the effective in-band radiance (measured in $W\text{-}m^{-2}\text{-}sr^{-1}$) for a given band n;

L(λ) is the spectral radiance at the sensor aperture; and

$R_n(\lambda)$ is the relative spectral radiance response for a given band n.

An alternative multiple linear regression approach is based on the LRMI bands having a strong correlation with the HRPI (Shettigara, 1992). Ordinary least

squares regression (OLS) is a commonly applied technique to determine weights using this method because of its computational simplicity (Cliche et al., 1985; Hill et al., 1999; Munechika et al., 1993; Rahman and Csaplovics, 2007; Shettigara, 1992; Zhang et al., 2006; Zhang, 1999, 2008). OLS calculates the model that best fit with the observed values by determining the unknown parameters (least squares estimators) for the dependent variables. It minimises the sum of squared residuals (or errors) between the observed and the modelled values.

$$\mathbf{OLS} = \sum_{i=1}^{n}(\mathbf{Y_i} - \boldsymbol{\varphi_0} - \boldsymbol{\varphi_1} \cdot \mathbf{X_1} - \boldsymbol{\varphi_2} \cdot \mathbf{X_2} - \cdots - \boldsymbol{\varphi_n} \cdot \mathbf{X_n})^2 \quad \textbf{.....(4.3)}$$

where:
The least squares estimators are those values of $\phi_0, \phi_1, \ldots, \phi_n$ that minimise OLS.

The least absolute deviation (LAD) regression, as used in SRM technique, estimates regression coefficients (band weights) ϕ_1 to ϕ_n by minimising the sum of the absolute values of the residuals. It is the oldest linear regression method to find parameters which best fits observational equations and was first proposed by R. J. Boscovich in 1757 and predates OLS regression, which was first proposed by C. F. Guass in 1794. It has never received full attention due to its computational intensity, but now with iterative computer programming it is practical (Dodge and Jurečková, 2000). In comparison to LAD regression, OLS regression only finds one solution and this can be very sensitive to outliers in the data (Giloni et al., 2006). A few outlying observations, even one, can spoil the least squares fit that may result in a severe estimation bias and drastically affect the correlation value (McKean and Sievers, 1987; Xia and Kamel, 2008). LAD is an important alternative to the OLS from the point of view of efficiency for longer-tailed error distributions which provides robust estimators that are unaffected by outlying observations (McKean and Sievers, 1987). Some early use of LAD estimators for digital aerial image matching provided improved subpixel matching accuracy in the presence of outlier points when compared with OLS (Calitz and Rüther, 1996). The formula for LAD is described in equation 4.4. LAD iterates until it minimises the sum of absolute deviations.

$$\mathbf{LAD} = \mathbf{Min}_{\boldsymbol{\varphi_n}} \sum_{i=1}^{n} |\mathbf{Y_i} - \sum_{i=1}^{n} \boldsymbol{\varphi_n} \cdot \mathbf{X_n}| \quad \textbf{.....(4.4)}$$

The advantage of LAD based spectral band weights is that it does not need to be recalculated for different images of the same sensor, unlike OLS calculated band weights.

The calculation of band weights using LAD and OLS for Quickbird and Vexcel images are demonstrated in the following sections and their performances are compared.

4.4 Implementing LAD and OLS for calculating band weights

4.4.1 Data used

Two sets of images are used for implementing and evaluating LAD and OLS for calculating band weights. The first set is a QuickBird sub-scene consisting of 500 x 500 pixels of LRMI (Figure 4.2*c*) and 2000 x 2000 pixels of HRPI; captured on 22 March 2007. These images display a typical habitat of emergent and submerged vegetation, which is located at the southern edge of Lake Taupo and is part of the Tongariro river delta. The image contains approximately 50% water, which is located in the upper half of the image. The rest of the image is composed of different herbaceous wetland vegetation. Structures such as roads, buildings and a boat marina are also visible.

The second set of images consists of Microsoft's Vexcel UltraCam-D dual-resolution aerial sensor was captured on 29 Jan 2009. An aerial frame of Vexcel's UltraCam-D sensor covers 3680 x 2400 pixels of LRMI (Figure 4.2*b*) and 11500 x 7500 pixels of HRPI. A sub-scene of 1152 x 768 pixels of LRMI and 3600 x 2400 pixels of HRPI is used for the analysis, and represents predominantly riparian environments of the Waikato River section and urban features within Hamilton city. These images are geometrically projected to UTM zone 60S. The QuickBird image has 2.4 m and 0.6 m resolution for the LRMI and HRPI respectively, whereas the Vexcel image has 28.125 cm and 9 cm resolution for the LRMI and HRPI respectively. They are both stored in 16-bit integer format. During analysis, all derived images were stored as 16-bit floating point.

In order to calculate multiple linear regression between LRMI and the HRPI, the HRPI is degraded so its spatial resolution matches with the LRMI. For the QuickBird, a pixel block average (or zonal mean) of 16 pixels of the HRPI produced the LRPI since the spatial resolution ratio (SRR) is 1:4. For the Vexcel image a pixel block average of 9 pixels was used. However, first the LRMI was up-sampled from 28.125 cm to 27 cm using nearest neighbour convolution to round the SRR to 1:3. The new size of the LRMI for the Vexcel sub-scene was 1200 x 800 pixels.

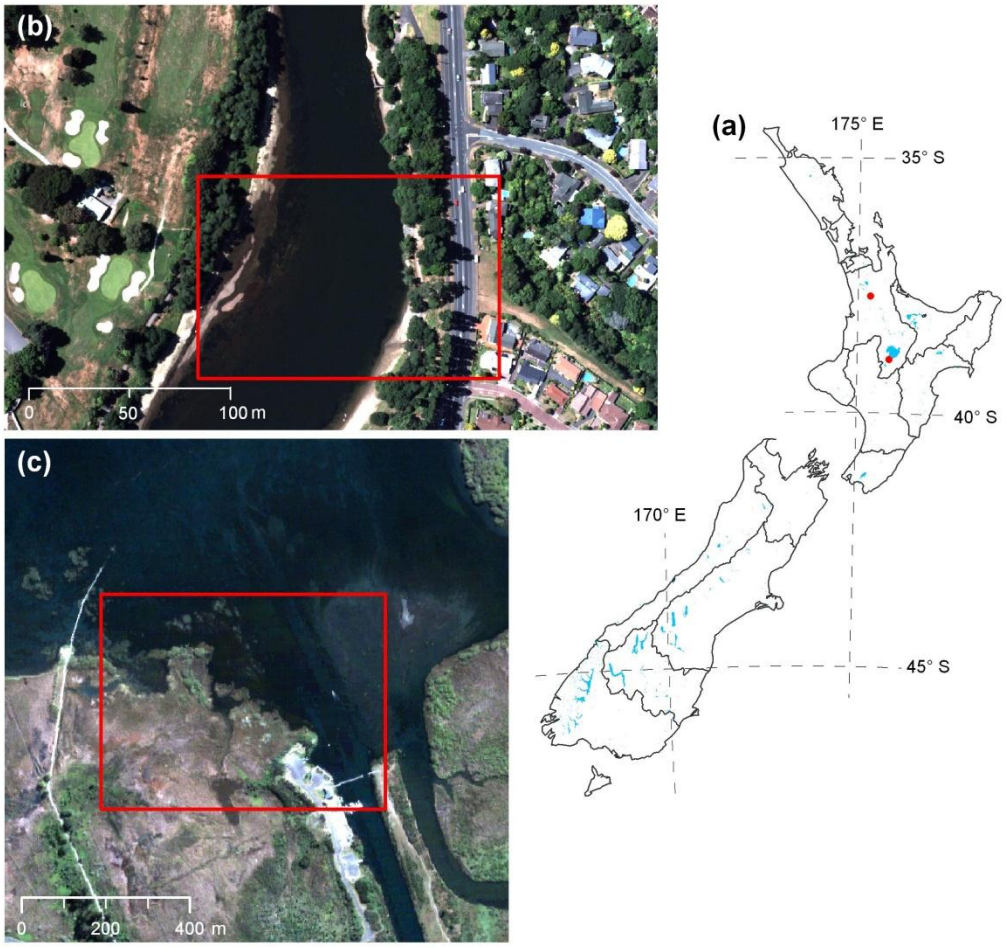

Figure 4.2: Images used for the evaluation of different methods for determining band weights for SRM DF; (a) index map showing locations of the images used – The Waikato river section within Hamilton city and the southern edge of the Lake Taupo. Sub-scenes of the true colour composites of (b) the Vexcel LRMI and (c) the QB LRMI. The square boxes in (b) and (c) are the extent of the zoomed-in areas in Figures 6–12.

4.4.2 Implementing LAD regression

To determine band weights for a sensor it is appropriate to find a set of images that have high image quality and good contrast. Sub-image polygons (Figure 4.3) were used that include relatively large, homogenous patches with good distribution of colours that stay well within the polygon boundary. This speeds up processing, and trims data to eradicate outliers such as clouds, shadows, water glare, and highly textured features (e.g. dense urban and some vegetation). Trimming also ensures that there is an equal representation of colours.

Figure 4.3: Sub-image colour polygons used for determining LAD-based regression coefficients.

Determining spectral band weights (ϕi) using LAD multiple linear regression is an iterative process. Initially all LRMI bands are assigned with ϕ = 1.0 to calculate a provisional weighted band sum (WBS) using a simple addition algorithm. WBS is z-score normalised so that the mean (μ) and standard deviation (σ) of WBS match the μ and σ of the HRPI using equation 3.7. An absolute difference image is calculated between the LRPI and provisional WBS. Instead of measuring the sum of the absolute difference, the μ and σ values are

measured. Each band weight was iteratively modified by 0.1 and the μ and σ values between iterations were calculated. The band weight combination with the least μ and σ values was determined optimal. If μ or σ increased while the other decreased, which will always happen after a large number of iterations, then the difference between the σ from its previous iteration was considered twice as important as the difference between the μ and its previous iteration.

For the QuickBird sensor, although band weights are established by ERDAS using many images, we determined a new set of spectral weights specific to the sub-scene used for this research, so that it could be compared with the OLS calculation for the same sub-scene. For Vexcel's UltraCam-D digital sensor, weights were calculated using only one scene. We strongly recommend readers to determine their own weights for Vexcel sensor images, if they wish to apply SRM.

4.4.3 Implementing OLS regression

The implementation of OLS in ERDAS Imagine software was built using spatial modeller and the algebraic expression shown in equation 4.5. This algebraic expression is based on Neter et al. (1996) and provides regression coefficients that can be used as band weights.

$$\begin{bmatrix}\varphi_0\\ \varphi_1\\ \vdots\\ \varphi_n\end{bmatrix} = \begin{bmatrix} N & \sum LRMI_1 & \sum LRMI_2 & \cdots & \sum LRMI_n \\ \sum LRMI_1 & \sum LRMI_1^2 & \sum LRMI_2 . LRMI_1 & \cdots & \sum LRMI_n . LRMI_1 \\ \vdots & \vdots & \vdots & \ddots & \vdots \\ \sum LRMI_n & \sum LRMI_1 . LRMI_n & \sum LRMI_2 . LRMI_n & \cdots & \sum LRMI_n^2 \end{bmatrix}^{-1} \cdot \begin{bmatrix} \sum LRPI \\ \sum LRMI_1 . LRPI \\ \vdots \\ \sum LRMI_n . LRPI \end{bmatrix} \quad \textbf{....(4.5)}$$

Where:

N = total number of pixels in the LRMI or LRPI image;

ϕ_0 is value of intercept while ϕ_1 to ϕ_4 are OLS regression based band weights for the Blue, Green, Red and NIR bands of the LRMI image.

The algebraic expressions used to calculate the coefficient of multiple determination (denoted by R^2) is shown in equation 4.6:

$$\mathbf{R^2 = 1 - \frac{SSE}{SST}} \quad \textbf{(4.6)}$$

Where:

SSE = Sum of squares due to errors; and

SST = Total sum of squares.

SSE and SST are calculated using equations 4.7 and 4.8 as:

$$\mathbf{SSE = \sum_{i=1}^{n}(Y_i - \hat{Y}_i)^2 = \sum LRPI^2 - \left(\begin{bmatrix} \varphi_0 \\ \varphi_1 \\ \vdots \\ \varphi_n \end{bmatrix}^T . \begin{bmatrix} \sum LRPI \\ \sum LRMI_1 . LRPI \\ \vdots \\ \sum LRMI_n . LRPI \end{bmatrix} \right)} \quad \textbf{(4.7)}$$

$$\mathbf{SST = \sum_{i=1}^{n}(Y_i - \overline{Y})^2 = \sum LRPI^2 - \{(\sum LRPI)^2/N\}} \quad \textbf{4.8)}$$

Where:

Y_i is the sample value of the dependent variable;

$\hat{Y}_i$ is the corresponding value estimated from the regression equation; and

$\overline{Y}$ is the mean of Y_i

The modifications performed on SRM method due to implementing LAD or OLS based regressions are summarised in a following flow diagram (as Figure 4.4). Table 4.1 shows the calculated band weight values of QB and Vexcel sensors using the LAD and OLS regression techniques.

Table 4.1: Spectral band weights for SRM using LAD and OLS regression techniques (the values in parenthesis show spectral weight in percentage)

Sensor	Blue (φ_1)	Green (φ_2)	Red (φ_3)	NIR (φ_4)
QB-ERDAS (sensor specific weights)	0.2 (5.71)	0.7 (20.0)	1.2 (34.29)	1.4 (40.0)
QB-LAD (scene specific weights)	0.6 (18.75)	0.7 (21.88)	0.6 (18.75)	1.3 (40.63)
QB-OLS (scene specific weights)	0.055 (5.37)	0.261 (25.57)	0.292 (28.69)	0.411 (40.37)
Vexcel-LAD (scene specific weights)	1.9 (34.55)	2.0 (36.36)	1.5 (27.27)	0.1 (1.82)
Vexcel-OLS (scene specific weights)	0.562 (33.36)	0.635 (37.71)	0.479 (28.42)	0.008 (1.50)

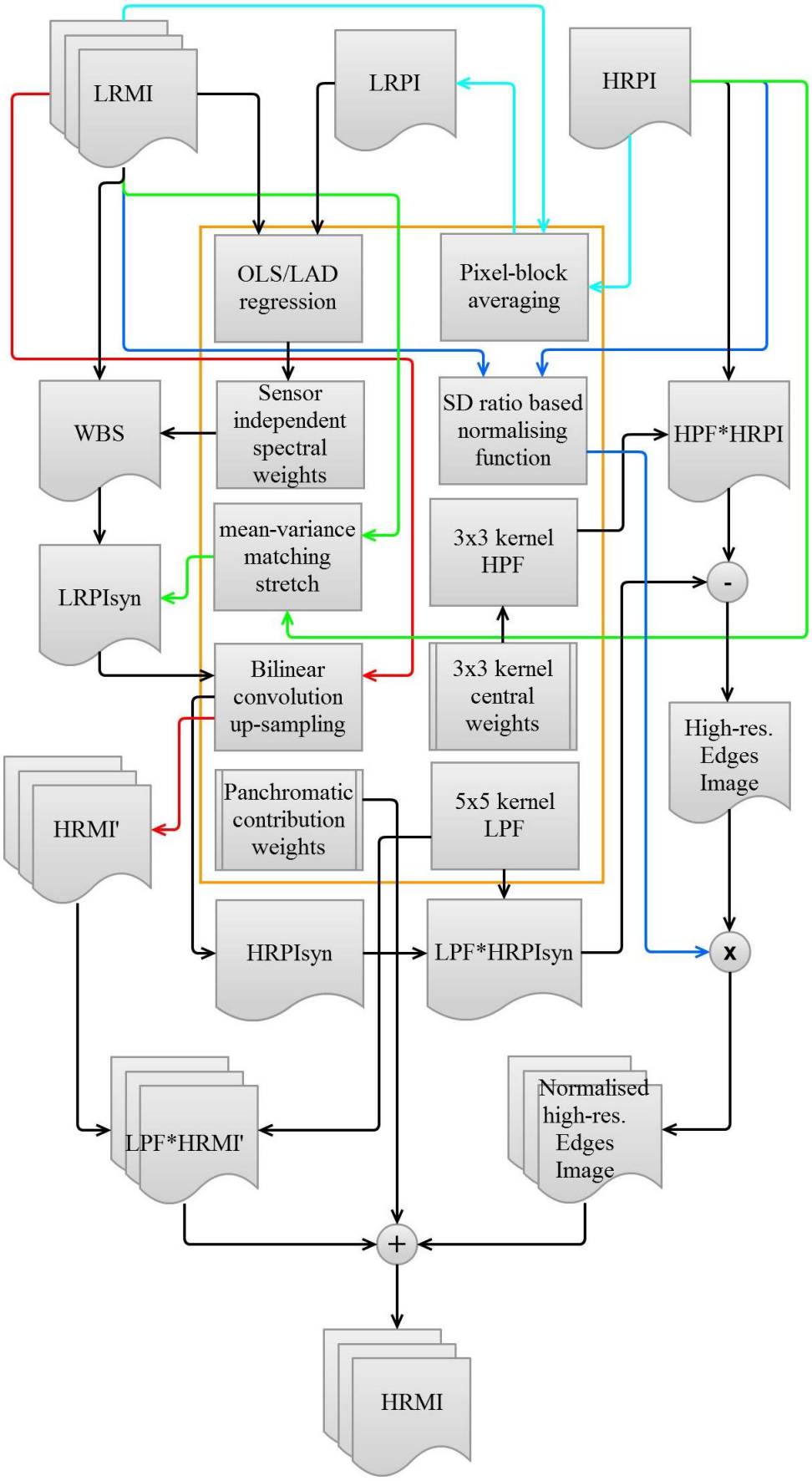

Figure 4.4: Flow diagram of LAD and OLS regression coefficients modification to SRM.

4.5 Methods for evaluating band weights

This research compares the performance of SRM data fusion using spectral band weights for QuickBird and Vexcel UltraCam-D sub-scenes calculated by LAD and OLS multiple linear regressions. This performance is compared qualitatively (visually) and by using quantitative spectral and spatial metrics. The use of both spectral and spatial metrics is important, as they tend to show opposite trends (Gangkofner et al., 2008). To evaluate the performance of data fusion methods, we degrade the resulting HRMI to the same spatial resolution as the original LRMI using pixel block averaging technique (Liu and Moore, 1998). To measure spectral quality, Pearson's correlation coefficient and root-mean squared error (RMSE) are used. To measure spatial quality, the RMSE of the Sobel filtered images are used (Gangkofner et al., 2008; Li et al., 2010; Pradhan et al., 2006). The RMSE between the HRMI and the HRPI is labelled Sobel filter RMSE-I, whereas the RMSE between the original LRMI and the degraded HRMI is labelled Sobel filter RMSE-II in the following sections. A comparison with the standard ERDAS SRM approach is also made for the QB image.

Image classification is also applied to analyse the performance of data fusion as this is a common end use(Nikolakopoulos, 2008). Unsupervised classification based on the Iterative Self-Organising Data Analysis Technique (ISODATA) was used (Tou and Gonzalez, 1974). Unsupervised rather than supervised classification was used because of the computational ease and its unbiased results (ERDAS, 2009). Ten arbitrary clusters for the QB and Vexcel sensor images were derived. The convergence threshold was set to 0.995 for both QB and Vexcel sensors, which means that if the spectral means of 99.5 % of pixels within arbitrary clusters are unchanged, the iterative process terminates. These unsupervised classifications results are assessed visually and quantitatively using their absolute difference from the ISODATA classified LRMI.

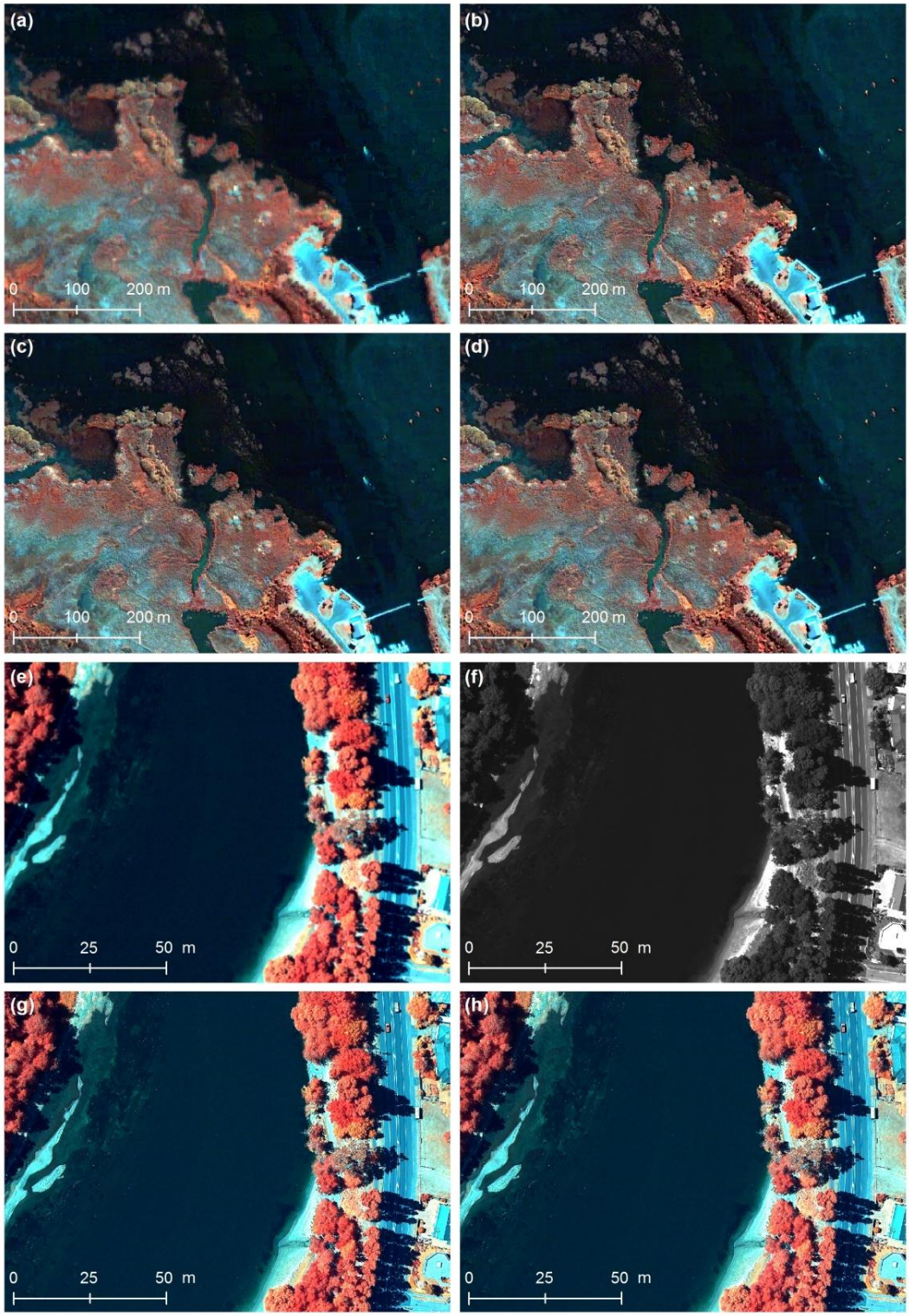

Figure 4.5: DF resulting from the use of different band weight calculations; (a) original QB image shown using a false colour composite (FCC) of LRMI bands 4, 2, 1 shown as R, G, B; (b) HRMI using ERDAS; (c) HRMI using LAD; (d) HRMI using OLS; (e) Vexcel's FCC of LRMI bands 4, 2, 1 shown as R, G, B; (f) HRPI; (g) HRMI using LAD and (h) HRMI using OLS spectral band weights.

4.6 Results and discussion

The fusion results using LAD and OLS regression based spectral weights for QB and Vexcel sensors are compared visually in Figure 4.5. QB-ERDAS abbreviation is used for the ERDAS supplied sensor specific spectral weights using LAD. Scene specific spectral weights for the QB and Vexcel using LAD and OLS are abbreviated as QB-LAD, QB-OLS, Vexcel-LAD and Vexcel-OLS. All images in figure 4.5 are displayed using the same colour lookup values and are stretched by three standard deviations. For both QB and Vexcel, LAD and OLS have performed similarly and there is visually insignificant difference between the results. Quantitative assessment is therefore needed to determine subtle variations in these results.

Figure 4.6 summarises the band averages of the quantitative metrics for all five methods. The results show that there is insignificant difference between LAD and OLS. For QB, LAD was slightly better, and for Vexcel, OLS was slightly better. The scene specific calculations for QB were also very similar to the QB ERDAS results. Table 4.2 shows the quantitative assessment for each band. Again, there is insignificant difference between LAD and OLS for any of the bands.

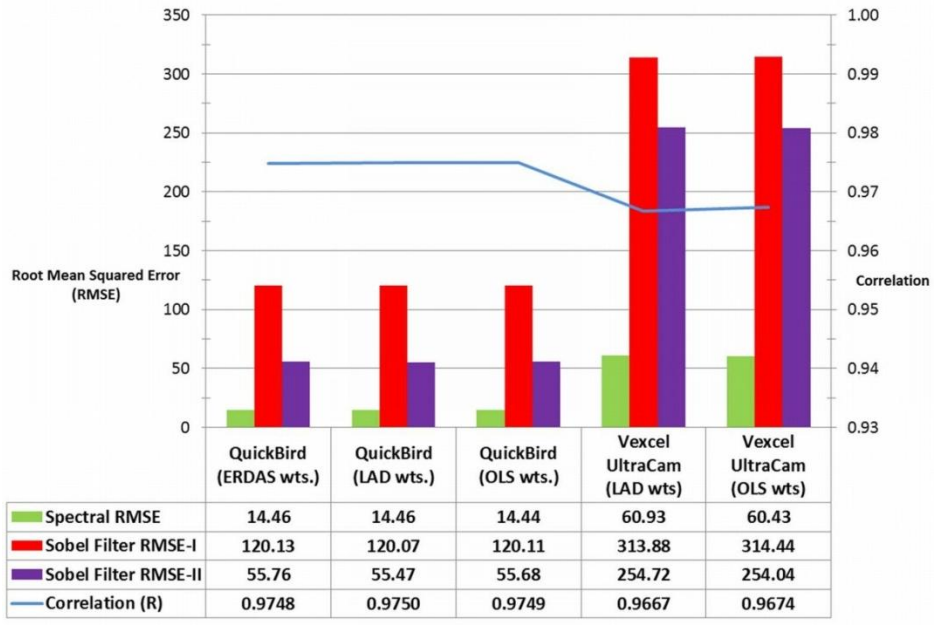

	QuickBird (ERDAS wts.)	QuickBird (LAD wts.)	QuickBird (OLS wts.)	Vexcel UltraCam (LAD wts)	Vexcel UltraCam (OLS wts)
Spectral RMSE	14.46	14.46	14.44	60.93	60.43
Sobel Filter RMSE-I	120.13	120.07	120.11	313.88	314.44
Sobel Filter RMSE-II	55.76	55.47	55.68	254.72	254.04
Correlation (R)	0.9748	0.9750	0.9749	0.9667	0.9674

Figure 4.6: Average correlation and root mean squared error metrics for different data fusion techniques

Table 4.2: Quantitative assessment of DF results for different bands.

Spectral band weights' calculation approach	Sensor	Spectral measure between LRMI and degraded HRMI bands								Spatial measure between HRMI & HRPI and LRMI and degraded HRMI bands							
		Correlation (R)				Spectral RMSE				Sobel Filter RMSE-I (between HRMI & HRPI)				Sobel Filter RMSE-II (between LRMI & degraded HRMI)			
		Blue	Green	Red	NIR	Blue	Green	Red	NIR	Blue	Green	Red	NIR	Blue	Green	Red	NIR
ERDAS	QB	0.970	0.975	0.976	0.979	4.19	8.62	8.87	36.16	**112.14**	**68.89**	**67.02**	232.47	15.99	32.75	34.26	140.06
LAD	QB	**0.970**	**0.975**	**0.976**	0.979	**4.18**	**8.60**	**8.82**	36.25	112.17	69.00	67.14	**231.95**	**15.89**	**32.49**	**33.94**	**139.55**
OLS	QB	0.970	0.975	0.976	**0.979**	4.19	8.62	8.85	**36.11**	112.16	68.92	67.06	232.32	15.99	32.76	34.21	139.75
LAD	Vexcel	0.969	0.968	0.968	0.962	23.13	44.17	60.19	116.22	**356.52**	**132.06**	136.40	**630.52**	94.63	178.70	247.69	497.86
OLS	Vexcel	**0.969**	**0.969**	**0.968**	**0.963**	**22.99**	**43.84**	**59.81**	**115.09**	356.61	132.41	**136.25**	632.48	**94.59**	**178.26**	**247.48**	**495.83**

Figure 4.7 shows the RMS error map for all four bands of QB HRMI using scene specific LAD and OLS approaches. There is insignificant difference between them; however, for the blue and NIR bands (figure 4.7a, d, e, h) there are darker coloured pixels over the water region in QB-LAD than QB-OLS. This suggests that QB-LAD is robust for dark features such as water, shades and submerged aquatic vegetation. The NIR RMSE, using either LAD or OLS, show higher values compared to the RMSE for the visible bands. This indicates a poor performance of data fusion for the NIR band, which is consistent with any data fusion technique because of the high standard deviation of this band (Hill et al., 1999).

Figure 4.8 shows RMSE map for all four bands of Vexcel HRMI using scene-specific LAD and OLS approaches. There is a slight improvement with OLS for the darker features such as water.

The unsupervised HRMI and LRMI classification results are shown in Figure 4.9 (QB) and Figure 4.10 (Vexcel). Visually, all HRMI classification results are similar for both QB and Vexcel.

The quantitative absolute difference results between LRMI and HRMI unsupervised classes shown in figure 4.11 further verify that there is no distinct advantage between LAD and OLS.

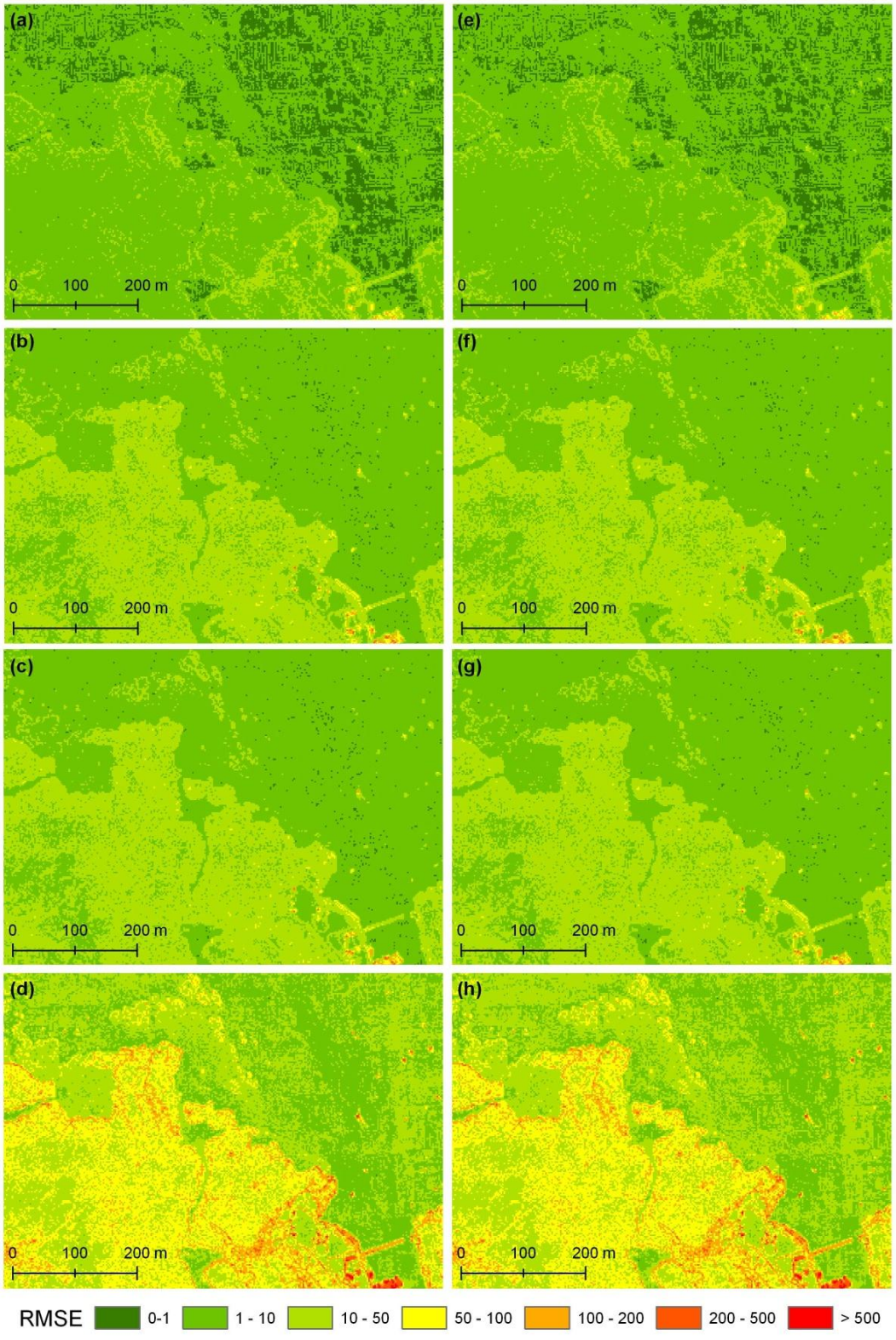

Figure 4.7: Spectral RMSE maps showing the error values for each pixel of blue, green, red and NIR bands of QuickBird image (a–d) using LAD spectral weights and (e–h) using OLS spectral weights.

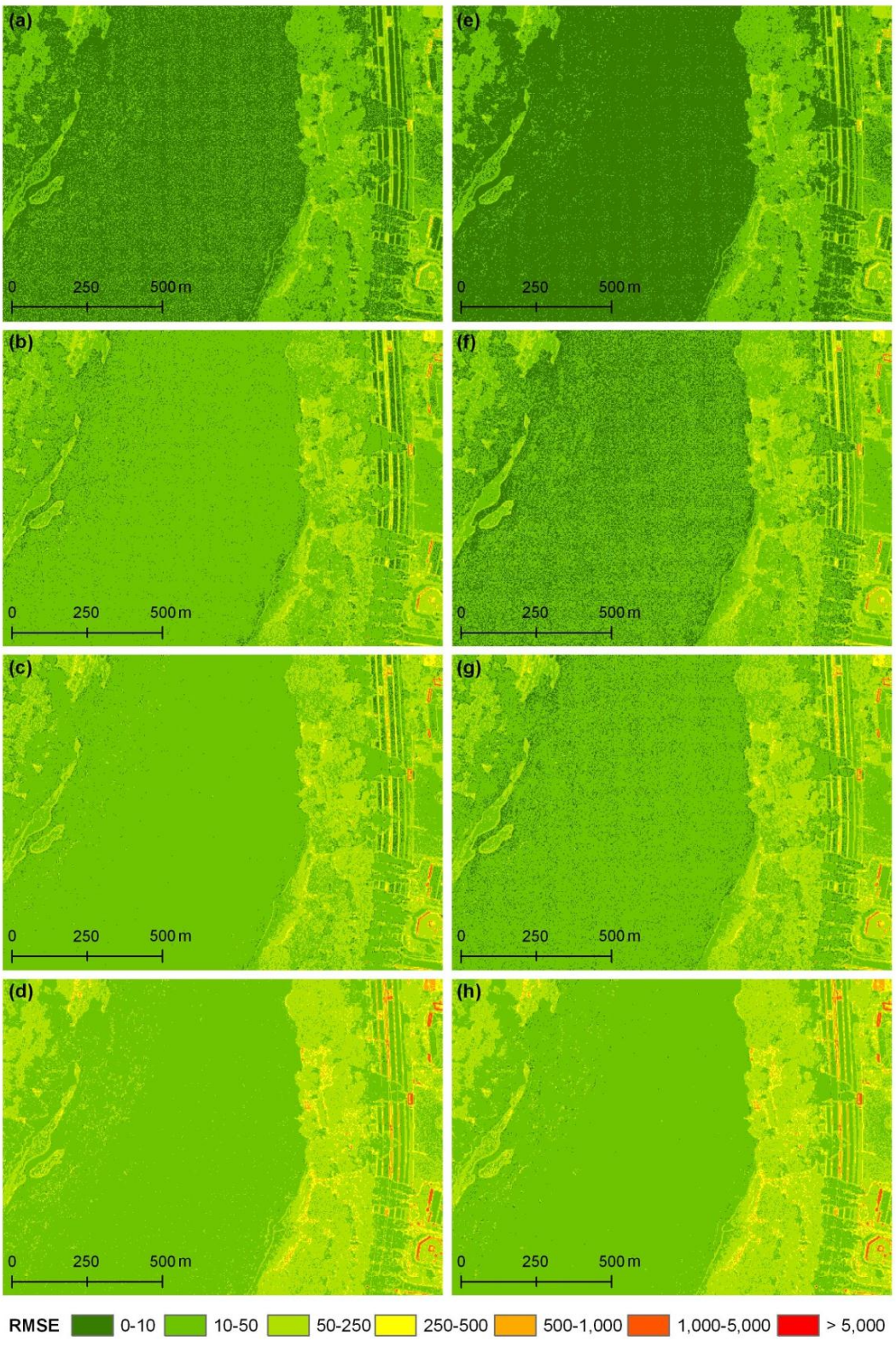

Figure 4.8: Spectral RMSE maps showing the error values for each pixel of blue, green, red and NIR bands of Vexcel image (a–d) using LAD spectral weights and (e–h) using OLS spectral weights.

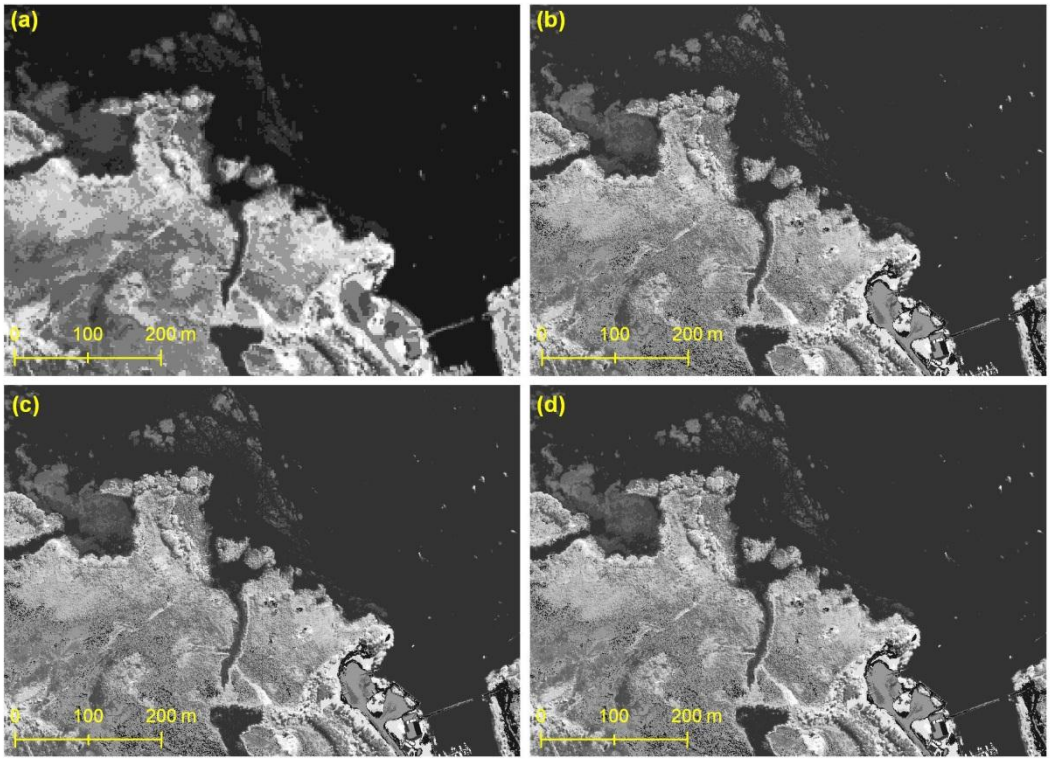

Figure 4.9: Unsupervised classification of DF results for QB image; (a) LRMI; and HRMIs using (b) ERDAS; (c) LAD and (d) OLS spectral band weights.

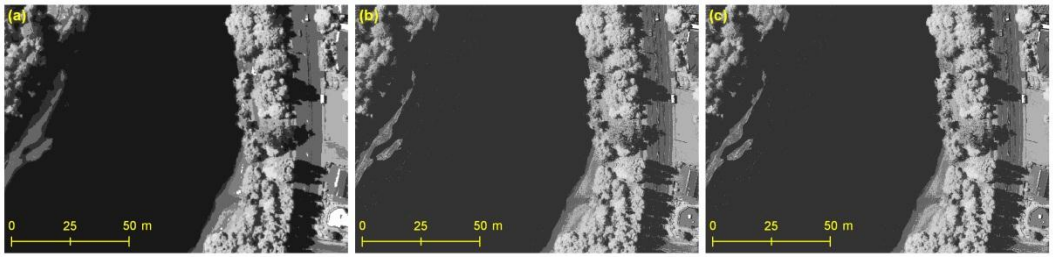

Figure 4.10: Unsupervised classification of DF results for Vexcel image; (a) LRMI; and HRMI's using (b) LAD and (c) OLS spectral band weights.

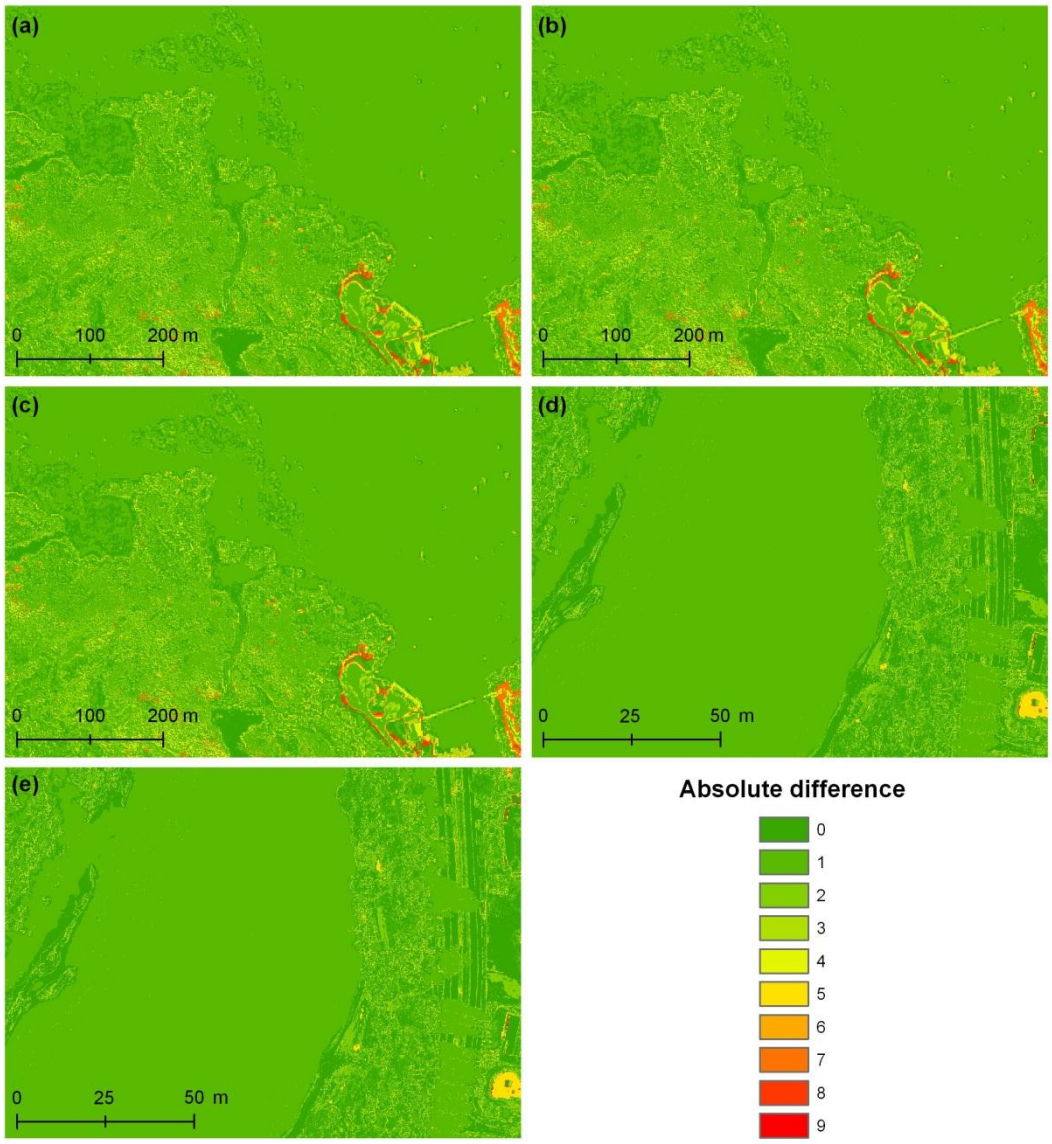

Figure 4.11: Absolute difference between LRMI and HRMI unsupervised classes; (a) QB-ERDAS; (b) QB-LAD; (c) QB-OLS; (d) Vexcel-LAD and (e) Vexcel-OLS spectral band weights.

4.7 Conclusions

This research concludes that there are some differences in the resulting band weights that are calculated from LAD or OLS regression techniques; however these differences make insignificant variations in the resulting fused images in terms of spectral and spatial quantitative metrics and qualitative assessment. However, since LAD is a cumbersome iterative process to compute, then OLS is a preferred method.

Wang et al. (2008) argued that the calculation of band weights adds computational burden to data fusion and therefore predetermined weights are

preferred. The computing of band weights in this was not particularly burdensome. The calculation of band weights using OLS for a full scene of QB took approximately 5 minutes on an Intel Core 2 CPU (2.4 GHz) with 2 GB system RAM using ERDAS Imagine spatial Modeller software. This could be integrated into an SRM tool. With much faster computers now available, this computational burden is not an issue. Given that band weights can be calculated for any set of LRMI and HRPI images that have spectral response overlap and correlation, image-processing software could build band weight calculations into the SRM data fusion technique. The LAD approach uses iterations, with each iteration taking approximately one minute. For this demonstration of LAD, there were 30 iterations to produce the band weights; therefore the LAD approach requires considerable computational time, which is why band weights are predetermined in SRM for a few selected sensors.

This research shows that there is insignificant difference between using predetermined band weights and user calculated band weights. Therefore, if predetermined weights are available for any sensor sets then they could be used. However, with the increasing number of satellite sensors and the potential combination of cross sensor images that can be used in data fusion, pre-determined weights will not always be available. In this case, image analysts will benefit from the OLS method to calculate their own band weights, and this should be integrated into the SRM technique to diversify its application.

Chapter 5

Effect of contrast and luminance normalisation to data fusion

5.1 Abstract

Subtractive Resolution Merge (SRM) is a contemporary method for data fusion that produces highly preserved spatial and spectral resolution. This method is limited to dual sensor platforms with specific band ratios between the high-resolution panchromatic image (HRPI) and the low-resolution multispectral image (LRMI). An additional problem with SRM is that some bands are over or under represented due to the global normalisation function applied. This provides two modifications that resolve these limitations. SRM builds a synthetic low-resolution panchromatic image (LRPI) from the weighted sum of the LRMI bands. This is modified by using a pixel block (zonal) averaging of the HRPI instead. The second modification is the use of a contrast and luminance index for the normalising function. These two modifications are tested on a QuickBird images (multispectral and panchromatic), as well as fusing SPOT-5 multispectral and an aerial photograph. The results show improved quantitative metrics and unsupervised classification compared to the standard SRM technique. Both of these modifications are grouped into a patent pending technique that is called Contrast and Luminance Normalised (CLN) fusion.

5.2 Introduction

Data fusion is an important image preparation tool for enhancing spatial detail in multispectral images. It integrates the spatial detail of a high-resolution panchromatic image (HRPI) with the spectral detail of a low-resolution multispectral image (LRMI) to produce a high-resolution multispectral image

(HRMI). There are many techniques available for data fusions, which have been reviewed, compared, and evaluated (Dong et al., 2009; Nikolakopoulos, 2008; Pohl and Van Genderen, 1998; Thomas et al., 2008; Wang et al., 2005). As explained earlier, these techniques follow a generic framework of image fusion (see Eq. 1.1) and determine high resolution spatial edges (HRSE) image from the HRPI alone or in combination with LRMIs. These edges are modulated using a set of scalar values (also called modulation coefficients or normalising function - NF) and injected into an up-sampled LRMI (Aiazzi et al., 2007a; Wang et al., 2010; Wang et al., 2005). Aiazzi et al. (2007b) and Dou et al. (2007) have demonstrated through their research that HRSE and NF are the main reasons for colour infidelity and spatial distortions during image fusion process and are therefore the focus of further research.

This chapter first provides a brief overview of the contemporary Subtractive Resolution Merge (SRM) technique and identifies its limitations. Two modifications are suggested to improve the performance of the SRM technique. The first modification uses a pixel block averaging of the HRPI to determine edge details, and the second modification applies a contrast and luminance index for the normalisation function. Both of these modifications are grouped into a patent pending technique that is called Contrast and Luminance Normalised (CLN) fusion. These modifications are demonstrated by fusing two pairs of images; QuickBird multispectral and panchromatic images, and SPOT-5 multispectral and an aerial photograph. Standard qualitative and quantitative techniques and unsupervised classification are used to show the improved performance.

5.3 SRM technique and its limitations

The SRM technique is already explained in Chapter 3; however, its mathematical form is expressed again to explain and compare proposed modifications with it. The SRM technique achieves the HRMI using the following equation:

$$\mathbf{HRMI_n} = (\mathbf{LPF} * \mathbf{LRMI'_n}) + (\mathbf{HPF} * \mathbf{HRPI} - \mathbf{LPF} * \mathbf{HRPI_{SYN}}) \times \mathbf{PCW} \times \mathbf{NF_n} \quad \textbf{.....(5.1)}$$

where:

HPF is a weighted focal mean;

$\mathrm{LRMI'_n}$ is an up-sampled LRMI using bilinear convolution

LPF is a simple focal arithmetic mean;

PCW is a panchromatic contribution weight;

NF is a normalising function $\left(\frac{\sigma \mathrm{LRMI_n}}{\sigma \mathrm{HRPI}}\right)$; and

n represents one of the n bands

A major disadvantage of SRM is that it is limited to fusing dual-resolution sensors where the spatial resolution ratio (SRR) between HRPI and LRMI is 1:4, such as QuickBird, IKONOS and FormoSat. There are opportunities to fuse images from numerous mono-resolution sensors, e.g. ASTER, RapidEye, WorldView-1 and aerial photography, as well as other dual-resolution sensors, e.g. GeoEye-1, WorldView-2, or DubaiSat etc. An additional weakness of SRM is the global statistical function that is used to normalise the band edges. As will be shown in this , this function over or under represents the edges in some bands. In particular, the near infrared (NIR) band is over-represented in an aquatic environment. This problem is not limited to SRM and applies to most data fusion techniques that use a normalisation function.

5.3.1 First modification to SRM – bypassing the use of band weights and a specific spatial resolution ratio

As described previously, the SRM technique calculates $\mathrm{LRPI_{SYN}}$ using weights for the LRMI, which are specific to a sensor. The SRM technique is therefore dependent on dual-resolution sensor images, such as QuickBird, IKONOS, and FormoSat. SRM is also dependant on the spatial resolution ratio (SRR) of LRMI to HRPI being 1:4. There are many sensors that do not have this ratio, such as Landsat-7 ETM+, SPOT-5 HRG (5 m HRPI), DubaiSat and EO1. Ideally, data fusion should be independent of the SRR and not require sensor specific weights for cross-sensor data.

Our first modification bypasses the use of band weights and a requirement for a fixed 1:4 SRR to produce a $HRPI_{SYN}$. Instead, the $HRPI_{SYN}$ is produced from the HRPI by first down-sampling using pixel-block averaging and then up-sampling using bilinear interpolation. We are calling this HRPI' because it is generated from the HRPI and not synthetically from the LRMI. The use of pixel-block averaging is a technique used in pixel block intensity modulation (PBIM) by Liu and Moore (1998); however PBIM is limited because it generates serious pseudo-edge effects or blocking artefacts around features with high contrast colour boundaries, such as between water and vegetation in the NIR band (Hill et al., 1999; Liu and Moore, 1998). The subtraction of HRPI' from HRPI generates similar edge details as the SRM, but has the advantage of not requiring band weights and can be applied to fuse cross-sensor images.

The bilinear up-sampling used above was compared with nearest neighbourhood (NN) and cubic convolution (CC) interpolation methods. For the QuickBird image, which has a 1:4 SRR, the best results were achieved when LRPI is up-sampled using the NN method. Since the modified technique is independent of the sensor, any SRR can be used for the fusion. In the case of a larger SRR, higher kernel low-pass filters are required to avoid blocking artefacts. It is found that a larger LPF modulation on the LRMI is computationally expensive and that may cause spatial artefacts like ghosting and blurring in the resulting products (Padwick et al., 2010). Alternatively, an up-sampling of LRMI to HRMI' using BL interpolation was used and this provided better spectral preservation, insignificant spatial edge smoothness, a visual improvement, and efficient computation. The equation for the first modification to SRM (MSRM-1) is:

$$\mathbf{HRMI_n} = \mathbf{LPF} * \mathbf{HRMI'_n} + (\mathbf{HPF} * \mathbf{HRPI} - \mathbf{LPF} * \mathbf{HRPI'}) \times \mathbf{PCW} \times \mathbf{NF_n} \quad \textbf{.....(5.2)}$$

where:

HRPI' is an up-sampled LRPI using bilinear interpolation; the LRPI is a mean of all pixels of HRPI over the LRMI pixel block;

HRMI' is an up sampled LRMI using bilinear interpolation; and

NF is a normalising function $\left(\frac{\sigma \mathrm{LRMI}_n}{\sigma \mathrm{HRPI}}\right)$

MSRM-1 still uses the same low-pass and high-pass modulations applied on the HRPI' and HRPI respectively to enhance edge detail even for the higher SRR. It also uses the same normalising function as SRM. The advantage of this modification is that the sensor specific band weights are not required.

5.3.2 Second modification to SRM – using a luminance and contrast indices for normalising spatial edges

The NF is a weight matrix that normalises a single layer spatial edges image according to the digital numbers of the individual LRMI bands before injecting the spatial edges into the LRMI. Two methods commonly used for the NF are the ratio between the standard deviations of the LRMI and HRPI (de Béthune et al., 1998b), and the ratio between the covariance of HRPI and LRMI and the variance of HRPI (Laben and Brower, 2000). Both these methods can be applied using global or local statistics (Aiazzi et al., 2007a; Choi et al., 2008; Gangkofner et al., 2008).

The SRM algorithm, which as previously stated, uses the ratio of the global standard deviations of the LRMI (for a particular band) and HRPI. This normalisation ratio was first introduced by de Béthune et al. (1998a; 1998b) in the local mean and variance matching (LMVM) method. The LMVM was a modification to the high-pass filter addition (HPFA) resolution merging technique, which was introduced earlier by (Schowengerdt, 1980). The HPF method adds an edge detailed image (calculated as a difference between the HRPI and its low-pass intensity modulated image) into the LRMI without any normalisation performed to it. Since the edge image tends a near-zero mean Gaussian curve distribution of data, its addition preserves the mean of the HRMI for all LPF window sizes, whereas the standard deviation, entropy, and deviation index values increase rapidly with the LPF window size. The use of the NF in the LMVM method thus preserved these spectral quantitative metrics for the bigger LPF window sizes (de Béthune et al., 1998a; 1998b).

The SRM technique determines the NF using global statistics of the LRMI and the HRPI whereas the LMVM technique determines it on a moving focal window. The global method is computationally fast and has been in practise for other methods such as the Modified Intensity Hue Saturation (Choi et al., 2008), and the Optimised High Pass Filter Addition (Gangkofner et al., 2008).

The role of NF is particularly important for reverse polarity images that contain features such as water and vegetation. For these features, the NIR band results in a high variance for its digital numbers in the LRMI. The NIR band, if compared to the visible bands, usually has a higher standard deviation than the HRPI. The normalising function in the SRM therefore over represents the edge details of the NIR band upon its injection to the LRMI. The NF can be reversed for the NIR by inversing the ratio but this has the effect of under representing the NIR edges. This highlights that the existing NF using either standard deviation ratio or covariance and variance ratio is not effective in normalising high spatial edge details of an image for the NIR.

The second modification (MSRM-2) uses the multiplication of contrast and luminance indices (Eq. 5.3 and 5.4 respectively) for the NF, as shown in Eq. 5.5. Contrast and luminance are important characteristics of an image. Contrast is a visual property that makes an object in an image distinguishable from other objects, and is determined by the variance of its brightness. Luminance is a brightness factor that is determined from the mean values of the image's digital numbers. The contrast and luminance of the edge detail derived from the HRPI are used to adjust the contrast and luminance of the LRMI before the edge detail is injected into the LRMI (or HRMI' if using the first modification).

Contrast and luminance distortion indices have been used to compare the quality of two images (Wang and Bovik, 2002). If these indices can be used for identifying image quality, then they can be used for generating quality image. The contrast distortion index compares two images based on the variance of brightness, while the luminance distortion index is derived from the mean of the digital numbers. The formulae we use for these indices are adapted from Wang

and Bovik (2002). These indices normalise the edge detail and preserve contrast and luminance properties based on both images.

$$\textbf{Contrast Distortion Index} = \frac{2 \cdot \sigma LRMI_n \cdot \sigma HRPI}{(\sigma LRMI_n^2 + \sigma HRPI^2)} \quad \textbf{(5.3)}$$

$$\textbf{Luminance Distortion Index} = \frac{2 \cdot \mu LRMI_n \cdot \mu HRPI}{(\mu LRMI_n^2 + \mu HRPI^2)} \quad \textbf{(5.4)}$$

$$\textbf{Contrast and Luminance NF} = \frac{2 \cdot \sigma LRMI_n \cdot \sigma HRPI}{(\sigma LRMI_n^2 + \sigma HRPI^2)} \cdot \frac{2 \cdot \mu LRMI_n \cdot \mu HRPI}{(\mu LRMI_n^2 + \mu HRPI^2)} \quad \textbf{(5.5)}$$

Table 5.1 compares the normalising weights using three different NFs - standard deviation, covariance and variance, and the contrast and luminance. The contrast and luminance NF method returns normalising weights less than one for all bands, while the other two methods return high normalising weights for NIR (1.85 and 1.76) and very low weights for the blue band (0.18 and 0.13). Normalising weights greater than one overly increase the mean and standard deviation of the fused image resulting in high brightness and contrast, and vice versa for very low normalising weights.

Both of these modifications are grouped into a method that is called the Contrast and Luminance Normalised (CLN) fusion. Figure 5.1 shows the flow diagram of the CLN fusion method.

Table 5.1: Effects of normalising function on band values for the QuickBird satellite image

Normalising Function	Equation	Normalising Weights for			
		Blue	**Green**	**Red**	**NIR**
Standard Deviation	$\frac{\sigma LRMI_n}{\sigma HRPI}$	0.18	0.40	0.43	1.85
Covariance-Variance	$\frac{Cov\,(LRMI_n, HRPI)}{Var(HRPI)}$	0.13	0.34	0.35	1.76
Contrast & Luminance	$\frac{2 \cdot \sigma LRMI_n \cdot \sigma HRPI}{(\sigma LRMI_n^2 + \sigma HRPI^2)} \cdot \frac{2 \cdot \mu LRMI_n \cdot \mu HRPI}{(\mu LRMI_n^2 + \mu HRPI^2)}$	0.35	0.69	0.62	0.82

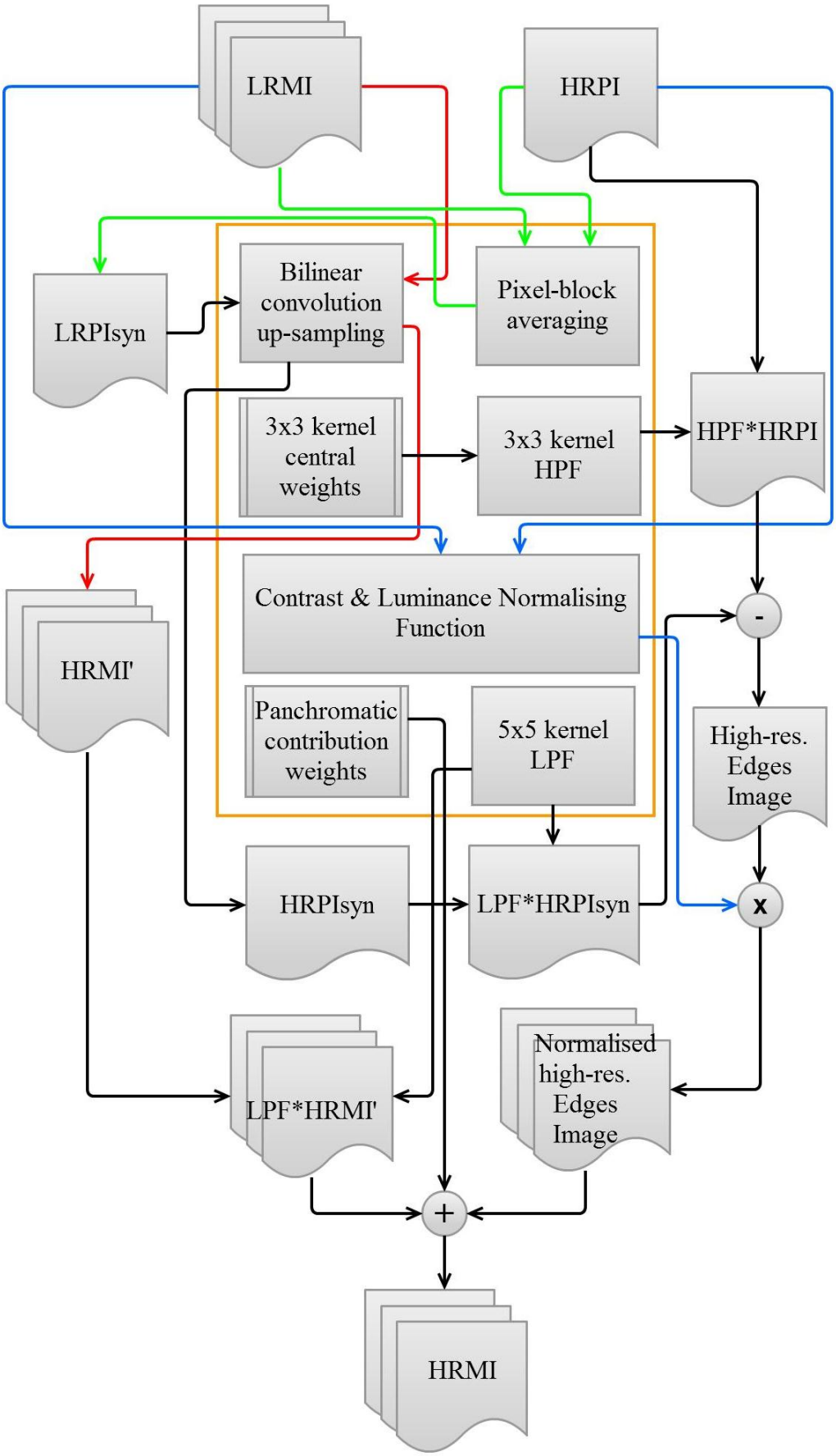

Figure 5.1: Flow diagram of the CLN fusion method.

The second set of images demonstrates the performances of these modifications for cross sensor applications. This set includes a Waikato region sub-scene of 180 x 120 pixels of SPOT-5 LRMI and a sub-scene of 2880 x 1920 pixels of a scanned colour aerial mosaic. These images (captured on the 29 December 2007 for SPOT and 27 November 2007 for the aerial image) represent predominantly lacustrine and riparian environments at the southern end of the Lake Karapiro along the Waikato River. These images were ortho-rectified by Landcare Research Ltd. and Terralink International Ltd. respectively. The spatial resolutions of SPOT-5 LRMI and the aerial image are 10 m and 0.625 m and are stored in 8-bit integer format. The principal component-1 (PC1) of the aerial image (Fig. 5.2f) is used as a surrogate for the HRPI (Fig. 5.2g). The SPOT LRMI (Fig. 5.2e) was re-positioned to less than 0.3 m along both axes to match its pixel geometry with the HRPI. During analysis, all derived images were stored as 8-bit floating point data.

For the SPOT LRMI and aerial HRPI data, MSRM-1+2 data fusion is performed using a default kernel central weight for the high-pass filter i.e. 17 and using 1.00 value of PCW. Two additional data fusion techniques, viz. principal component substitution (PCS) and optimised high-pass filter addition (OHPFA) are applied on these datasets to evaluate the performance of MSRM-1+2 against these widely and commonly used methods.

For PCS, ERDAS Imagine software offers three re-sampling choices for PCS; nearest neighbour (NN), bilinear (BL), and cubic convolution (CC). A BL re-sampling method is used as this generated a visually superior outcome as compared to NN. For the OHPFA, the default values are used, i.e. HPF kernel of 15 x 15 with central weight of 224 and a PCW of 1.35.

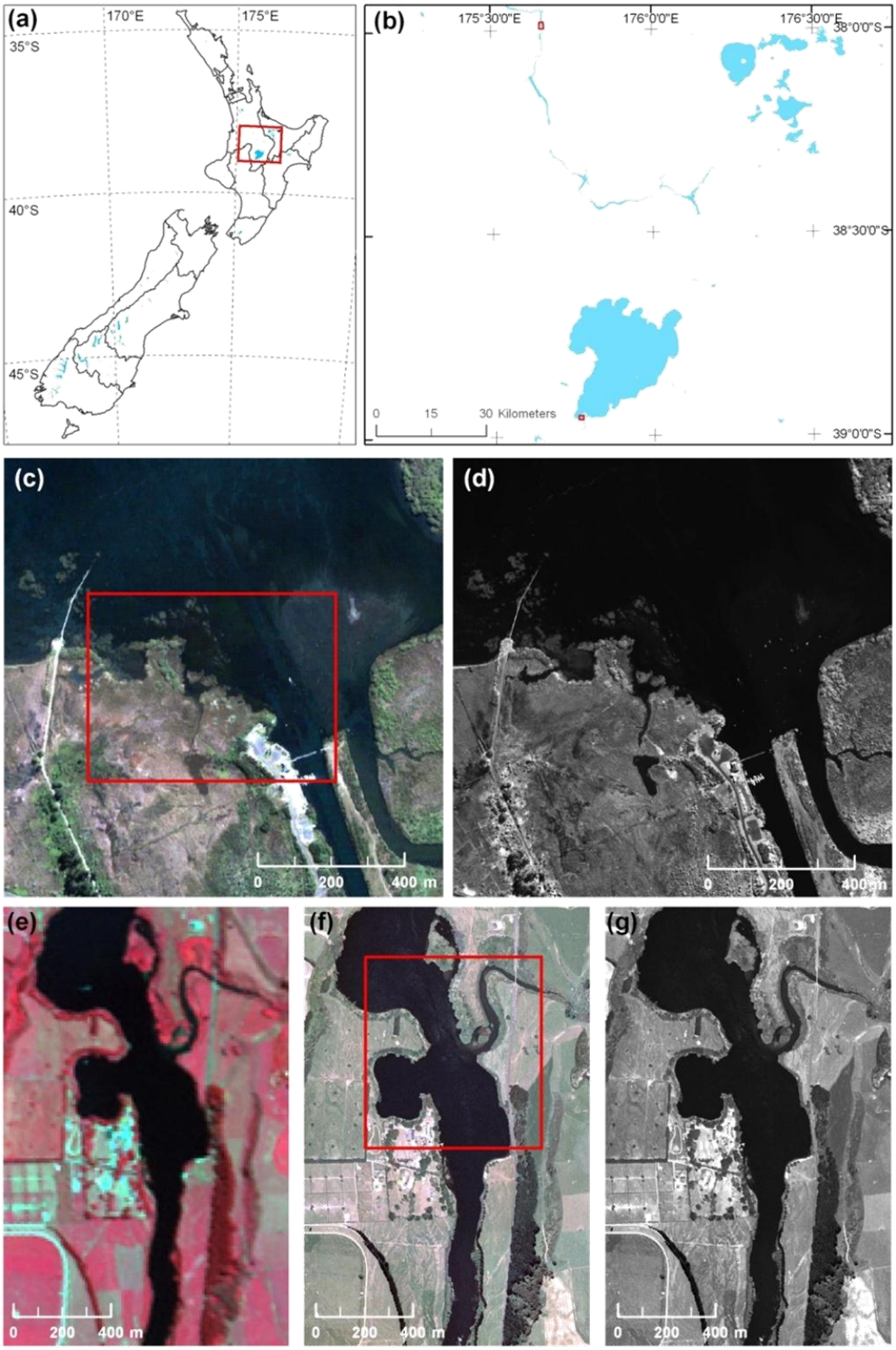

Figure 5.2: The images used for the evaluation of data fusion techniques; (a) Index map; (b) Location map of the images used – Southern edges of the Lake Karapiro and the Lake Taupo, NZ; (c) Sub-scene of the true colour composite of the QuickBird LRMI; (d) QB HRPI; (e) Sub-scene of the false colour composite of the SPOT LRMI; (f) Scanned colour aerial mosaic; and (g) Derived HRPI from the colour aerial mosaic. The square boxes in (b) and (f) are the extent of the zoomed-in areas shown in Fig. 5.2 and Fig. 5.5.

5.4 Methods for evaluating data fusion techniques

This research compares SRM, Modified SRM-1, Modified SRM-2, and Modified SRM 1+2 techniques qualitatively by visual inspection and quantitatively by means of spectral and spatial metrics (Gangkofner et al., 2008). We degrade the resulting HRMI to the same spatial resolution as the original LRMI and these are quantitatively compared (Li et al., 2010; Wald et al., 1997). To measure spectral quality, Pearson's correlation coefficient and root-mean squared error (RMSE) are used. To measure spatial quality, the RMSE of the Sobel filtered images are used (Gangkofner et al., 2008; Pradhan et al., 2006). The RMSE between the HRMI and the HRPI is labelled Sobel filter RMSE-I, whereas the RMSE between the original LRMI and the degraded HRMI (to the same resolution as the original LRMI) is labelled Sobel filter RMSE-II in the following sections.

Image classification is also applied to analyse the performance of the data fusion as this is a common end use (Nikolakopoulos, 2008). The purpose of the classification algorithm used in this research is to show that the spectral distortion effects are minimal, and there is an enhancement of the land cover edges (Colditz et al., 2006). de Carvalho et al. (2004) suggest that the high preservation of spectral information and spatial enhancement may improve the efficiency of spectral based classification, whether it would be supervised or unsupervised. Unsupervised classification based on the Iterative Self-Organising Data Analysis Technique (ISODATA) was used (Tou and Gonzalez, 1974). Unsupervised rather than supervised classification (such as maximum likelihood classification) was used because of the computational ease and its unbiased results (ERDAS, 2009; Xie et al., 2008). Thompson et al. (1998), in their study for coastal and river corridor mapping, have concluded that unsupervised classification can be an acceptable alternative to supervised classification due to the wide spectral variation between surface classes such as between water and vegetation. Five arbitrary clusters for the resulting images were derived. The convergence threshold was set to 0.995 for both QB as well as SPOT-5 and aerial

sensors, which means that if the spectral means of 99.5 % of pixels within arbitrary clusters are unchanged, the iterative process terminates.

Based on the ground knowledge of the region, these clusters were grouped into 4 land cover classes. For the QB image, these classes are; (i) water, (ii) freshwater vegetation (such as submerged and emergent vegetation and water logged terrestrial vegetation), (iii) sparse terrestrial vegetation (dominated by reeds), and (iv) dense terrestrial vegetation (such as grasses and trees). The low reflectance of development features such as roads have been assigned automatically to 'freshwater vegetation', while some high reflectance features are grouped as 'sparse terrestrial vegetation'. For the SPOT-5 and aerial image, four land cover classes are; (i) water, (ii) forest, (iii) grass, and (iv) urban structures.

Teggi et al. (2003) used classification comparison between the original image and the enhanced images using different fusion techniques as an instrument to measure the distortion of pixel spectra (caused due to the fusion method). They argued that fusion methods which yield low classification uncertainties and possess high similarity with the original classified data are assumed better. Congalton (2001) uses the classification difference images as a first step towards assessing the accuracy of spatial information. If one of the classification maps is assumed to be correct, then the difference between these images is a spatial error. Therefore, unsupervised classification results from the fused images are assessed visually and quantitatively using their difference from the ISODATA classified LRMI. The number of pixels for each class were used to show the overall percentage agreement for both images.

With the data fusion of the SPOT-5 and aerial image, it was not possible to compare the modifications with SRM because SRM cannot be applied across sensors. Instead, a comparison was made with principal component substitution (PCS), and optimised high-pass filter addition (OHPFA).

5.5 Results and discussion

Figure 5.3 provides a qualitative assessment of the four different data fusion techniques for a zoomed in area of the QB LRMI (Fig. 5.1*c*). All images in Figure 5.3*a-d* are displayed using the same colour lookup values and are stretched by three standard deviations. All methods, except MSRM-1, appear similar in quality and standout as being significantly sharp. There is visually insignificant difference and therefore quantitative assessment is required.

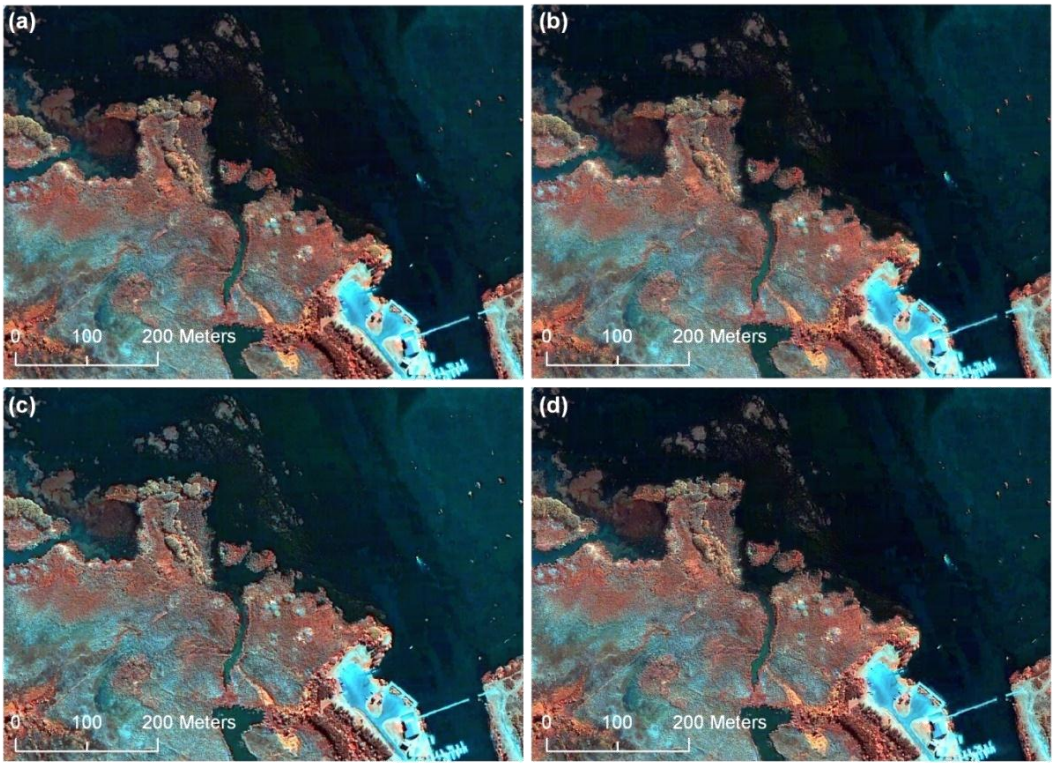

Figure 5.3: Qualitative assessment of the four different data fusion techniques; (a) Subtractive Resolution Merge; (b) Modified SRM-1; (c) Modified SRM-2; and (d) Modified SRM-1+2

Figure 5.4 summarises the band averages for the correlation and RMSE metrics for the different data fusion techniques. The results are mixed but MSRM-1+2 is quantitatively superior using two of the four metrics, and compared to SRM is superior for all the metrics. The use of contrast and luminance normalisation has nearly halved the Sobel filter RMSE-I value. The use of a pixel block averaging of the HRPI (MSRM-1) is superior to SRM for three of the four quantitative metrics but has a visually softer appearance. MSRM-2 and

MSRM-1+2 have similar low values for Spectral and Sobel RMSE values but MSRM-1+2 has a higher correlation with the original LRMI.

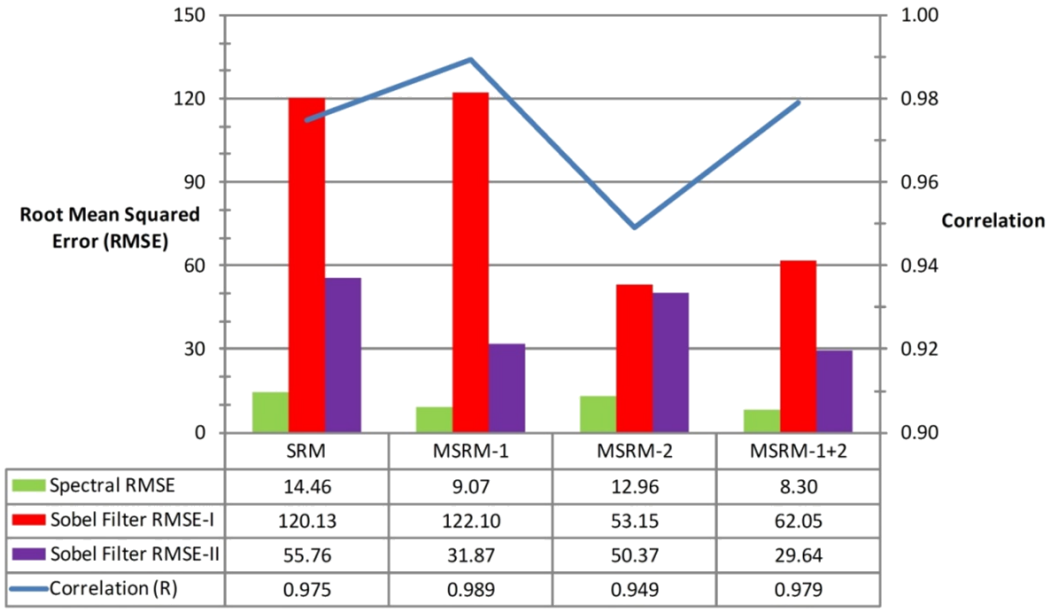

	SRM	MSRM-1	MSRM-2	MSRM-1+2
Spectral RMSE	14.46	9.07	12.96	8.30
Sobel Filter RMSE-I	120.13	122.10	53.15	62.05
Sobel Filter RMSE-II	55.76	31.87	50.37	29.64
Correlation (R)	0.975	0.989	0.949	0.979

Figure 5.4: Average correlation and RSME metrics for each data fusion techniques

Table 5.2 shows the quantitative assessment for each band. Although MSRM-1+2 performances best overall, at the individual band level it only performs best for the NIR band. The MSRM-1 is closest to the original LRMI for the three visual bands using both spectral quantitative metrics. For the MSRM-1 method, every band of the degraded HRMI other than the NIR band is found to have a very strong spectral correlation (98% or better) with LRMI. Both, the SRM and MSRM-1 techniques generate higher edge RMS error (Sobel Filter RMSE-I) for the NIR band. For the Sobel RMSE-II (between degraded HRMI and the LRMI), the MSRM-1 performs better than SRM for all the bands. For the SRM and MSRM-1, a high spatial edge RMSE for the NIR band suggests that the existing NF performs poorly.

Table 5.2: Quantitative assessment for each band of the QuickBird image

Techniques	Spectral measure between LRMI and degraded HRMI bands								Spatial measure between HRMI & HRPI and LRMI and degraded HRMI bands							
	Correlation (R)				Spectral RMSE				Sobel Filter RMSE-I (between HRMI & HRPI)				Sobel Filter RMSE-II (between LRMI & degraded HRMI)			
	Blue	Green	Red	NIR	Blue	Green	Red	NIR	Blue	Green	Red	NIR	Blue	Green	Red	NIR
SRM	0.970	0.975	0.976	0.979	4.19	8.62	8.87	36.16	112.14	68.89	67.02	232.47	15.99	32.75	34.26	140.06
MSRM-1	**0.986**	**0.989**	**0.990**	0.992	**2.88**	**5.59**	**5.73**	22.08	114.60	73.89	73.71	226.18	**11.53**	**20.90**	**21.08**	73.99
MSRM-2	0.914	0.935	0.952	0.995	7.19	13.89	12.49	18.26	**82.73**	**32.42**	**39.67**	**57.76**	28.80	55.30	49.94	67.43
MSRM-1+2	0.964	0.974	0.981	**0.998**	4.27	8.89	8.06	**11.51**	87.56	41.90	50.19	68.52	17.61	33.13	30.16	**37.65**

The second modification, which deals with the normalising function (NF) and is represented by MSRM-2 and MSRM-1+2, decreases the spatial RMSE of the NIR band to lower values, as would be expected since the NF value (Table 5.1) is less. The edge RMSE-I for MSRM-1+2 when compared with SRM, is reduced for all the bands, which shows that a contrast and luminance normalised method preserves spatial edges better than the existing SRM NF method. Although, the spectral metrics of the MSRM-1+2 are slightly lower than SRM for the visible bands, these metrics have been improved drastically for the NIR band.

Figure 5.5 shows the NIR RMSE map for the four different data fusion techniques. SRM and MSRM-1 have higher NIR change for most of the vegetation types. The MSRM-2 and MSRM-1+2 have the lower overall errors (Fig. 5.5c & 5.5d) and the major errors are located around high contrast features, such as infrastructure.

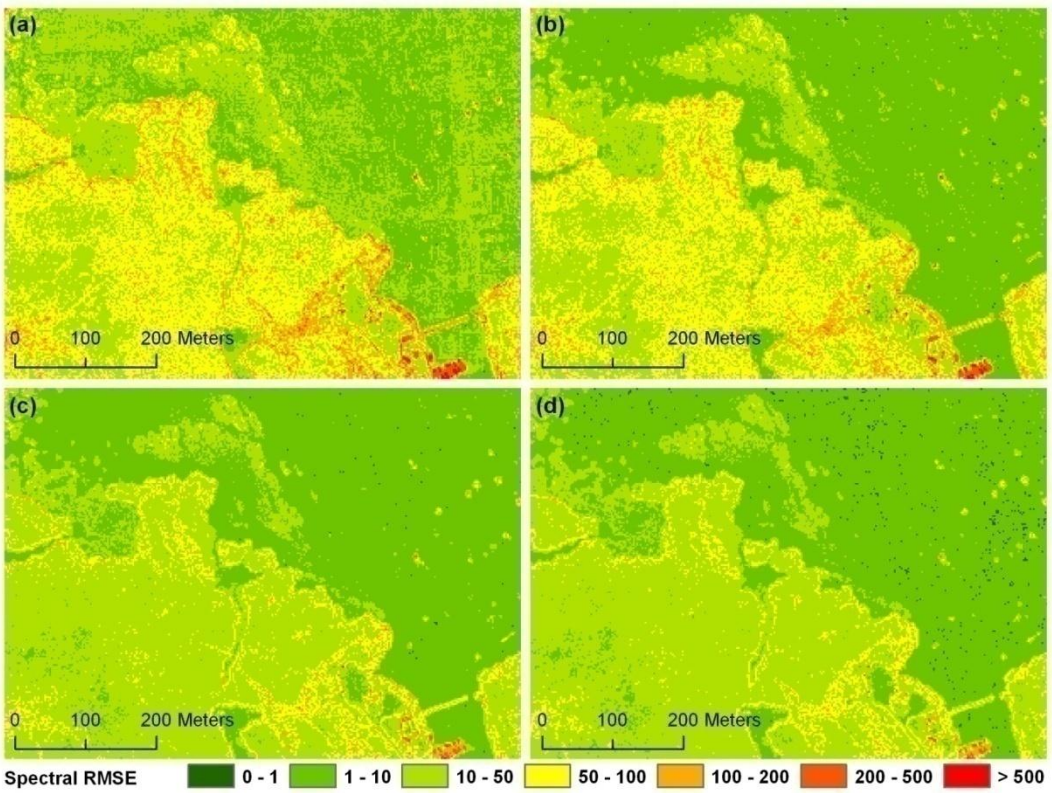

Figure 5.5: Spectral RMSE maps showing the error value for each pixel of band 4 (NIR); (a) SRM; (b) MSRM-1; (c) MSRM-2; and (d) MSRM-1+2

Figure 5.6 shows the RMSE map for the three different data fusion methods (PCS, OHPFA and MSRM-1+2) applied on the SPOT-5 SWIR band (band

4). It is clear that MSRM-1+2 has the least variations in the dynamic range during the fusion compared to PCS and OHPFA. In contrast to MSRM-1+2, PCS and OHPFA both have higher error for water features.

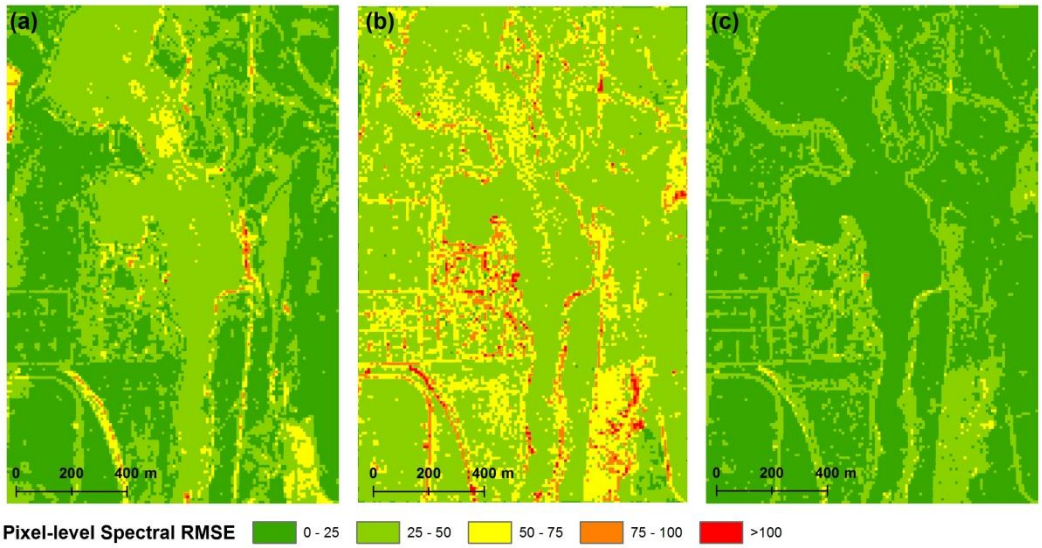

Figure 5.6: Spectral RMSE maps showing the error value for each pixel of band 4 (SWIR); (a) PCS; (b) OHPFA; and (c) MSRM-1+2

Figure 5.7 shows the qualitative assessment of the fused SPOT LRMI and the HRPI derived from the aerial image. All images in Figure 5.7a-d are displayed using the same colour lookup values and are stretched by three standard deviations. This qualitative assessment shows that PCS is rich in colours and appearing visually superior over OHPFA and MSRM-1+2.

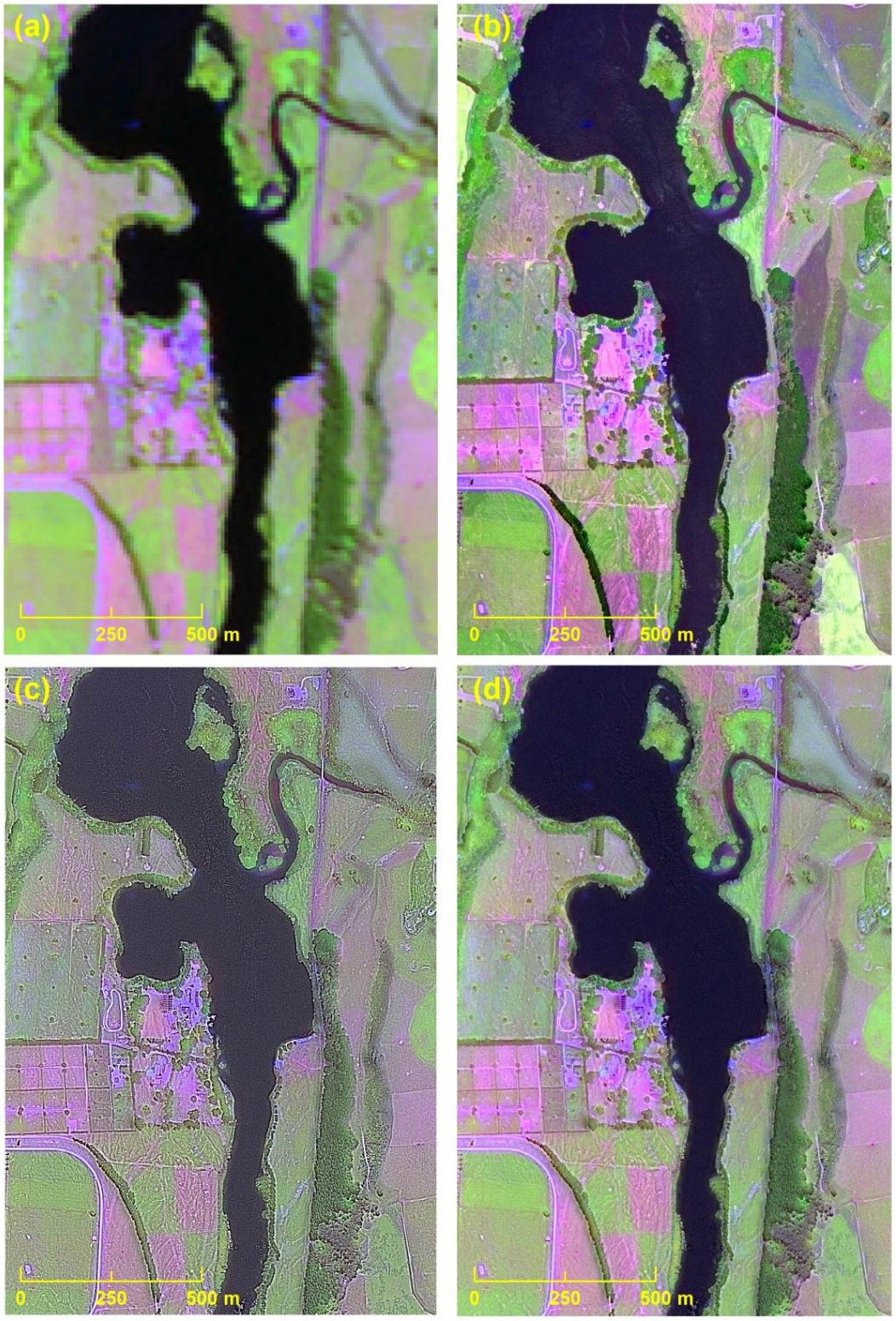

Figure 5.7: Data fusion of SPOT LRMI and the HRPI derived from the aerial image; (a) Colour composite of original SPOT LRMI bands 4, 3, 2 shown as R, G, B; (b) principal component substitution; (c) optimised high-pass filter addition; and (d) MSRM-1+2

Figure 5.8 summarises the results from the quantitative evaluation metrics and Table 5.3 shows the quantitative assessment for each band. The

RMSE metrics for MSRM-1+2 are reduced spectrally and spatially and clearly show that MSRM-1+2 has outperformed the other techniques.

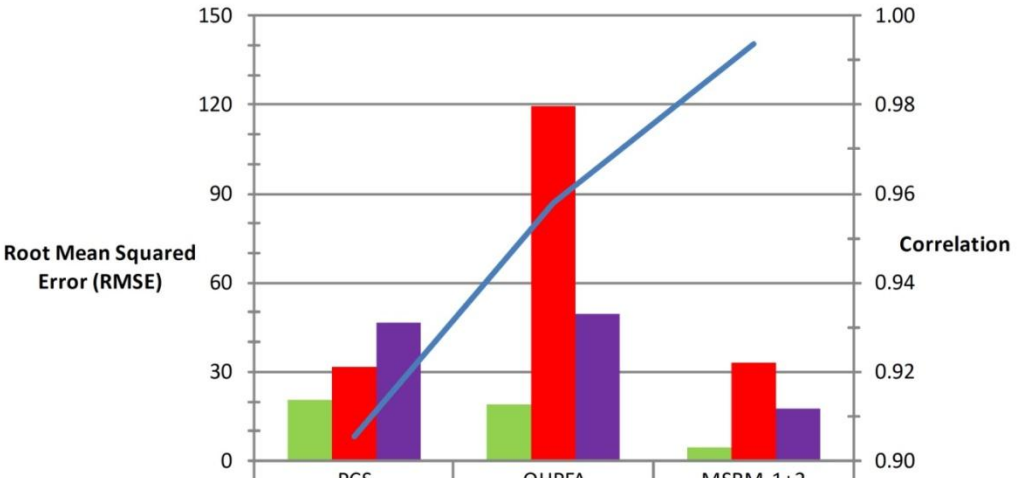

	PCS	OHPFA	MSRM-1+2
Spectral RMSE	20.353	19.156	4.367
Sobel Filter RMSE-I	31.439	119.253	33.028
Sobel Filter RMSE-II	46.700	49.528	17.822
Correlation (R)	0.905	0.958	0.994

Figure 5.8: Average correlation and RSME metrics for each data fusion techniques using SPOT LRMI and aerial HRPI data

Table 5.3: Quantitative assessment for each band of the QuickBird image

Techniques	Spectral measure between LRMI and degraded HRMI bands								Spatial measure between HRMI & HRPI and LRMI and degraded HRMI bands							
	Correlation (R)				Spectral RMSE				Sobel Filter RMSE-I (between HRMI & HRPI)				Sobel Filter RMSE-II (between LRMI & degraded HRMI)			
	Green	Red	NIR-I	NIR-II	Green	Red	NIR-I	NIR-II	Green	Red	NIR-I	NIR-II	Green	Red	NIR-I	NIR-II
PCS	0.903	0.916	0.908	0.894	12.77	15.03	25.72	27.90	49.98	44.28	**19.03**	**12.46**	30.55	35.53	57.77	62.95
OHPFA	0.952	0.951	0.962	0.967	12.50	15.84	24.02	24.27	64.73	86.71	160.00	165.58	38.23	50.66	61.05	48.17
MSRM-1+2	**0.991**	**0.993**	**0.995**	**0.997**	**3.67**	**4.11**	**5.13**	**4.55**	**22.52**	**30.25**	39.20	40.14	**14.55**	**16.86**	**21.92**	**17.95**

The unsupervised HRMI and LRMI classification results are shown in Figure 5.9 (for QB image) and Figure 5.10 (for SPOT-5/aerial image). A fusion process incorporates spatial details of the HRPI into the fused image which results in an increase of texture that often leads to undesired speckled classification. Colditz et al. (2006) have argued that an image fusion technique is considered good for image classification purposes if it generates less speckled classes. For the QB image, MSRM-2 and MSRM-1+2 both have the least speckled classes and create larger contiguous patches of the same land cover classes as compared to the SRM and MSRM-1.

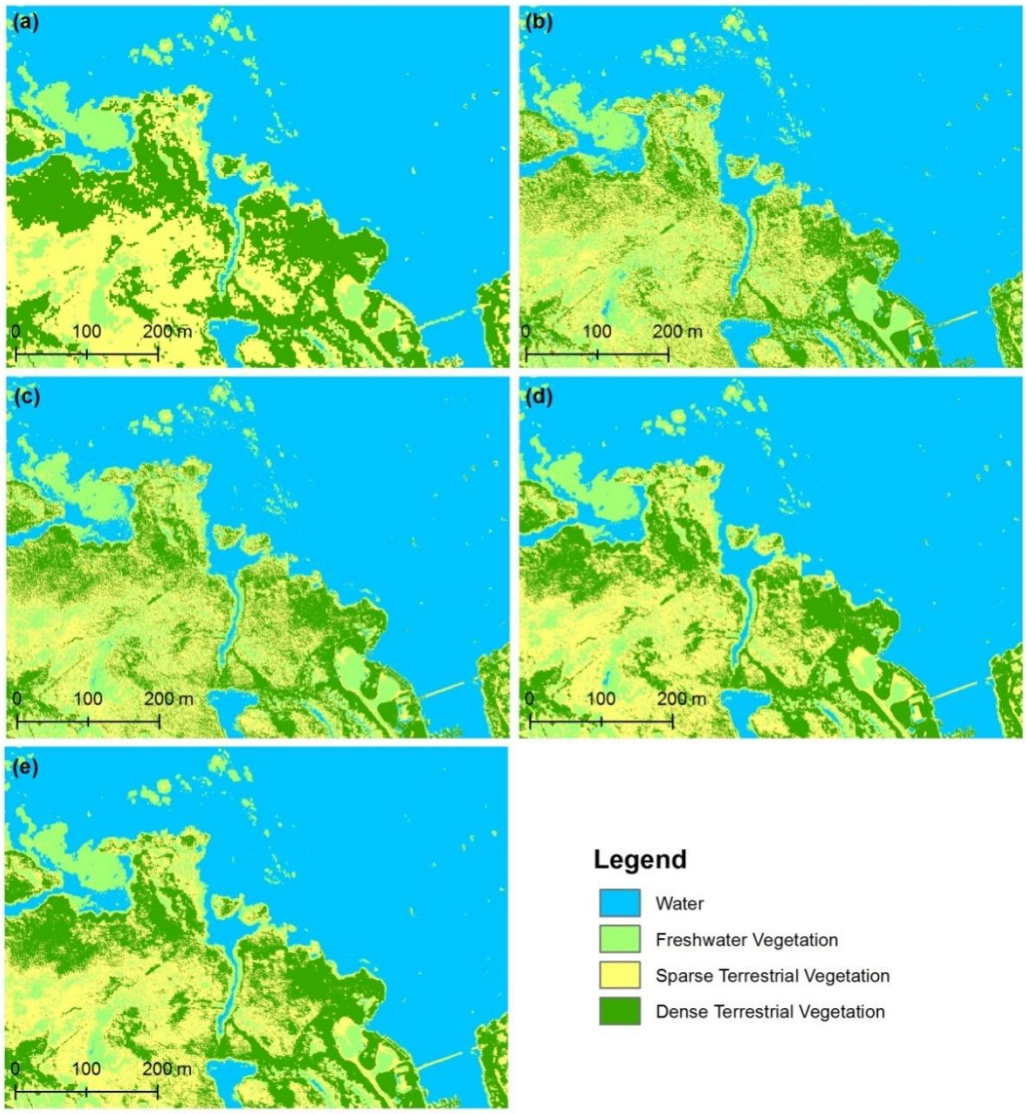

Figure 5.9: Unsupervised classification based landcover maps for QB image; (a) original LRMI; and fused HRMI's using (c) SRM; (d) MSRM-1; (e) MSRM-2; and (f) MSRM-1+2 techniques

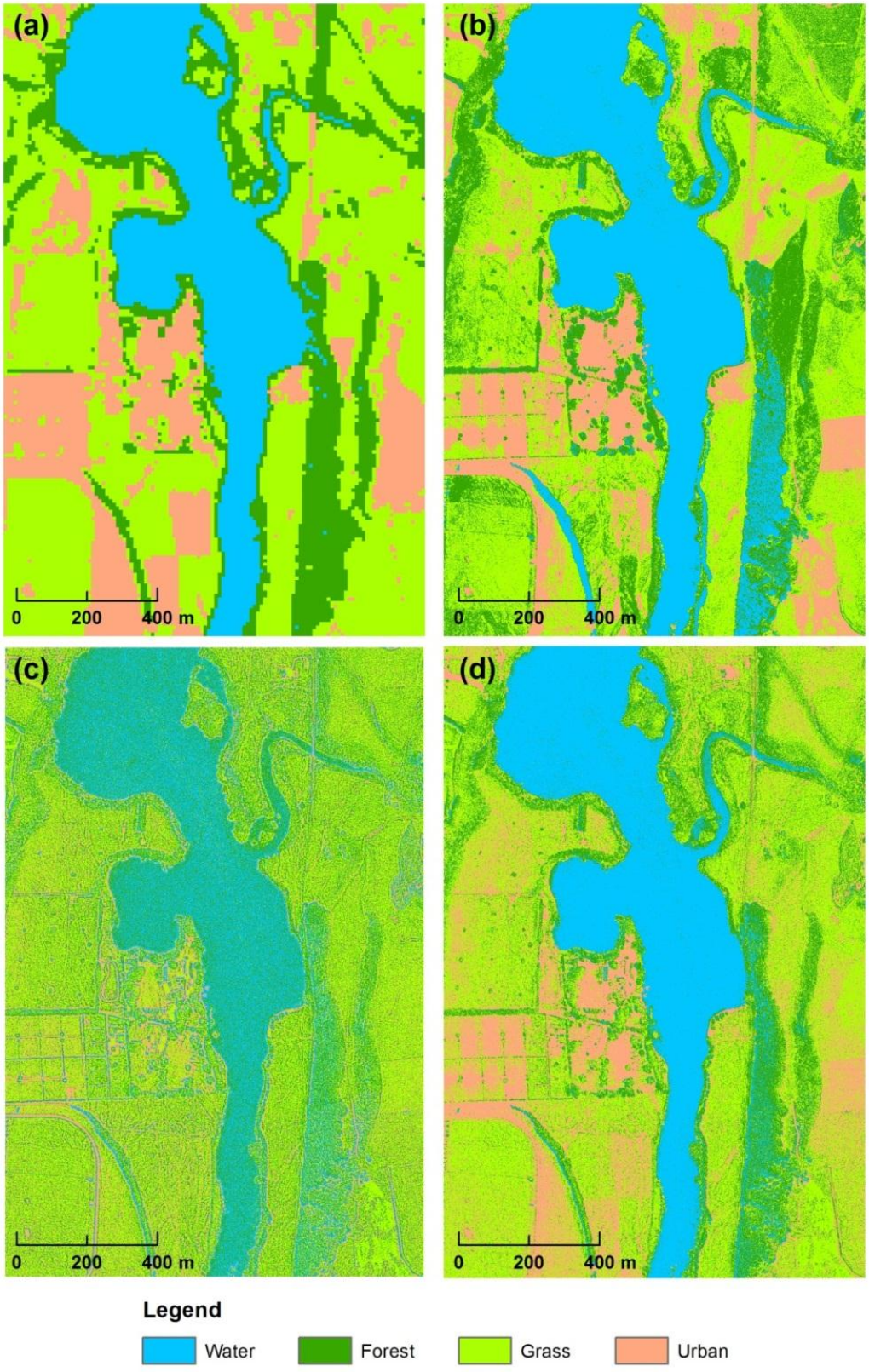

Figure 5.10: Unsupervised classification of data fusion results for SPOT/aerial image; (a) SPOT LRMI; and SPOT/aerial HRMIs using (b) PCS; (c) OHPFA; and (d) MSRM-1+2

For the SPOT-5/aerial image fused data, OHPFA technique has produced a highly speckled classification, which limits its ability for correct edge detection. The PCS technique has produced the least speckled classes, however; it is erroneously showing a dark shaded forest class as water, which is due to high spectral RMS errors in fused pixels for this class (see Fig. 5.6a).

The difference in classification results between the initial LRMI image and the different data fused images are shown in Figure 5.11 for the QB image and Figure 5.12 for the SPOT/aerial image. Class-by-class change detection comparisons (calculated by computing zonal statistics for each land cover class) between the results of unsupervised classification of the original and fused images are shown in Tables 5.4 (for QB image) and 5.5 (for SPOT/aerial images). These classification difference maps graphically quantify change and show areas of classification agreement and disagreement as shades of yellow and grey respectively. With data fusion, there should be classification improvements to the edges of features and this will show as a change. Changes, as shown in Fig. 5.11 and 5.12 should be limited to the edges rather than the centre of features. The MSRM-1+2 fusion method (Figs. 5.11d and 5.12c) has the least number of changed pixels (Table 5.4) and these are distributed along the edges. This clearly shows the effectiveness of the MSRM-1+2 fusion technique over the other methods.

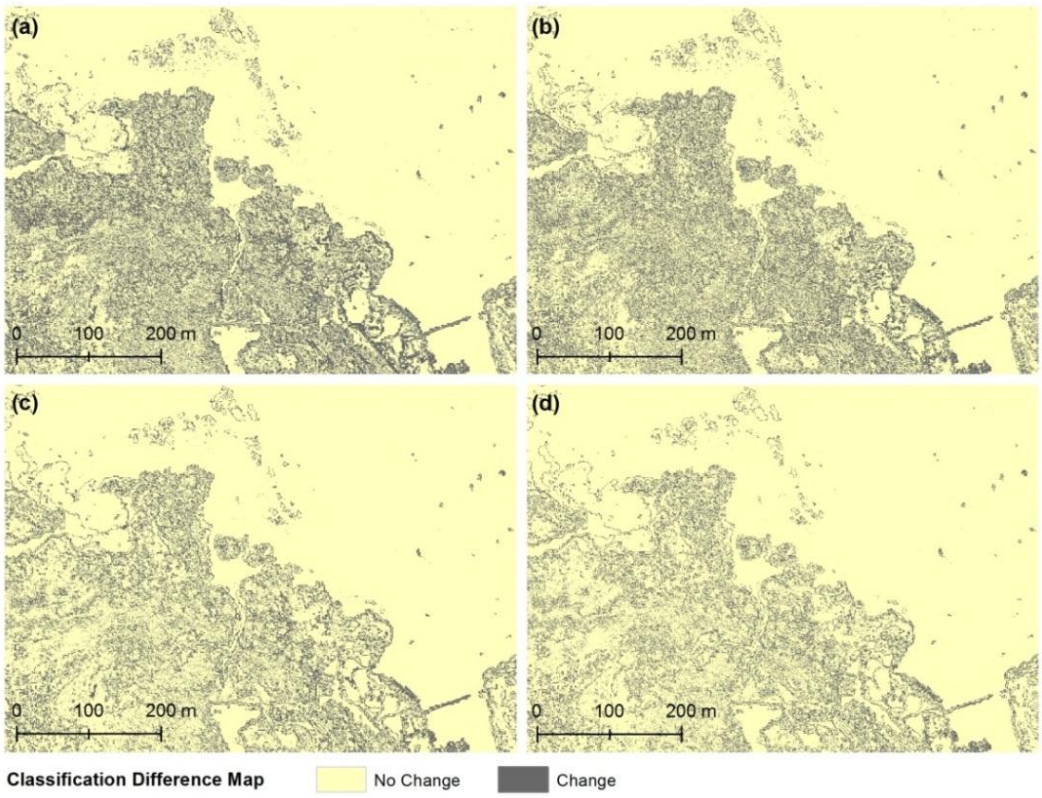

Figure 5.11: Change detection map between LRMI and HRMI land cover classes; (a) SRM; (b) MSRM-1; (c) MSRM-2; and (d) MSRM-1+2.

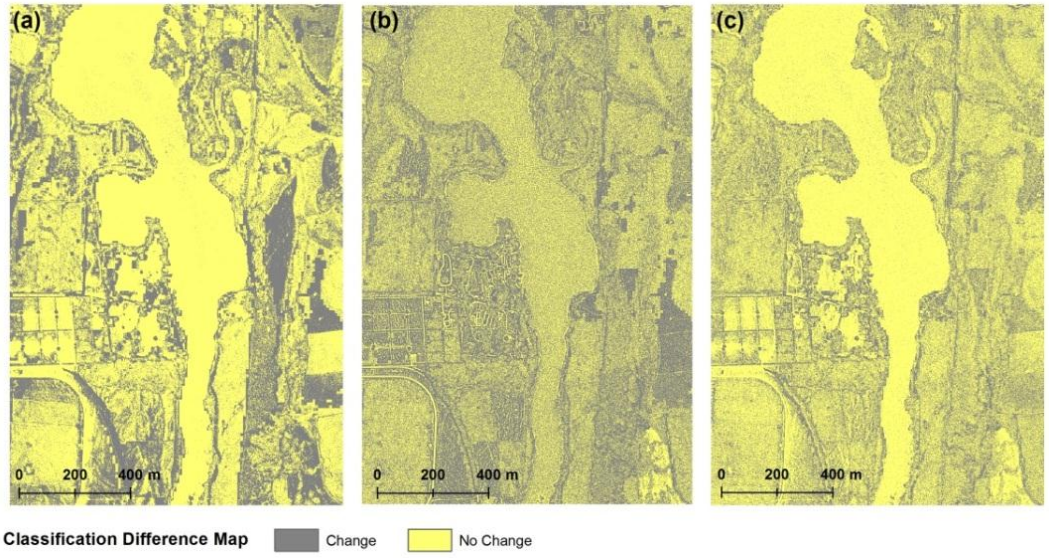

Figure 5.12: Change detection between LRMI and HRMI unsupervised classes; (a) PCS; (b) OHPFA; and (c) MSRM-1+2

Table 5.4: Classification change detection statistics (similarity %) between original and different fused images for QB dataset

Unsupervised classification comparison between LRMI and HRMI	Water	Freshwater Vegetation	Sparse Terrestrial Vegetation	Dense Terrestrial Vegetation	Overall Similarity (%)
SRM	99.17	61.86	54.07	64.35	80.25
MSRM-1	99.23	69.94	58.86	70.31	83.06
MSRM-2	**99.40**	72.77	69.70	78.51	87.20
CLN	99.35	**77.01**	**72.54**	**81.64**	**88.69**

Table 5.5: Classification change detection statistics (similarity %) between original and different fused images for SPOT-5/aerial photo dataset

Unsupervised classification comparison between LRMI and HRMI	Water	Forest	Grass	Urban	Overall Similarity (%)
PCS	**96.74**	46.77	62.22	56.60	66.06
OHPFA	59.53	35.24	49.95	25.66	45.21
CLN	95.18	**55.22**	**64.07**	**59.38**	**68.42**

5.6 Conclusions

This research demonstrated two modifications to the SRM technique. The first modification uses pixel-block (zonal) average of the HRPI, which negates the need to calculate a synthetic HRPI using band weights and the dependence on images from dual resolution sensors. The second modification uses contrast and luminance indices to normalise the edge data, which preserves the relative band intensities for the edges. The computational efficiency of these modifications is comparable to SRM because it uses similar global and focal functions.

The combination of these modifications produces a fused image with less spectral and spatial distortion than the standard SRM. This reduction in distortion is particularly the case with the NIR band. This is important because NIR is used for vegetation and land use mapping.

The SRM method offers a user-controlled PCW to choose a balance between spectral distortion and spatial edges. For the standard SRM technique, higher spatial edges are reduced in the NIR band by reducing the PCW from its

default of 1.0. It is observed that this compromises the spatial edge details within the visible bands. A contrast and luminance NF ensures that no band is over or under represented and reduces the range of NF weights for all the bands.

A review of statistics of selected full scenes of QuickBird images showed that certain images whose histograms are skewed (due to the dominance of certain features such as a large vegetation field) or possess bi- or multi-modal data (such as contrasting water and vegetation features) tend to show higher standard deviation of the NIR band than the HRPI data. Moreover, certain visible bands such as blue have lower standard deviations, which result in poor spatial contrast of this band. A conventional NF thus under and over represent certain edges for these extreme bands. Most QuickBird scenes of New Zealand have this limitation due to the contrasting landscape. A contrast and luminance NF will maintain a balance of spectral and spatial distortions in the fused outcome.

This has demonstrated a method using SPOT LRMI and colour aerial photography that can fuse cross sensors data. This independence of sensor is a major advantage because of the increasing mix of aerial and satellite images captured. We are calling MSRM-1+2 Contrast and Luminance Normalised (CLN) fusion, because it is a significant adjustment to the standard SRM technique, and the application of contrast and luminance indices is original for data fusion. Hill et al. (1999, p.6) stated that the NIR band "is generally considered the most problematic channel for image fusion" and should not be significantly distorted because of its importance for vegetation mapping. CLN fusion will help resolve this major issue.

Chapter 6

Conclusions and research implications

The overall motivation for this research was to investigate the use of remote sensing for mapping freshwater aquatic environments. A review of images available for New Zealand showed that image data is rapidly improving and that there is a wide selection of images available, and there will be an even greater selection available in the future. Of particular importance is the utilisation of regional and national data sharing arrangements, such as KiwImage/QuickBird (kiwImage, n.d.), LUCAS/SPOT-5 (MfE, 2010), and WRAPS (E. W., n.d.). These have the advantage of being freely available to regional and central government agencies.

Freshwater mapping using remotely sensed data requires the selection of suitable sensors capable of detecting and differentiating narrow and elongated margins of diverse and heterogeneous vegetation with surrounding water of varying quantity and quality. For such purpose, a combination of high spatial, spectral, radiometric and temporal resolution RS sensor which is capable of capturing large spatial extents is required. There is no ideal sensor which can offer these resolution qualities; however through data fusion (DF), these qualities can be achieved. This research, therefore, focused on exploring the use of DF and the associated complexities. As described in the introduction, specific research questions were identified and these have been addressed as follows.

6.1 What are the best DF techniques for aquatic environment data and what are their limitations?

In order to answer this question, DF techniques were classified into three groups: (i) spatially-centric (LMVM, OHPFA, MSRM-1, and MSRM-1+2 – also

referred as CLN), (ii) spectrally-centric (BT, and PCS), and (iii) hybrid (SRM-ERDAS, SRM-OLS, SRM-LAD, and MSRM-2).

This research concludes that in general the spatially-centric DF techniques performed best in preserving the spatial and spectral integrity of the multispectral data for different freshwater environments. Hybrid techniques, which assimilate spatially-centric processing into their inherent spectrally-centric algorithms, in general out-performed the spectrally-centric techniques.

The original SRM-ERDAS and marginally inferior OHPFA techniques out-performed other DF methods. SRM-ERDAS uses a more robust processing framework that preserves edges and has an efficient modulation when compared to the OHPFA technique. However, the SRM-ERDAS techniques can only fuse data for a limited range of sensors whose spectral band weights are predetermined and provided by the software. OHPFA does not have this limitation. A limitation with both the SRM-ERDAS and the OHPFA techniques was a profound spatial edges error associated with high-variant semi-aquatic images. This was found to be due to an ineffective use of a global normalisation function, which did not compensate for the high variance of NIR band in aquatic images. These limitations were subsequently addressed in the following research questions.

6.2 What is the contribution of the spectral bands for different spectrally centric DF techniques?

This research has shown that the contribution of the spectral band weights varies significantly between the different DF techniques. For example the PCS used 70 % of the NIR band for the QuickBird image, while the SRM used only 40 % and the BT 33 %. This variation resulted in significant differences in the resulting fused images.

This research has demonstrated how band weights can be calculated using OLS and LAD regressions, and that these weights can be used for SRM-ERDAS DF. This removes the limitation of SRM-ERDAS being restricted to images

with predetermined band weight. The OLS and LAD regression had similar performance; however, the OLS regression is a preferred method due to its efficiency.

6.3 How to normalise the spatial edges for freshwater environments?

This research demonstrated that existing normalising functions built into DF techniques fail to properly account for the variance in multispectral bands, which becomes particularly problematic for images of freshwater environments that are bimodal. This creates over-represented edges for different bands. For the images analysed in this study, the NIR band was over represented.

A solution to this problem was discovered by using a contrast and luminance index to normalise the spatial edges. This normalising function was integrated into the MSRM-1 technique to create a new technique called contrast and luminance normalisation (CLN) fusion. This technique was qualitatively and quantitatively shown to improve image quality both spectrally and spatially. In particular, CLN fusion minimised the over-representation of the spatial edges of the NIR band. It also improved the classification of aquatic vegetation mapping. Not only does CLN fusion outperform SRM, but overcomes the many limitations of SRM. Unlike SRM, CLN is capable of fusing multi-sensor, multi-platform, multi-temporal, and multi-resolution data because it does not rely on predefined band weights.

6.4 Limitations and future research

This research was applied to small areas distributed over three sites related to freshwater environments and used only four different images – QB, Vexcel, SPOT-5, and aerial images. Without further research, care is needed to generalise the results to other environments and may be different for other images. The performance of DF techniques has not been tested for terrestrial or marine environments. In a marine environment, submerged seaweeds, and

corals are generally present rather than emergent vegetation. In a terrestrial environment there are many other extreme contrast features such as desert and snow. Testing in other environments and scaling-up to larger areas for a range of land-cover types is recommended.

Although many different DF techniques have been reviewed in this research there are opportunities to consider other techniques. A spatially-centric group of techniques employing multi-resolution analysis has not been included in this research because the initial focus of the research was on SRM, which uses a different framework. The range of DF techniques tested also needed to be limited for practical reasons.

The CLN fusion technique derived from this research is a spatially-centric DF technique because it bypasses the band weights. It therefore partially resembles the multi-resolution analysis framework, which decomposes each image into a series of band-pass images. Multi-resolution analysis techniques overcome the problem of spectral distortion but add aliasing or pseudo-edges effects in the resultant image (Alparone et al., 2007; Khan et al., 2008). The CLN fusion technique performs a single step decomposition of the HRPI using pixel block averaging (PBA). It is recommended to evaluate the performance of CLN fusion against similar spatially-centric techniques.

A recurring issue with the evaluation of data fusion techniques is the absence of a reference image for comparison of results (Pohl and Van Genderen, 1998; Wald et al., 1997). Therefore, a range of techniques have been used for evaluating the results from this research. This includes simulating existing data by down-sampling the results to a lower resolution to compare with the input data, down-sampling the input data to lower resolutions then enhancing back to the same resolution to compare with the input data, qualitative and quantitative comparisons, and unsupervised classification. Qualitative assessment is required to show that an improvement exists, and quantitative analysis is used to determine spectral and spatial consistency with the input images. Image classification is a relevant measure of fusion performance, as this is a desired end

use, which was the case with this research. Future research could focus on testing classes based on existing land-cover types rather than unbiased arbitrary clusters.

6.5 Implications for mapping freshwater environments

There are definite advantages in using the CLN fusion technique for mapping freshwater vegetation. As mentioned previously, there are national and regional level multi-platform images available that have a range of spatial and spectral resolutions. Modern data fusion techniques, such as SRM, cannot fuse data across platforms and have major problems with band normalisation. The CLN technique addresses these problems. SPOT-5 can now be merged with colour aerial photographs such as WRAPS for the Waikato region. SPOT-5 has the NIR band which is an advantage for vegetation mapping when compared with aerial photography such as WRAPS. SPOT-5 also has the added advantage of being cheaper than QB. It is also quicker to process and has less seasonal variability across images. The CLN fusion technique using SPOT-5 and aerial images can produce the same spatial resolution images as QB data.

The ability to generate high spectral and spatial resolution images by using data fusion means that detailed maps of freshwater environments can be produced. The vegetation of wetlands, lake fringes, and large rivers, such as the Waikato River, can be mapped.

This research has not only developed a new fusion technique, i.e. CLN, but also a spatial model for deriving band weights using OLS regression. These methods can be built into existing commercial software for wider application. The contrast and luminance index has been shown to enhance the SRM technique. It could also be used to enhance other data fusion techniques that use a normalisation function, such as OHPFA.

Data fusion techniques are becoming increasingly relevant, since remotely sensed data from a range of new sensors are becoming available. Research on DF techniques to fuse multi-platform and multi-resolution data is

therefore important. As demonstrated by this research, the performance of DF techniques can be improved. This research has focused on freshwater environments, and shown that a high variance in spectral bands creates problems but that through research these can be resolved. DF research is therefore a productive research endeavour that needs to be pursued for a range of image platforms and environments.

Appendix A

Calculating quantitative evaluation algorithms using ERDAS model maker

A.1 Pearson's correlation coefficient

Pearson's correlation coefficient is the most popular similarity metric in image fusion (Wang et al. 2005). It measures the similarity between two or more paired datasets and is determined as the ratio of the covariance to the product of the standard deviations. In its current context, it measures the spectral similarity by determining the degree of linear relationship between the original LRMI and the fused HRMI, which is at same resolution as the LRMI after degradation using pixel-block averaging low-pass modulation. It ranges from -1 to +1, where -1 indicates a complete dissimilarity and +1 a perfect match between two images. The problem with the correlation coefficient is it's insensitivity to a constant gain and bias between two images. It is determined as;

$$\mathbf{r}\,(\mathbf{X}|\mathbf{Y}) = \frac{\mathbf{Cov}\,(\mathbf{X},\mathbf{Y})}{\mathbf{SD_X \cdot SD_Y}} \quad \textbf{(A.1)}$$

where n is the number of pixels in any band of image X (i.e. $HRMI_{DEG}$) or Y (i.e. LRMI).

Covariance (or Cov) is the measure of common variation observed in two or more datasets (de Smith et al., 2009) and is determined as;

$$\mathbf{Cov}\,(\mathbf{X},\mathbf{Y}) = \frac{\mathbf{1}}{\mathbf{n}}\sum_{\mathbf{i=1}}^{\mathbf{n}}(\mathbf{X_i} - \overline{\mathbf{X}})(\mathbf{Y_i} - \overline{\mathbf{Y}}) \quad \textbf{(A.2)}$$

where $\overline{X}$ is the arithmetic mean of X

Likewise, standard deviation (or SD) is a square root of the average squared difference of dataset from its mean. Mathematically, it can be represented as;

$$\mathbf{SD}_X = \sqrt{\frac{1}{\mathbf{n}}\sum_{\mathbf{i=1}}^{\mathbf{n}}(\mathbf{X_i} - \overline{\mathbf{X}})^2} \quad \textbf{(A.3)}$$

$$\mathbf{SD}_\mathbf{Y} = \sqrt{\frac{1}{\mathbf{n}}\sum_{\mathbf{i=1}}^{\mathbf{n}}(\mathbf{Y_i} - \overline{\mathbf{Y}})^2} \quad \textbf{(A.4)}$$

A.2 Root mean squared error (RMSE)

The Root Mean Square Error (RMSE) measures the standard error between the LRMI and the degraded HRMI (Li et al. 2010) and more sensitive way to measure spectral infidelity than Pearson's correlation (Gangkofner et al. 2008; Pradhan et al. 2006). It is achieved as;

$$\mathbf{RMSE} = \sqrt{\frac{1}{n}\sum_{\mathbf{i=1}}^{\mathbf{n}}(\mathbf{HRMI_{DEG}} - \mathbf{LRMI})^2} \quad \textbf{(A.5)}$$

where n is the number of pixels of any band of the LRMI.

RMSE can be calculated at a global level and a pixel level. The global RMSE value indicates how close both datasets match, however it does not provide any detail about which features have changed or the magnitude of these changes. Such changes can be assessed qualitatively if mapped at the pixel level. A flow diagram of the global RMSE calculation process is shown in Fig. A.1.

To calculate RMSE at pixel level, the LRMI mask was used that had unique value for every individual pixel of the LRMI. Therefore, the value of n in such case is 16 for the QB data, since there are 16 pixels of the HRMI that fall within a pixel of the LRMI. A flow diagram of the pixel level RMSE calculation process is shown in Fig. A.2.

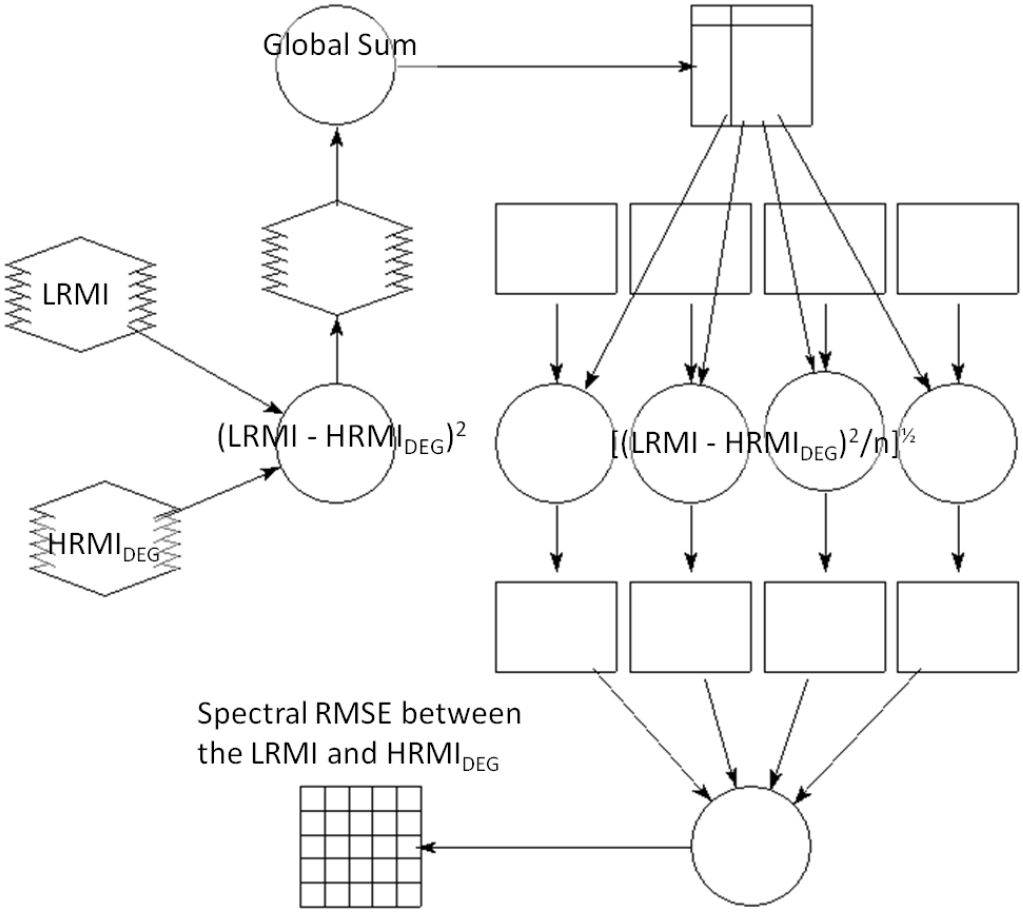

Figure A.1: ERDAS spatial modeller flow diagram showing the process of calculating a global spectral RMSE between the degraded HRPI and LRMI

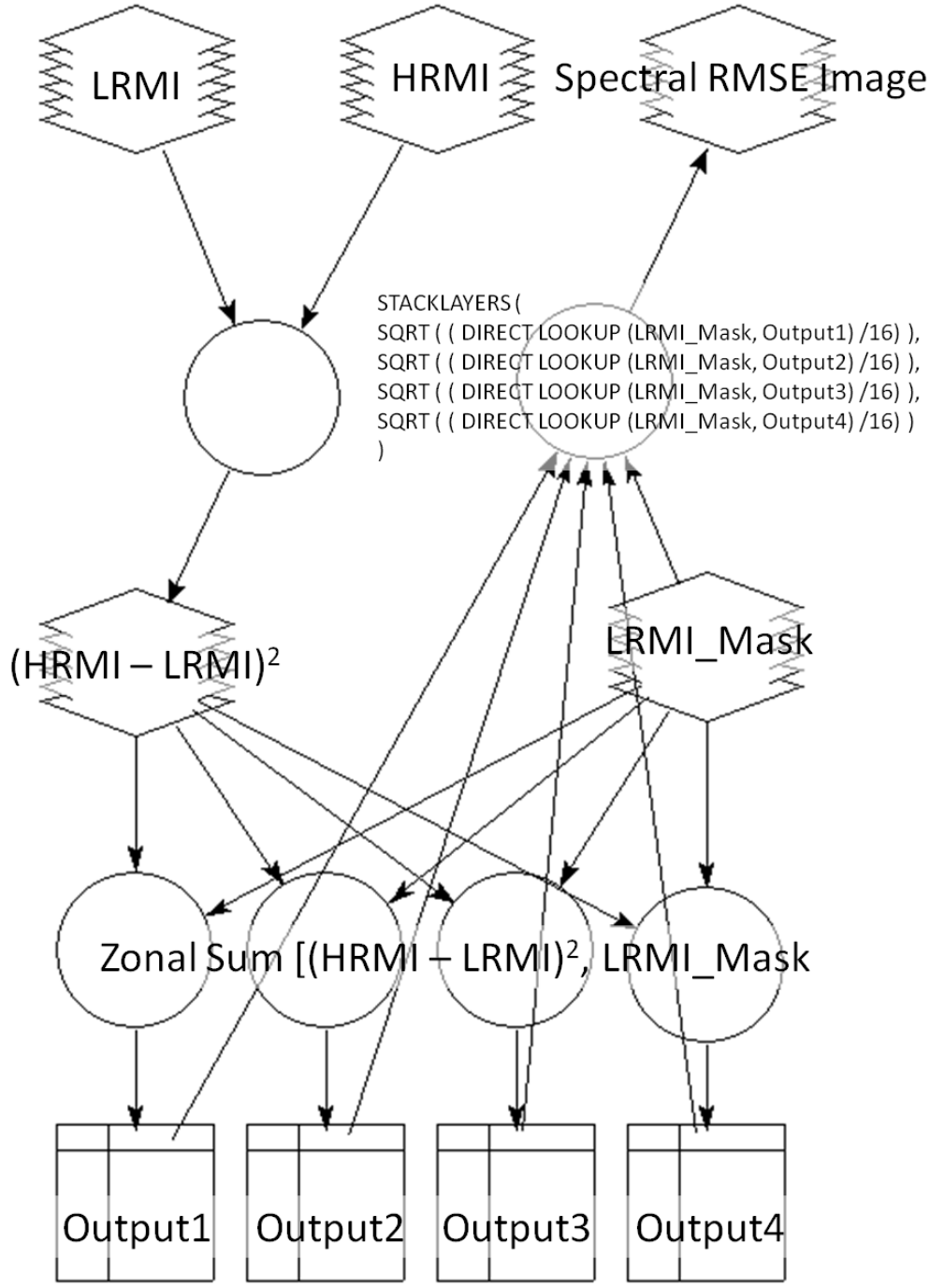

Figure A.2: ERDAS spatial modeller flow diagram showing the process of calculating spectral RMSE between the degraded HRPI and LRMI at a pixel level

A.3 Spatial RMSE using the Sobel filter

The Sobel filter based RMSE is a quantitative method for comparing the absolute edge magnitude difference of the HRPI and the fused HRMI. The horizontal and vertical edges of the HRMI and HRPI are generated using two 3 x 3-kernel Sobel filters, in horizontal and vertical directions. The Euclidian distance

of these two horizontal and vertical edge intensities returns an edge magnitude. The equation for the Sobel filter edge magnitude is:

$$\mathbf{M} = \sqrt{\mathbf{M_x^2} + \mathbf{M_y^2}} \quad \textbf{(A.6)}$$

Where:

$$\mathrm{M_x} = \begin{bmatrix} -1 & 0 & +1 \\ -2 & 0 & +2 \\ -1 & 0 & +1 \end{bmatrix} * \text{Image and } \mathrm{M_y} = \begin{bmatrix} -1 & -2 & -1 \\ 0 & 0 & 0 \\ +1 & +2 & +1 \end{bmatrix} * \text{Image}$$

A flow diagram of the process is shown in the Fig. A.3.

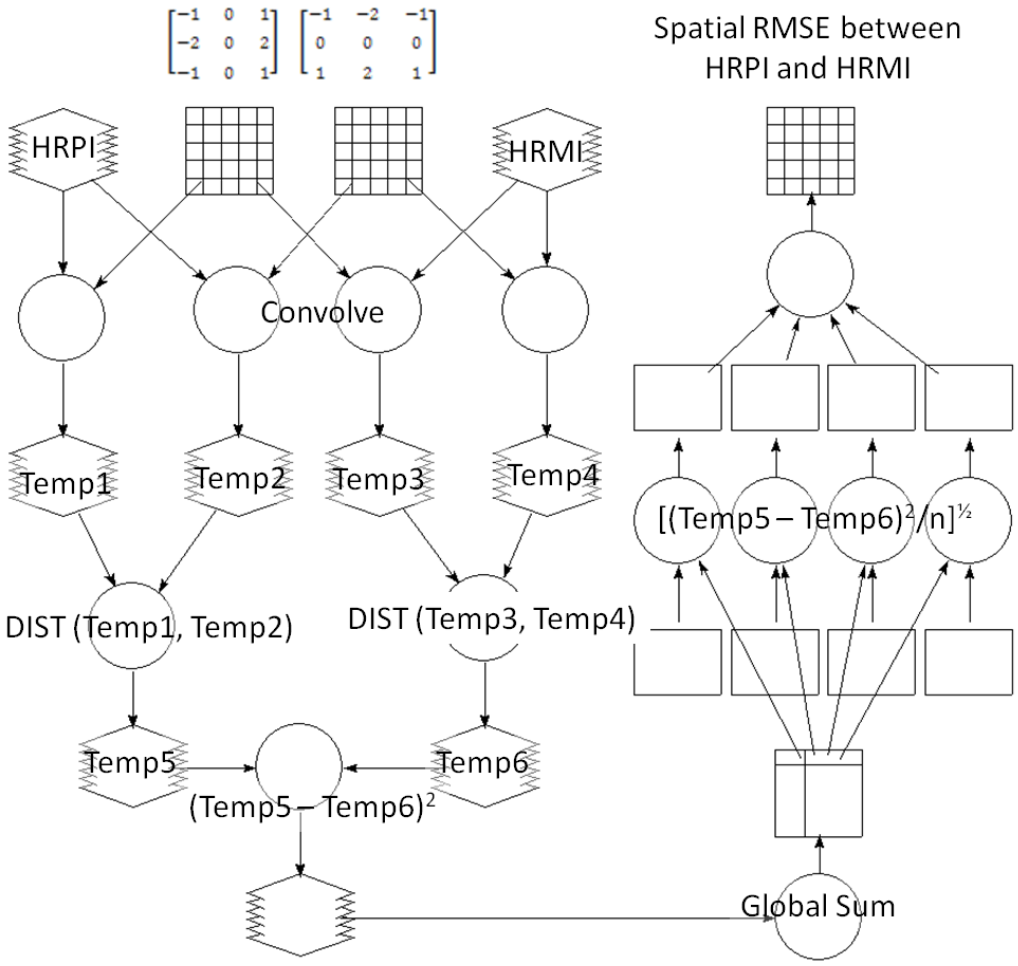

Figure A.3: ERDAS spatial modeller flow diagram showing the process of calculating spatial RMSE between the HRPI and HRMI

Appendix B

Calculating multiple linear regression using ERDAS model maker

B.1 Overview

The model calculates multivariate linear regression between an independent variable (referred as Y) and four dependent variables (referred as X_1, X_2, X_3 and X_4) using the ordinary least squares estimation technique. ERDAS spatial modeller utility has been used to calculate regression coefficients (i.e. φ_0, φ_1, φ_2, φ_3, *and* φ_4) and coefficients of determination (R^2).

B.2 Calculations

The model loads a single band panchromatic image Y (i.e., the degraded HRPI or $HRPI_{DEG}$) and a four-band image X (i.e., the blue, green, red, and infrared bands of the LRMI) to calculate regression coefficients and R^2. Table B.1 shows the temporary variables, which are computed from these images and arranged in different arrays (matrixes) during the calculations;

Table B.1: Description of temporary variables used in the multivariate regression model

Temporary Variables	Description
N	Total number of observations (i.e., pixels) of an independent or a dependent variable
$\sum Y$, $\sum X_1$, $\sum X_2$, $\sum X_3$, $\sum X_4$	The sum of all the digital numbers (DNs) of the independent (Y or $HRPI_{DEG}$) and dependent variables (X_1, X_2, X_3 and X_4 representing Blue, Green, Red and NIR respectively)
$\sum(Y.Y)$ or $\sum(Y)^2$ and from $\sum(X_1.X_1)$ or $\sum(X_1)^2$ to $\sum(X_4.X_4)$ or $\sum(X_4)^2$	The sum of the squares of all the DNs of the $HRPI_{DEG}$ and LRMI bands

Temporary Variables	Description
$\sum Y.\sum Y$ or $(\sum Y)^2$	The square of the sum of all the DNs of the $HRPI_{DEG}$
From $\sum(Y.X_1)$ to $\sum(Y.X_4)$	The sum of the multiple of the HRPI and any band of the LRMI
From $\sum(X_1.X_2)$ to $\sum(X_1.X_4)$; $\sum(X_2.X_3)$; $\sum(X_2.X_4)$; and $\sum(X_3.X_4)$	The sum of the multiple of any two different bands of the LRMI

To find regression coefficients, these variables are grouped in the following two matrices.

$$\mathbf{A} = \begin{bmatrix} \mathbf{N} & \sum \mathbf{X_1} & \sum \mathbf{X_1} & \sum \mathbf{X_3} & \sum \mathbf{X_4} \\ \sum \mathbf{X_1} & \sum (\mathbf{X_1})^2 & \sum (\mathbf{X_2} \cdot \mathbf{X_1}) & \sum (\mathbf{X_3} \cdot \mathbf{X_1}) & \sum (\mathbf{X_4} \cdot \mathbf{X_1}) \\ \sum \mathbf{X_1} & \sum (\mathbf{X_1} \cdot \mathbf{X_2}) & \sum (\mathbf{X_2})^2 & \sum (\mathbf{X_3} \cdot \mathbf{X_2}) & \sum (\mathbf{X_4} \cdot \mathbf{X_2}) \\ \sum \mathbf{X_1} & \sum (\mathbf{X_1} \cdot \mathbf{X_3}) & \sum (\mathbf{X_2} \cdot \mathbf{X_3}) & \sum (\mathbf{X_3})^2 & \sum (\mathbf{X_4} \cdot \mathbf{X_3}) \\ \sum \mathbf{X_1} & \sum (\mathbf{X_1} \cdot \mathbf{X_4}) & \sum (\mathbf{X_2} \cdot \mathbf{X_4}) & \sum (\mathbf{X_3} \cdot \mathbf{X_4}) & \sum (\mathbf{X_4})^2 \end{bmatrix} \quad \textbf{.....(B.1)}$$

$$\mathbf{B} = \begin{bmatrix} \sum \mathbf{Y} \\ \sum (\mathbf{Y} \cdot \mathbf{X_1}) \\ \sum (\mathbf{Y} \cdot \mathbf{X_2}) \\ \sum (\mathbf{Y} \cdot \mathbf{X_3}) \\ \sum (\mathbf{Y} \cdot \mathbf{X_4}) \end{bmatrix} \quad \textbf{.....(B.2)}$$

The regression coefficients are calculated using the following equation;

$$\mathbf{C} = \begin{bmatrix} \boldsymbol{\varphi_0} \\ \boldsymbol{\varphi_1} \\ \boldsymbol{\varphi_2} \\ \boldsymbol{\varphi_3} \\ \boldsymbol{\varphi_4} \end{bmatrix} = \mathbf{B} \cdot \mathbf{A}^{-1} \quad \textbf{.....(B.3)}$$

The R^2 is calculated using the following set of equations;

$$\textbf{SSE (sum of squares due to errors)} = \sum(Y)^2 - C^T \cdot B \quad \textbf{.....(B.4)}$$

$$\textbf{SST (Total sum of squares)} = \sum(Y)^2 - (\sum Y)^2/N \quad \textbf{.....(B.5)}$$

$$\mathbf{R^2} = \mathbf{1} - \frac{\mathbf{SSE}}{\mathbf{SST}} \quad \textbf{.....(B.6)}$$

The modeller flow diagram to calculate multivariate linear regression is shown in the Figure B.1 as;

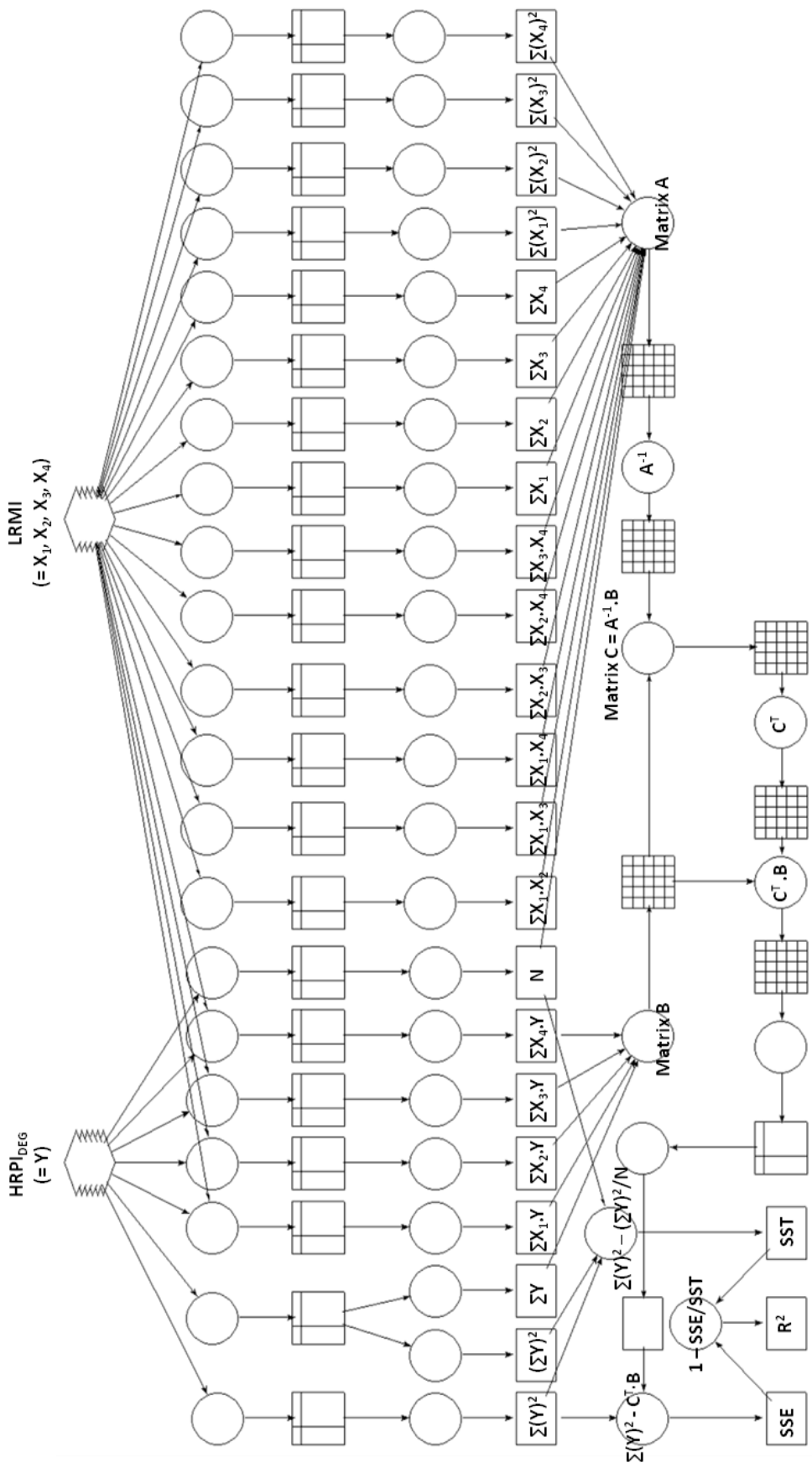

Figure B.1: ERDAS spatial modeller flow diagram showing the process of calculating multivariate linear regression between the degraded HRPI and four-band LRMI

References

Aiazzi, B., Alparone, L., Baronti, S., Garzelli, A., Lotti, F., Nencini, F., Selva, M., 2007a. Context-sensitive pan-sharpening of multispectral images, in: Falcidieno, B., Spagnuolo, M., Avrithis, Y., Kompatsiaris, I., Buitelaar, P. (Eds.), Semantic Multimedia: 2nd International conference on semantic and digital media technologies (SAMT 2007). Springer Berlin/Heidelberg, Genoa, Italy, pp. 121-125.

Aiazzi, B., Baronti, S., Selva, M., 2007b. Improving Component Substitution Pansharpening Through Multivariate Regression of MS+Pan Data. IEEE Transactions on Geoscience and Remote Sensing 45, 3230-3239.

Alexander, D., 2008. Remote sensing and the coast: Development of advanced techniques to map nuisance macro-algae in estuaries. New Zealand Geographer 64, 157-161.

Alparone, L., Wald, L., Chanussot, J., Thomas, C., Gamba, P., Bruce, L.-M., 2007. Comparison of pansharpening algorithms: Outcome of the 2006 GRS-S data fusion contest. IEEE Transactions on Geoscience and Remote Sensing 45, 3012-3021.

Amarsaikhan, D., Blotevogel, H.H., van Genderen, J.L., Ganzorig, M., Gantuya, R., Nergui, B., 2010. Fusing high-resolution SAR and optical imagery for improved urban land cover study and classification. International Journal of Image and Data Fusion 1, 83-97.

Amarsaikhan, D., Douglas, T., 2004. Data fusion and multisource image classification. International Journal of Remote Sensing 25, 3529-3539.

Arbuckle, C.J., Huryn, A.D., Israel, S.A., 1998. Applications of remote sensing and GIS to wetland inventory: Upland bogs, in: Firns, P. (Ed.), Tenth Annual Colloquium of the Spatial Information Research Centre, 16 - 19 Nov., University of Otago, New Zealand, pp. 15 - 24.

Arbuckle, C.J., Huryn, A.D., Israel, S.A., 1999. Landcover classification in the Taieri River catchment, New Zealand: A focus on the riparian zone. Geocarto International 14, 10 - 16.

Artigas, F.J., Yang, J.S., 2006. Spectral discrimination of marsh vegetation types in the New Jersey Meadowlands, USA. Wetlands 26, 271-277.

Ashraf, S., Brabyn, L., Hicks, B.J., 2007. Remote sensing of freshwater habitats for large rivers and lakes of the Waikato region using sub-pixel classification, CBER Contract Report 63. Centre for Biodiversity and Ecology Research, The University of Waikato, Hamilton, NZ, p. 76 pp.

Ashraf, S., Brabyn, L., Hicks, B.J., 2008. Evaluating remote sensing data classification techniques for mapping freshwater habitats: Trial application in the Tongariro River delta, Lake Taupo, CBER Contract Report 87. Centre for Biodiversity and Ecology Research, The University of Waikato, Hamilton, NZ, p. 33 pp.

Ashraf, S., Brabyn, L., Hicks, B.J., 2009. Remote sensing of freshwater environments: Trial application in the Lower Waikato River, CBER Contract Report 103. Centre for Biodiversity and Ecology Research, The University of Waikato, Hamilton, NZ, p. 20 pp.

Ashraf, S., Brabyn, L., Hicks, B.J., 2012. Image data fusion for the remote sensing of freshwater environments. Applied Geography 32, 619-628.

Ashraf, S., Brabyn, L., Hicks, B.J., 2011. Alternative solutions for determining the spectral band weights for the subtractive resolution merge technique. International Journal of Image and Data Fusion, DOI: 10.1080/19479832.2011.607473

Ashraf, S., Brabyn, L., Hicks, B.J., Collier, K., 2010. Satellite remote sensing for mapping vegetation in New Zealand freshwater environments: A review. New Zealand Geographer 66, 33-43.

Ausseil, A.-G.E., Dymond, J.R., Shepherd, J.D., 2007. Rapid Mapping and Prioritisation of Wetland Sites in the Manawatu–Wanganui Region, New Zealand. Environmental Management 39, 316-325.

Becker, B.L., Lusch, D.P., Qi, J., 2005. Identifying optimal spectral bands from in situ measurements of Great Lakes coastal wetlands using second-derivative analysis. Remote Sensing of Environment 97, 238-248.

Becker, B.L., Lusch, D.P., Qi, J., 2007. A classification-based assessment of the optimal spectral and spatial resolutions for Great Lakes coastal wetland imagery. Remote Sensing of Environment 108, 111-120.

Belliss, S.E., 1984. Remote sensing in New Zealand: A status report. International Journal of Remote Sensing 5, 877 - 881.

Boloorani, A.D., 2008. Remotely sensed data fusion as a basis for environmental studies: Concepts, techniques and applications, PhD Thesis, Mathematics and Natural Science Faculties. Georg-August-Universität, Göttingen, Germany, p. 166.

Boloorani, A.D., Kappas, M., Erasmi, S., 2005. Hyper-spectral/high-resolution data fusion: Assessing the quality of EO1-Hyperion/Spot-Pan & Quickbird-MS fused images in spectral domain, in: Heipke, C., Jacobsen, K., Gerke, M. (Eds.), ISPRS Hannover Workshop 2005: High-Resolution Earth Imaging for Geospatial Information. Institute of Photogrammetry and GeoInformation (IPI), Hannover, Germany, pp. 5, Un-paginated CD-ROM.

Booth, D.T., Cox, S.E., Simonds, G., 2007. Riparian monitoring using 2-cm GSD aerial photography. Ecological Indicators 7, 636-648.

Calitz, M.F., Rüther, H., 1996. Least Absolute Deviation (LAD) image matching. ISPRS Journal of Photogrammetry and Remote Sensing 51, 223-229.

Cetin, M., Musaoglu, N., 2009. Merging hyperspectral and panchromatic image data: qualitative and quantitative analysis. International Journal of Remote Sensing 30, 1779-1804.

Chambers, P.A., Kalff, J., 1985. The influence of sediment composition and irradiance on the growth and morphology of Myriophyllum spicatum L. Aquat. Bot. 22, 253-263.

Chavez Jr., P.S., Sides, S.C., Anderson, J.A., 1991. Comparison of three different methods to merge multiresolution and multispectral data: Landsat TM and SPOT panchromatic. Photogrammetric Engineering & Remote Sensing 57, 295-303.

Chen, Y., Deng, L., Li, J., Li, X., Shi, P., 2006. A new wavelet-based image fusion method for remotely sensed data. International Journal of Remote Sensing 27, 1465 - 1476.

Choi, J.W., Kim, H.J., Ryu, K.Y., Kim, Y.I., 2008. A new adaptive image fusion technique for IKONOS satellite imagery, in: Blouke, M.M., Bodegom, E. (Eds.), Conference on Sensors, Cameras, and Systems for Industrial/Scientific Applications IX. SPIE, San Jose, CA, pp. N1-N10.

Clayton, J., Edwards, T., 2006. LakeSPI - A method for monitoring ecological condition in New Zealand lakes. Technical Report, Version 2. National Institute of Water & Atmospheric Research Ltd, Hamilton, p. 67.

Cliche, G., Bonn, F., Teillet, P., 1985. Integration of the SPOT panchromatic channel into its multispectral mode for image sharpness enhancement. Photogrammetric Engineering & Remote Sensing 51, 311-316.

Coates, M.J., Folkard, A.M., 2009. The effects of littoral zone vegetation on turbulent mixing in lakes. Ecological Modelling 220, 2714-2726.

Coffey, B.T., Clayton, J.S., 1988. New Zealand waterplants: A guide to plants found in New Zealand freshwaters. Ruakura Agricultural Centre, Hamilton, New Zealand.

Colditz, R.R., Wehrmann, T., Bachmann, M., Steinnocher, K., Schmidt, M., Strunz, G., Dech, S., 2006. Influence of image fusion approaches on classification accuracy: a case study. International Journal of Remote Sensing 27, 3311-3335.

Collier, K., Kelly, J., Champion, P., 2007. Regional guidelines for ecological assessments of freshwater environments. Aquatic plant cover in wadeable

streams. Environment Waikato Technical Report 2006/47. Environment Waikato, Hamilton, NZ.

Collier, K.J., Cooper, A.B., Davies-Colley, R., Rutherford, J.C., Smith, C.M., Williamson, R.B., 1995. Managing riparian zones: A contribution to protecting New Zealand's rivers and streams, First ed. Department of Conservation, Wellington, New Zealand.

Congalton, R.G., 2001. Accuracy assessment and validation of remotely sensed and other spatial information. The International Journal of Wildland Fire 10, 321-328.

Congalton, R.G., Birch, K., Jones, R., Schriever, J., 2002. Evaluating remotely sensed techniques for mapping riparian vegetation. Computers and Electronics in Agriculture 37, 113-126.

Cramer, M., 2005. Digital airborne cameras - status and future, in: Heipke, C., Jacobsen, K., Gerke, M. (Eds.), ISPRS Hannover Workshop 2005: High-Resolution Earth Imaging for Geospatial Information. Institute of Photogrammetry and GeoInformation (IPI), Hannover, Germany, pp. Unpaginated, on CD-ROM.

Crippen, R.E., 1989. A simple spatial filtering routine for the cosmetic removal of scan-line noise from Landsat TM P-Tape imagery. Photogrammetric Engineering & Remote Sensing 55, 327-331.

Cromarty, P., Scott, D.A., 1995. A Directory of Wetlands in New Zealand. Department of Conservation, Wellington, New Zealand.

Dalke, P.D., 1937. The cover map in wildlife management. The Journal of Wildlife Management 1, 100-105.

de Béthune, S., Muller, F., Binard, M., 1998a. Adaptive intensity matching filters: a new tool for multi-resolution data fusion, Multi-Sensor Systems and Data Fusion for Telecommunications, Remote Sensing and Radar AGARD, Neuilly-sur-Seine, France, Lisbon, Portugal, pp. 671–680.

de Béthune, S., Muller, F., Donnay, J.-P., 1998b. Fusion of multispectral and panchromatic images by local mean and variance matching filtering techniques, in: Ranchin, T., Wald, L. (Eds.), 2nd International Conference on Fusion of Earth data: merging point measurements, raster maps and remotely sensed images. SEE/URISCA, Sophia Antipolis, France, pp. 1-6.

de Carvalho, L.M.T., Acerbi Jr., F.W., Clevers, J.G.P.W., Fonseca, L.M.G., de Jong, S.M., 2004. Multiscale feature extraction from images using wavelets, in: de Jong, S.M., van der Meer, F.D. (Eds.), Remote sensing image analysis: including the spatial domain Kluwer Academic Publishers, Dordrecht, The Netherlands, pp. 237-270.

de Smith, M.J., Goodchild, M.F., Longley, P.A., 2009. Geospatial Analysis - A Comprehensive Guide to Principles, Techniques and Software Tools, 3 ed. Matador, Leicester, UK.

Dodge, Y., Jurečková, J., 2000. Adaptive Regression. Springer-Velrag Inc., New York.

Dong, J., Zhuang, D., Huang, Y., Fu, J., 2009. Advances in multi-sensor data fusion: algorithms and applications. Sensors 9, 7771-7784.

Dou, W., Chen, Y., Li, X., Sui, D.Z., 2007. A general framework for component substitution image fusion: An implementation using the fast image fusion method. Computers & Geosciences 33, 219-228.

E. W., n.d. Aerial Photography - WRAPS 2006 - GIS Layer. Environment Waikato, Retrieved January 19, 2010, from http://www.ew.govt.nz/environmental-information/REDI/1120590/.

ERDAS, 2009. ERDAS Imagine ver. 9.2 Software Help Document, November 2009 ed. ERDAS Inc., Norcross, GA.

Eser, P.C., 1998. PhD Thesis: Ecological patterns and processes of the South Taupo wetland, North Island, New Zealand, with special reference to nature conservation management. School of Biological Sciences, Victoria University of Wellington, Wellington.

Everitt, J.H., Fletcher, R.S., Elder, H.S., Yang, C., 2008. Mapping giant salvinia with satellite imagery and image analysis. Environ. Monit. Assess. 139, 35-40.

Everitt, J.H., Yang, C., Deloach, C.J., 2005. Remote sensing of giant reed with QuickBird satellite imagery. J. Aquat. Plant Manage. 43, 81-85.

Everitt, J.H., Yang, C., Fletcher, R.S., Davis, M.R., Drawe, D.L., 2004. Using aerial color-infrared photography and QuickBird satellite imagery for mapping wetland vegetation. Geocarto International 19, 15 - 22.

Fox III, L., Garrett, M.L., Heasty, R., Torres, E., 2002. Classifying wildlife habitat with Pan-sharpened Landsat-7 imagery, in: Morain, S., Budge, A. (Eds.), ISPRS Comission I Mid-Term Symposium on Integrated Remote Sensing at the Global, Regional and Local Scale in conjunction with Pecora 15/Land Satellite Information IV Conference. ISPRS, Denver, CO.

Frohn, R., Reif, M., Lane, C., Autrey, B., 2009. Satellite remote sensing of isolated wetlands using object-oriented classification of Landsat-7 data. Wetlands 29, 931-941.

Frohn, R.C., Autrey, B.C., Lane, C.R., Reif, M., 2011. Segmentation and object-oriented classification of wetlands in a karst Florida landscape using multi-season

Landsat-7 ETM+ imagery. International Journal of Remote Sensing 32, 1471-1489.

Gangkofner, U.G., Pradhan, P.S., Holcomb, D.W., 2008. Optimizing the high-pass filter addition technique for image fusion. Photogrammetric Engineering & Remote Sensing 74, 1107-1118.

Gao, J., 1999. A comparative study on spatial and spectral resolutions of satellite data in mapping mangrove forests. International Journal of Remote Sensing 20, 2823-2833.

Gao, J., Chen, H.F., Zhang, Y., Zha, Y., 2004. Knowledge-based approaches to accurate mapping of mangroves from satellite data. Photogramm. Eng. Remote Sens. 70, 1241-1248.

Garguet-Duport, B., Girel, J., Chassery, J.-M., Pautou, G., 1996. The use of multiresolution analysis and wavelets transform for merging SPOT panchromatic and multispectral image data. Photogrammetric Engineering & Remote Sensing 62, 1057-1066.

Genkai-Kato, M., 2007. Macrophyte refuges, prey behaviour and trophic interactions: Consequences for lake water clarity. Ecology Letters 10, 105-114.

Gillespie, A.R., Kahle, A.B., Walker, R.E., 1986. Colour enhancement of highly correlated images-I. Decorrelation and HSI contrast stretches. Remote Sensing of Environment 20, 209-235.

Gillespie, A.R., Kahle, A.B., Walker, R.E., 1987. Colour enhancement of highly correlated images-II. Channel ratio and "chromaticity" transformation techniques. Remote Sensing of Environment 22, 343-365.

Giloni, A., Simonoff, J.S., Sengupta, B., 2006. Robust weighted LAD regression. Computational Statistics & Data Analysis 50, 3124-3140.

Gilvear, D., Hunter, P., Higgins, T., 2007. An experimental approach to the measurement of the effects of water depth and substrate on optical and near infra-red reflectance: a field-based assessment of the feasibility of mapping submerged instream habitat. International Journal of Remote Sensing 28, 2241-2256.

Goetz, S.J., 2006. Remote sensing of riparian buffers: Past progress and future prospects. J. Am. Water Resour. Assoc. 42, 133-143.

Haest, B., Biesemans, J., Horsten, W., Everaerts, J., Camp, N.V., Valckenborgh, J.V., 2009. Radiometric Calibration of Digital Photogrammetric Camera Image Data, ASPRS 2009 Annual Conference. ASPRS, Baltimore, Maryland.

Harding, J., Mosley, P., Pearson, C., Sorrell, B., 2004. Freshwaters of New Zealand. New Zealand Hydrological Society Inc. and New Zealand Limnological Society Inc., Christchurch.

Harvey, K.R., Hill, G.J.E., 2001. Vegetation mapping of a tropical freshwater swamp in the Northern Territory, Australia: A comparison of aerial photography, Landsat TM and SPOT satellite imagery. International Journal of Remote Sensing 22, 2911 - 2925.

Hill, J., Diemer, C., Stöver, O., Udelhoven, T., 1999. A local correlation approach for the fusion of remote sensing data with different spatial resolutions in forestry applications. International Archives of Photogrammetry and Remote Sensing 32, pp. 8, Un-paginated CD-ROM.

Holliday, C.T., 1950. Seeing the Earth from 80 miles up. National Geographic Oct 1950, 98, 511.

Horler, D.N.H., Dockray, M., Barber, J., 1983. The red edge of plant leaf reflectance. International Journal of Remote Sensing 4, 273 - 288.

Hunter, P.D., Gilvear, D.J., Tyler, A.N., Willby, N.J., Kelly, A., 2010. Mapping macrophytic vegetation in shallow lakes using the Compact Airborne Spectrographic Imager (CASI). Aquatic Conservation: Marine and Freshwater Ecosystems 20, 717-727.

Israel, S.A., Fyfe, J.E., 1996. Determining the sensitivity of SPOT XS imagery for monitoring intertidal and sublittoral vegetation of Otago Harbour. Conservation Advisory Science Notes No. 131. Department of Conservation, Wellington, p. 21.

James, W.F., Barko, J.W., Butler, M.G., 2004. Shear stress and sediment resuspension in relation to submersed macrophyte biomass. Hydrobiologia 515, 181-191.

Jensen, J.R., Hodgson, M.E., Christensen, E., Mackey Jr., H.E., Tinney, L.R., Sharitz, R., 1986. Remote sensing inland wetlands: A multispectral approach. Photogammetric Engineering & Remote Sensing 52, 87-100.

Johansen, K., Phinn, S., 2006. Mapping structural parameters and species composition of riparian vegetation using IKONOS and landsat ETM plus data in Australian tropical savannahs. Photogramm. Eng. Remote Sens. 72, 71-80.

Johansen, K., Phinn, S., Dixon, I., Douglas, M., Lowry, J., 2007. Comparison of image and rapid field assessments of riparian zone condition in Australian tropical savannas. Forest Ecology and Management 240, 42-60.

Joyce, K.E., 2004. A method of mapping live coral cover using remote sensing, PhD Thesis, School of Geography, Planning and Architecture. University of Queensland, Brisbane, Australia, p. 137.

Khan, M.M., Chanussot, J., Condat, L., Montanvert, A., 2008. Indusion: Fusion of Multispectral and Panchromatic Images Using the Induction Scaling Technique. Geoscience and Remote Sensing Letters, IEEE 5, 98-102.

kiwImage, n.d. All of Government Imagery - Project KiwImage. New Zealand Defence Force, Retrieved January 19, 2010, from http://www.kiwimage.govt.nz.

Laben, C.A., Brower, B.V., 2000. Process for enhancing the spatial resolution of multispectral imagery using pan-sharpening. US Patent # 6,011,875, USPTO. Eastman Kodak Company (Rochester, NY), United States.

Li, S., Li, Z., 2010. Effects of image fusion algorithms on classification accuracy, in: Liu, Y., Chen, A. (Eds.), 2010 18th International Conference on Geoinformatics. Institute of Electrical and Electronics Engineers, Beijing, China, pp. 1-6.

Li, S., Li, Z., Gong, J., 2010. Multivariate statistical analysis of measures for assessing the quality of image fusion. International Journal of Image and Data Fusion 1, 47-66.

Li, W., Zhang, Q., Zhang, Y., 2007. Research on the fusion methods with high information preservation, Fourth International Conference on Fuzzy Systems and Knowledge Discovery (FSKD 2007). IEEE, Haikou, China, pp. 487-491.

Ling, Y., Ehlers, M., Usery, E.L., Madden, M., 2007. FFT-enhanced IHS transform method for fusing high-resolution satellite images. ISPRS Journal of Photogrammetry and Remote Sensing 61, 381-392.

Liu, J.G., 2000. Smoothing filter-based intensity modulation: A spectral preserve image fusion technique for improving spatial details. International Journal of Remote Sensing 21, 3461 - 3472.

Liu, J.G., Moore, J.M., 1998. Pixel block intensity modulation: adding spatial detail to TM band 6 thermal imagery. International Journal of Remote Sensing 19, 2477 - 2491.

Lonard, R.I., Judd, F.W., Everitt, J.H., Escobar, D.E., Davis, M.R., Crawford, M.M., Desai, M.D., 2000. Evaluation of color-infrared photography for distinguishing annual changes in riparian forest vegetation of the lower Rio Grande in Texas. Forest Ecology and Management 128, 75-81.

Maheu-Giroux, M., de Blois, S., 2005. Mapping the invasive species Phragmites australis in linear wetland corridors. Aquat. Bot. 83, 310-320.

Mallinis, G., Emmanoloudis, D., Giannakopoulos, V., Maris, F., Koutsias, N., 2011. Mapping and interpreting historical land cover/land use changes in a Natura 2000 site using earth observational data: The case of Nestos delta, Greece. Applied Geography 31, 312-320.

Malthus, T.J., Karpouzli, E., 2003. Integrating field and high spatial resolution satellite-based methods for monitoring shallow submersed aquatic habitats in the Sound of Eriskay, Scotland, UK. International Journal of Remote Sensing 24, 2585 - 2593.

McKean, J.W., Sievers, G.L., 1987. Coefficients of determination for least absolute deviation analysis. Statistics & Probability Letters 5, 49-54.

Meenakshisundaram, V., 2005. Quality Assessment of Ikonos and Quickbird Fused Images for Urban Mapping, M.Sc. Thesis, Department of Geomatics Engineering. University of Calgary, Calgary, Canada, p. 107.

Melendez-Pastor, I., Navarro-Pedreño, J., Gómez, I., Koch, M., 2010. Detecting drought induced environmental changes in a Mediterranean wetland by remote sensing. Applied Geography 30, 254-262.

MfE, 2007. Environment New Zealand 2007. Ministry for the Environment, Wellington, p. 456.

MfE, 2010. Land Use and Carbon Analysis System: Satellite imagery interpretation guide for land-use classes. Ministry for the Environment, Wellington, p. 25.

Midwood, J., Chow-Fraser, P., 2010. Mapping floating and emergent aquatic vegetation in coastal wetlands of Eastern Georgian Bay, Lake Huron, Canada. Wetlands 30, 1141-1152.

Mount, R.E., 2006. Small format digital aerial photography for mapping and monitoring seagrass habitats in shallow temperate marine waters, School of Geography and Environmental Studies. University of Tasmania, Hobart, p. 185.

Muller, E., 1997. Mapping riparian vegetation along rivers: Old concepts and new methods. Aquat. Bot. 58, 411-437.

Munechika, C.K., Warnick, J.S., Salvaggio, C., Schott, J.R., 1993. Resolution enhancement of multispectral image data to improve classification accuracy. Photogramm. Eng. Remote Sens. 59, 67-72.

Nagler, P., Glenn, E.P., Hursh, K., Curtis, C., Huete, A., 2005. Vegetation mapping for change detection on an arid-zone river. Environ. Monit. Assess. 109, 255-274.

Naiman, R.J., Décamps, H., 1997. The Ecology of Interfaces: Riparian Zones. Annu. Rev. Ecol. Syst. 28, 621-658.

Narumalani, S., Zhou, Y.C., Jensen, J.R., 1997. Application of remote sensing and geographic information systems to the delineation and analysis of riparian buffer zones. Aquat. Bot. 58, 393-409.

Neter, J., Kutner, M.H., Nachtsheim, C.J., Wasserman, W., 1996. Applied Linear Statistical Models, 4 ed. McGraw-Hill Inc., Boston.

Nikolakopoulos, K.G., 2008. Comparison of Nine Fusion Techniques for Very High Resolution Data. Photogammetric Engineering & Remote Sensing 74, 647-659.

NZ Soil Bureau, 1954. General Survey of the soils of North Island, New Zealand. Soil Bureau Bulletin 5. DSIR, Wellington.

NZ Soil Bureau, 1968. General Survey of the soils of South Island, New Zealand. Soil Bureau Bulletin 27. DSIR, Wellington.

Okun, N., Mehner, T., 2005. Distribution and feeding of juvenile fish on invertebrates in littoral reed (Phragmites) stands. Ecology of Freshwater Fish 14, 139-149.

Otazu, X., González-Audícana, M., Fors, O., Núñez, J., 2005. Introduction of sensor spectral response into image fusion methods. Application to wavelet-based methods. IEEE Transactions on Geoscience and Remote Sensing 43, 2376-2385.

Ozesmi, S.L., Bauer, M.E., 2002. Satellite remote sensing of wetlands. Wetlands Ecology and Management 10, 381-402.

Padwick, C., Deskevich, M., Pacifici, F., Smallwood, S., 2010. WorldView-2 Pan-Sharpening, ASPRS 2010 Annual Conference: Opportunities for Emerging Geospatial Technologies. ASPRS, San Diego, California.

Pohl, C., Van Genderen, J.L., 1998. Multisensor image fusion in remote sensing: concepts, methods and applications. International Journal of Remote Sensing 19, 823-854.

Pradhan, P.S., King, R.L., Younan, N.H., Holcomb, D.W., 2006. Estimation of the number of decomposition levels for a wavelet-based multiresolution multisensor image fusion. IEEE Transactions on Geoscience and Remote Sensing 44, 3674-3686.

Rahman, M.M., Csaplovics, E., 2007. Examination of image fusion using synthetic variable ratio (SVR) technique. International Journal of Remote Sensing 28, 3413-3424.

Raitala, J., Jantunen, H., Lampinen, J., 1985. Application of landsat satellite data for mapping aquatic areas in north-eastern Finland. Aquat. Bot. 21, 285-294.

Ranchin, T., Wald, L., 2000. Fusion of high spatial and spectral resolution images: The ARSIS Concept and its implementation. Photogramm. Eng. Remote Sens. 66, 49-61.

Risley, E.M., 1967. Developments In The Application of Earth Observation Satellites To Geographic Problems. The Professional Geographer 19, 130-132.

Riyahi, R., Kleinn, C., Fuchs, H., 2009. Comparison of different image fusion techniques for individual tree crown identification using Quickbird images, in:

Heipke, C., Jacobsen, K., Müller, S., Sörgel, U. (Eds.), ISPRS Hannover Workshop 2009: High-Resolution Earth Imaging for Geospatial Information. ISPRS, Hannover, Germany, pp. Un-pagenated.

Robb, C., Bright, J., 2004. Values and uses of water, in: Harding, J., Mosley, P., Pearson, C., Sorrell, B. (Eds.), Freshwaters of New Zealand. New Zealand Hydrological Society Inc. and New Zealand Limnological Society Inc., Christchurch, pp. 42.41-42.13.

Sawaya, K.E., Olmanson, L.G., Heinert, N.J., Brezonik, P.L., Bauer, M.E., 2003. Extending satellite remote sensing to local scales: land and water resource monitoring using high-resolution imagery. Remote Sensing of Environment 88, 144-156.

Schowengerdt, R.A., 1980. Reconstruction of multispatial, multispectral image data using spatial frequency content. Photogrammetric Engineering & Remote Sensing 46, 1325-1334.

Schowengerdt, R.A., 2007. Remote sensing - models and methods for image processing, Third edition ed. Academic Press, Burlington.

Schulz, M., Rinke, K., Kohler, J., 2003. A combined approach of photogrammetrical methods and field studies to determine nutrient retention by submersed macrophytes in running waters. Aquat. Bot. 76, 17-29.

Shalaby, A., Tateishi, R., 2007. Remote sensing and GIS for mapping and monitoring land cover and land-use changes in the Northwestern coastal zone of Egypt. Applied Geography 27, 28-41.

Shettigara, V.K., 1992. A generalized component substitution technique for spatial enhancement of multispectral images using a higher resolution data set. Photogramm. Eng. Remote Sens. 58, 561-567.

Silva, T., Costa, M., Melack, J., Novo, E., 2008. Remote sensing of aquatic vegetation: theory and applications. Environ. Monit. Assess. 140, 131-145.

Sirguey, P., Mathieu, R., Arnaud, Y., Khan, M.M., Chanussot, J., 2008. Improving MODIS spatial resolution for snow mapping using wavelet fusion and ARSIS concept. IEEE Geoscience and Remote Sensing Letters 5, 78-82.

Sotheran, I.S., FosterSmith, R.L., Davies, J., 1997. Mapping of marine benthic habitats using image processing techniques within a raster-based geographic information system. Estuar. Coast. Shelf Sci. 44, 25-31.

Stephens, P.R., 1991. Remote sensing in New Zealand. Geocarto International 6, 90 - 92.

Svab, A., Ostir, K., 2006. High-resolution Image Fusion: Methods to Preserve Spectral and Spatial Resolution. Photogrammetric Engineering & Remote Sensing 72, 565-572.

Tansey, K., Chambers, I., Anstee, A., Denniss, A., Lamb, A., 2009. Object-oriented classification of very high resolution airborne imagery for the extraction of hedgerows and field margin cover in agricultural areas. Applied Geography 29, 145-157.

Teggi, S., Cecchi, R., Serafini, F., 2003. TM and IRS-1C-PAN data fusion using multiresolution decomposition methods based on the 'a tròus' algorithm. International Journal of Remote Sensing 24, 1287 - 1301.

Thomas, C., Ranchin, T., Wald, L., Chanussot, J., 2008. Synthesis of multispectral images to high spatial resolution: A critical review of fusion methods based on remote sensing physics. IEEE Transactions on Geoscience and Remote Sensing 46, 1301-1312.

Thomas, H.H., 1920. Aircraft photography in the service of science. Nature 105 457-459.

Thompson, S., Grüner, I., Gapare, N., 2003. New Zealand Land Cover Database version 2, Illustrated guide to target classes. Ministry for the Environment, Wellington, N.Z.

Thompson, S., Grüner, I., Gapare, N., 2004. New Zealand Land Cover Database 2 user guide. Ministry for the Environment, Wellington, N.Z.

Thomson, A.G., 1998. Supervised versus unsupervised methods for classification of coasts and river corridors from airborne remote sensing. International Journal of Remote Sensing 19, 3423 - 3431.

Tou, J.T., Gonzalez, R.C., 1974. Pattern recognition principles. Addison-Wesley Publishing Company, Reading, Massachusetts, USA.

Valta-Hulkkonen, K., Pellikka, P., Tanskanen, H., Ustinov, A., Sandman, O., 2003. Digital false colour aerial photographs for discrimination of aquatic macrophyte species. Aquat. Bot. 75, 71-88.

Wald, L., Ranchin, T., Mangolini, M., 1997. Fusion of satellite images of different spatial resolutions: Assessing the quality of resulting images. Photogrammetric Engineering & Remote Sensing 63, 691-699.

Walker, S., Price, R., Rutledge, D., Stephens, R.T.T., Lee, W.G., 2006. Recent loss of indigenous cover in New Zealand. New Zealand Journal of Ecology 30, 169-177.

Wang, L., Cao, X., Chen, J., 2008. ISVR: An improved synthetic variable ratio method for image fusion. Geocarto International 23, 155 - 165.

Wang, Z., Bovik, A.C., 2002. A universal image quality index. IEEE Signal Processing Letters 9, 81-84.

Wang, Z., Liu, S., You, S., Huang, X., 2010. Simulation of Low-Resolution Panchromatic Images by Multivariate Linear Regression for Pan-Sharpening IKONOS Imageries. IEEE Geoscience and Remote Sensing Letters 7, 515-519.

Wang, Z., Ziou, D., Armenakis, C., Li, D., Li, Q., 2005. A comparative analysis of image fusion methods. IEEE Transactions on Geoscience and Remote Sensing 43, 1391-1402.

Ward, J.C., Lambie, J.S., 1999. Monitoring changes in wetland extent: An environmental performance indicator for wetlands. Final report - project phase 1. Lincoln Environmental, Lincoln University, Canterbury, NZ.

Water and Soil Division, 1979. Our land resources. National Water and Soil Conservation Organisation, Water and Soil Division, Ministry of Works and Development, Wellington.

Weber, R.M., Dunno, G.A., 2001. Riparian vegetation mapping and image processing techniques, Hopi Indian Reservation, Arizona. Photogramm. Eng. Remote Sens. 67, 179-186.

Wolter, P.T., Johnston, C.A., Niemi, G.J., 2005. Mapping submergent aquatic vegetation in the US Great Lakes using Quickbird satellite data. International Journal of Remote Sensing 26, 5255-5274.

Xia, Y., Kamel, M.S., 2008. A generalized Least Absolute Deviation method for parameter estimation of autoregressive signals. IEEE Transactions on Neural Networks 19, 107-118.

Xie, Y., Sha, Z., Yu, M., 2008. Remote sensing imagery in vegetation mapping: a review. Journal of Plant Ecology 1, 9-23.

Yang, J., Zhang, J., Li, H., Sun, Y., Pu, P., 2010. Pixel level fusion methods for remote sensing images: a current review, in: Wagner, W., Székely, B. (Eds.), ISPRS Technical Commission VII Symposium – 100 Years: ISPRS Advancing Remote Sensing Science. ISPRS, Vienna, Austria, pp. 680-686.

Yang, X., 2007. Integrated use of remote sensing and geographic information systems in riparian vegetation delineation and mapping. International Journal of Remote Sensing 28, 353-370.

Yocky, D.A., 1996. Multiresolution wavelet decomposition image merger of Landsat Thematic Mapper and SPOT panchromatic data. Photogrammetric Engineering & Remote Sensing 62, 1067-1074.

Yuan, L., Zhang, L.-Q., 2008. Mapping large-scale distribution of submerged aquatic vegetation coverage using remote sensing. Ecological Informatics 3, 245-251.

Zhang, J., Yang, J., Zhao, Z., Zhang, Y., Li, H., 2006. Block-regression-based fusion of optical and SAR imagery for features enhancement, in: Kerle, N., Skidmore, A.K. (Eds.), From Pixels to Processes, ISPRS Mid-term Symposium 2006. ISPRS, Enschede, The Netherlands, pp. 1-6.

Zhang, Y., 1999. A new merging method and its spectral and spatial effects. International Journal of Remote Sensing 20, 2003 - 2014.

Zhang, Y., 2008. System and method for image fusion, US Patent 7,340,099 B2, United States, p. 12.

Zhang, Y., Hong, G., 2005. An IHS and wavelet integrated approach to improve pan-sharpening visual quality of natural colour IKONOS and QuickBird images. Information Fusion 6, 225-234.